

**A STUDY OF THE STELLAR POPULATIONS
IN GALAXIES FROM INTEGRATED SPECTRA**

A Thesis
Submitted for the degree of
Doctor of Philosophy in the Faculty of Science
BANGALORE UNIVERSITY

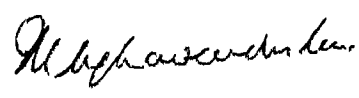
By
ASHOK KUMAR PATI

**INDIAN INSTITUTE OF ASTROPHYSICS
BANGALORE-560 034
INDIA
JULY 1988**

Certificate

The thesis entitled 'A Study of the Stellar Populations in Galaxies from Integrated Spectra' is a record of work done by Ashok Kumar Pati, and has not formed the basis for the award to him of any Degree, Diploma, Associateship, Fellowship or other similar titles. This thesis represents independent work on the part of Ashok Kumar Pati.


Prof. J.C. Bhattacharyya
Indian Institute of Astrophysics
Bangalore-560 034


Prof. K.S. Raghavendra Rao
Department of Physics
Bangalore University
Bangalore

Supervisors.

July 1988
Bangalore

Declaration

The work forming the subject matter of this thesis was entirely carried out by me under the supervision of Dr. J.C. Bhattacharyya and Dr.K.S. Raghavendra Rao. This work has not been submitted to any Institute or University for the award of any degree, diploma, associateship or fellowship.

July 1988
Bangalore


Ashok Kumar Pati

ACKNOWLEDGEMENTS

My interest in the field of galaxies in general and the use of population synthesis in studying stellar populations in galaxies, in particular, was kindled by the late M.K. Vainu Bappu under whose supervision this work was started. Dr. M.K. Vainu Bappu was always unfailing in his enthusiasm to inspire new comers to the field of astronomy to produce work of the highest quality. I shall always remain grateful to him for having provided constant encouragement and guidance.

I am thankful to Prof. J.C. Bhattacharyya both as my Supervisor and as the Director of the Indian Institute of Astrophysics for unfailing encouragement during the years that it took to complete this dissertation. I am grateful to Prof. K.S. Raghavendra Rao of the Bangalore University who, as co-supervisor took great interest in the progress of the work and helped me with the procedures at the University.

My colleagues at the Indian Institute of Astrophysics have spent time and effort in discussing problems relating to this work and in providing ideas and encouragement. I would like to especially thank Drs. D.C.V. Mallik, T.P. Prabhu, M. Parthasarathy and K.K. Ghosh. K.K. Ghosh, especially, often took

over many aspects of my duties as System Manager of the VAX computer installation, thereby allowing me time to work on this dissertation. T.P. Prabhu was a constant source of encouragement by virtue of his intense interest in the correct methods of reduction and analysis. He rendered invaluable help in the final days of preparation of the thesis, especially in the layout of the figures and in checking that everything was as it should be.

I am grateful to Mr. A.Mohd. Batcha, who went out of his way to do the entire typing of the thesis, mainly during sleepless nights. His excellent typing ability greatly relieved the tension and worries of the last days before the deadline of submission.

I also thank Mrs. A. Vagiswari, Mr. H.N. Manjunath and Ms. Christina Louis of the library for taking pains to locate and readily make available books, journals and other sources of reference. Mrs. and Mr. Krishna-moorthy and others at the binding section of the library did an excellent job of the final presentation. The library staff, especially Mr. Venkatesh, have readily spent long hours making xerox copies, for which I am grateful.

The VAX 11/780 computer system was used heavily for a lot of the work in this dissertation; many people

were directly or indirectly responsible for its constant operation. I would especially like to thank Messrs. V. Chandramouli, K. Subramani. The observing assistance at VBO was never lacking and I would like to especially thank Messrs. Jaykumar, Kuppuswamy and Rosario.

I would like to acknowledge the support of the European Southern Observatory in allotting observing time on the 1.5 m telescope and the use of the data reduction facility. The use of the STARLINK software package running on the VAX system at VBO is also acknowledged.

Dr. A.J. Pickles was very helpful in promptly providing the standard stellar library spectra compiled by him, the OPTIMA set of routines for optimisation and other routines for use in population synthesis. I would like to acknowledge the use of this material.

My wife has had a trying time with my long absences from home during the last few months of this work which were also the first few months of our marriage. Without her patience, understanding and support, it would have been impossible to bring this dissertation to a comprehensive end.

Lastly, I am grateful to my mother and my late father for having provided support and encouragement during all these long years.

July 1988

ASHOK KUMAR PATI

CONTENTS

| | | <u>Page</u> |
|-------------|--|-------------|
| Chapter I | INTRODUCTION | .. I-1 |
| | I.1 The Stellar Content of Galaxies | .. I-2 |
| | I.2 Determination of the stellar content of galaxies | .. I-4 |
| | I.2.1 Spectroscopy, equivalent widths and line ratios | .. I-4 |
| | I.2.2 Photometry | .. I-7 |
| | I.2.3 Spectrophotometry | .. I-10 |
| | I.3 Aims of Population Synthesis | I-17 |
| | I.4 Outline of this dissertation | I-20 |
| Chapter II | INSTRUMENTATION | .. II-1 |
| | II.1 Instrumentation at the Vainu Bappu Observatory | .. II-1 |
| | II.1.1 The Cassegrain Image Tube Spectrograph (CITS) | .. II-3 |
| | II.1.2 Intensity Calibration | .. II-6 |
| | II.1.3 PDS Microdensitometer | .. II-7 |
| | II.1.4 VAX 11/780 Computer System at VBO | .. II-9 |
| | II.2 Instrumentation used at the European Southern Observatory (ESO) | .. II-9 |
| | II.2.1 The ESO 1.5 m telescope | .. II-9 |
| | II.2.2 The Boller & Chivens Spectrograph at the ESO 1.5 m telescope | .. II-10 |
| | II.2.3 The Reticon Detector System | II-12 |
| | II.2.4 ESO Data Analysis Facility | .. II-15 |
| Chapter III | OBSERVATIONS | .. III-1 |
| | III.1 Observations at the ESO 1.5 m Telescope | .. III-2 |
| | III.1.2 Parameters of Observations | .. III-3 |
| | III.1.3 Objects Observed | .. III-6 |

CONTENTS

| | | <u>Page</u> |
|------------|---|-------------|
| | III.1.3.1 Flux Standard Stars .. | III-7 |
| | III.1.3.2 Synthesis Stellar Library Stars .. | III-8 |
| | III.1.3.3 Observations of Galaxies .. | III-10 |
| | III.2 Observations carried out at VBO .. | III-15 |
| Chapter IV | ... DATA REDUCTIONS AND PRESENTATION OF DATA .. | IV-1 |
| | IV.1 Reductions of Spectra obtained at ESO .. | IV-1 |
| | IV.1.2 Data Formats .. | IV-3 |
| | IV.1.3 Shifts in Wavelength and Flat field exposures .. | IV-4 |
| | IV.1.4 Wavelength Calibration .. | IV-5 |
| | IV.1.5 Sky Subtraction .. | IV-8 |
| | IV.1.6 Flat Field Correction .. | IV-10 |
| | IV.1.7 Instrument response curve | IV-11 |
| | IV.1.8 Conversion of spectra to fluxes .. | IV-15 |
| | IV.1.9 Errors in flux calibration | IV-18 |
| | IV.2 Further reductions and formatting for population synthesis .. | IV-19 |
| | IV.2.1 Removal of sky absorption bands .. | IV-21 |
| | IV.2.2 Residual wavelength correction and rebinning of star spectra for synthesis .. | IV-26 |
| | IV.2.3 Parameters of stellar group spectra .. | IV-28 |
| | IV.2.4 Augmented Stellar Library for Synthesis .. | IV-32 |
| | IV.2.5 Reddening Correction for Galaxy Spectra .. | IV-33 |
| | IV.2.6 Shifting to rest frame wavelength, rebinning, normalising of galaxy spectra .. | IV-34 |
| | IV.3 Photographic Data .. | IV-35 |

CONTENTS

| | | | | <u>Page</u> |
|------------|---------|---|----|-------------|
| Chapter V | ... | ANALYSIS AND SYNTHESIS MODELS | .. | V-1 |
| | V.1 | Spectra, Spectral lines and indices | .. | V-1 |
| | V.2 | Method of Population Synthesis | .. | V-12 |
| | V.2.1 | Stellar library parameters | .. | V-16 |
| | V.2.2 | Constraints on Synthesis Solutions | .. | V-22 |
| | V.2.3 | Weights used for synthesis | | V-26 |
| | V.2.4 | Population Synthesis of observed Galaxies | .. | V-27 |
| | V.2.4.1 | Results for NGC 4472 | .. | V-29 |
| | V.2.4.2 | NGC 3308 | .. | V-31 |
| | V.2.4.3 | NGC 5128 | .. | V-34 |
| Chapter VI | ... | SUMMARY AND FUTURE DIRECTIONS | .. | VI-1 |
| References | ... | | .. | R-1 |

Chapter I

INTRODUCTION

The study of the composition and evolution of galaxies is one of far reaching importance for astronomy. The traceback of the evolution of galaxies with time is indeed the single most important sequence chronicling the evolution of the known universe, since the early epoch of formation of galaxies. Since their formation galaxies have evolved, due to the evolution of constituent stars, due to recurring formation of new generations of stars from matter left over after the initial epoch of formation, matter expelled by evolving stars into the interstellar medium and matter falling into the galaxy from the environment. The evolution of galaxies is also greatly influenced by dynamical interaction between neighbouring galaxies. Unravelling this complex scenario in terms of present day understanding of these aspects of evolution is an arduous task and is perhaps one of the most important aims of extragalactic research.

From a pragmatic point of view the dynamical interaction between galaxies and its effect on evolution is not yet a tractable problem; further, the question of large amounts of gaseous matter falling

into galaxies and ensuing large scale star-formation activity is comparatively rare and detailed observations do not exist to permit systematic studies of such events and their influence on galaxy evolution. The role that the dynamics of large star-forming clouds plays in galaxy evolution is also not clearly understood. It would thus seem right for the present that studies of galaxy evolution have largely concentrated on 'normal' galaxies showing no or minimal signs of violent star formation, non-thermal activity or dynamical interaction with neighbouring galaxies. The vast majority of galaxies are of this type and in this dissertation we shall be concerned with such objects.

I.1. The Stellar Content of Galaxies:

The light of galaxies (from the ultraviolet to the near infrared region of the spectrum) comes largely from the photospheres of the stars constituting them. Since formation, the light from any given galaxy i.e. the integrated spectral energy distribution (SED), has continuously changed simply because the stellar content has continuously changed. The stellar content changes since stars evolve in accordance with their masses and heavy element abundances, more massive stars dying earlier and being replaced by less massive stars in the production of the integrated radiation.

The stellar content further changes if new generations are evolving.

The determination of the stellar content of galaxies is thus an important aspect of studies of the evolution of galaxies. Except for the nearest bright galaxies where some of the brightest stars can be resolved, such studies are entirely confined to an analysis of the integrated light from a mixture of unresolved stellar components. The essential aim is to determine the relative proportions of these components. The technique of population synthesis, in various forms, has been used to synthesize the photometric colours, the energy distributions and the spectra of galaxies, from a mixture of stars of different spectral types, luminosity classes and element abundances, for which the corresponding data have also been collected.

The distribution of stars on the Hertzsprung-Russell (HR) diagram thus derived allows the determination of several parameters including the average metallicity of the galaxy, the main sequence turnoff point and the corresponding age of the last major star formation activity, and estimates of subsequent star formation rates from relative proportions of young stars. These parameters, coupled with models for the evolution of galaxies, enables the determination (to the extent permitted by current knowledge of stellar

evolution) of the history of star formation (the star formation rate or SFR at different times) and the initial mass function (IMF).

I.2. Determination of the stellar content of galaxies:

The essential technique of matching observed spectral properties of galaxies with a combination of corresponding data for known individual stars in our Galaxy is fairly old. The first such attempt was that of Whipple, made over fifty years ago (Whipple 1935). He outlined a method for measuring equivalent widths of lines and colours for a galaxy and for many stars of different spectral classes and luminosities; the numbers of the latter were adjusted and an integrated spectrum computed to obtain the best fit to the galaxy observations. The large data base of observations of line equivalent widths and colours covering all portions of the HR diagram and similar accurate data for galaxies was just not available at the time; so in practice this work could not be carried out, to the required degree of completeness.

I.2.1. Spectroscopy, equivalent widths and line ratios:

Early attempts to assess the stellar content of galaxies from spectroscopic observations include the

work of Morgan and Mayall (1957). From low dispersion spectra they concluded that the equivalent spectral type of the galaxies changed with the wavelength range observed, becoming progressively earlier at shorter wavelengths. They used the MK (Yerkes) system, following the general schemes of classification of composite systems for globular clusters (Morgan 1956), to assign equivalent spectral types to galaxies. For M31 they derived a type of around F8 for $\lambda 3900\text{\AA}$, the 'cyanogen giant stars' gG8 to gK3 for $\lambda 3880\text{\AA}$ to 4300\AA , types K4 to K5 for $\lambda 4600\text{\AA}$ and M giants in the red and near infrared. Their work highlighted the need for wide spectral coverage in attempting to explain the stellar content of galaxies.

Following the suggestion of Whipple (1935), that equivalent widths of lines are more sensitive than colours in determining the stellar content, G. and A. de Vaucouleurs (1958, 1959) made an attempt to quantitatively synthesize a spectrum of the Large Magellanic Cloud in the range $\lambda 3700\text{-}4900\text{\AA}$. Their model which best fitted the observed spectrum required 62% of the blue light to come from B stars, 10% from A stars, 5% from F stars and 17% from evolved G and K stars. The discovery of the He I line at 3820\AA in their spectrum of the LMC led to the requirement of a large number of B stars.

Spinrad (1962) used line strengths in the spectral region $\lambda \sim 4000-6800\text{\AA}$, to study the stellar content in several galaxies. He used several important luminosity discriminants in the green and near-infrared region of the spectrum. Using these luminosity dependent spectral lines (especially the NaI 'D' lines), he gave a model for the nucleus of M31 and for giant elliptical galaxies, where most of the light was accounted for by an old population I base with a significant fraction of late spectral type, red dwarf stars added.

The spectroscopic studies mentioned above and some others not specifically referred to here, have all been done photographically. It must be pointed out that the photographic method has several disadvantages: night sky emission cannot be easily subtracted, emulsions have low quantum efficiency, especially in the near-infrared region of the spectrum and the process of calibrating from densities to relative intensities introduces further errors. Also, it is usually not possible to obtain accurate absolute fluxes using observations of standard stars with known fluxes. However, photographic techniques can be applied for limited spectral regions observed at higher spectral resolutions, as has been done by Rose (1985).

Rose used photographic image tube spectra in the region $\lambda \sim 3400$ to 4500\AA with a resolution of 2.5\AA , to

form relative line strength ratios of neighbouring lines which are used as indicators of temperature, luminosity and metal abundance. He found that hot stars contributed only 2% to the integrated spectrum of elliptical galaxies at $\lambda \sim 4000\text{\AA}$. The line indices $\text{CaII H} + \text{H}\epsilon / \text{Ca II K}$ could be matched by including a small metal-poor population that contributes 8% of the light at 4000\AA . He also showed that the presence of a substantial fraction of stars of intermediate age (as suggested in O'Connell 1980) in elliptical galaxies differentiates between them and the metal-rich Galactic globular clusters. Williams (1976), also used photographic image tube spectra in the range $\lambda \sim 3800$ to 6800\AA with a resolution of 2\AA , to synthesize observed line indices in the nuclear regions of ten galaxies.

I.2.2. Photometry:

The first quantitative attempt to use photometric colours for obtaining the stellar content of galaxies involved a six-colour photometric system by Stebbins and Whitford (1948) covering the wavelength range between 3500\AA and 10300\AA with average filter bandpasses of around 1000\AA . Comparison of their colours for some bright elliptical galaxies with a dwarf mid-G spectral type star gave colour excesses at both the ultraviolet and infrared wavelengths. Though the coverage of the HR diagram was again incomplete, the results showed

that broad-band colours of a galaxy are fairly insensitive to differences in stellar population models.

Intermediate band filter photometry has been used by several observers in attempting population synthesis (Wood 1966, 1969; Mc Clure and van den Bergh 1968; Faber 1972). Filters with band passes of the order of 100\AA were generally chosen to cover several points in the continuum as well as spectral features discriminating between stellar types. Wood (1966) employed twelve-colour observations to find that models patterned after an old galactic cluster population like M67, enriched with a few late-type giants, many dwarfs of late spectral type and some horizontal branch stars fitted the galaxy observations well.

Mc Clure and van den Bergh (1968) observed over 200 stars, 70 clusters and 56 galaxies on an intermediate band system covering the Balmer discontinuity, the discontinuity at 4000\AA due to line blanketing, the violet CN absorption and the G-band due to MgH. They derived reddening-free indices which were used as classification criteria for different types of stars and the metallicities of globular clusters. These indices, however, did not permit segregation of the effects of stellar metal abundance on the integrated

light of the cluster and the effects produced by the distribution of stars in the cluster colour-magnitude diagram. By studying the cyanogen index, they concluded that light from the semistellar nucleus of M31 and the core of the elliptical galaxy NGC 4472 was dominated by stars of very high metal abundance (cyanogen rich giant stars).

Faber (1972) used the method of quadratic programming to synthesize the stellar populations of M31, M32 and M81 and typical elliptical galaxies. She applied the synthesis technique to both 10-colour photometry as well as to 38-colour spectrophotometric indices (Spinrad and Taylor 1971). She concluded, in essence, that the technique yields good mean line strengths in external galaxies. However, her work did not confirm an enriched late spectral type dwarf sequence and she stated that the technique was not sensitive to the relative numbers of lower main sequence stars between K0V and M7V. The dwarf to giant star ratios and the mass to luminosity ratios were hence very uncertain.

Synthesis using broad band or intermediate band photometric data has several disadvantages: it is difficult to reproduce photometric systems accurately at different observatories, the filters and bandpasses must be chosen with prior knowledge of which spectral features and continuum points to look for. The spectral

features of interest can shift out of the filter band-passes as galaxies of higher redshift are observed. Moreover, as the studies discussed above indicate, even intermediate band photometry yields colours and indices which are not sensitive to all the possible ingredients in the stellar mix making up a typical galaxy.

I.2.3. Spectrophotometry:

Since photographic emulsions used in traditional spectroscopy are difficult to calibrate accurately and are not sensitive enough in some wavelength regions of interest (e.g. the near infrared), and since broad and intermediate band photometry does not provide sufficient coverage of the spectrum to discriminate between various stellar types, the spectrophotometer or spectrum scanner (as it is often called) became an obvious choice for galaxy spectrum synthesis.

In a typical scanner, the light is dispersed by a grating and a portion of the spectrum as determined by an exit slit is sampled by a photomultiplier tube. By rotating the grating in steps, the entire spectrum (as limited by the grating and photomultiplier efficiency) can be scanned or selected points in the spectrum can be sampled in a manner similar to photometry. In the last decade and a half solid state

array detectors such as the Reticon array and the charge coupled device (CCD) arrays have enabled the sampling of a large number of adjacent points in the spectrum simultaneously, with the 'bandpass' of photometry being replaced by the dimension (along the dispersion direction) of each pixel in the array.

The earliest attempts in scanning the spectrum of galaxies are those of Code (1959) and van den Bergh and Henry (1962). From the strength of the ultraviolet and blue CN bands, they both concluded that late-type giant stars contributed a large portion of the light from the nucleus of M31.

Spinrad & Taylor (1971) did very comprehensive work in deriving the population models for the nuclear regions of the galaxies M31, M32 and M81. They used the scanner as a tunable filter and measured fluxes at 36 points in the spectrum between 3600\AA and 10700\AA . The passband for the measurements was 16\AA for $\lambda < 5360\text{\AA}$ and 32\AA for $\lambda > 5360\text{\AA}$. These passbands covered many continuum points as well as luminosity and temperature sensitive spectral lines. The stellar data base covered 37 distinct stellar types. They found an appreciable contribution to the light from M31 to be from lower main sequence dwarf stars (as late as M8 V), giving a ratio of the total mass from stars to the total visible light from them (M/L ratio)

of 44. Their model for M31 required strong-lined giant stars and metal weak stars were completely excluded. The main sequence turn off derived was at G0 V, indicating an old population. Their model for M81 (not considering emission lines in the spectrum) was similar to that for M31 except that more giant M stars were required. For M32 they did not require as many late type dwarf stars as for M31 and the strong lined giant stars were not required to be present.

Another comprehensive study applying a population synthesis technique based on linear programming to narrow band spectrophotometric data was that of O'Connell (1976). He used a spectrum scanner to cover the spectral region from 3000 to 10800Å with bandpasses of about 16Å for $\lambda \leq 5050\text{Å}$, 26Å for $5050\text{Å} \leq \lambda \leq 7400\text{Å}$ and 130Å for longer wavelengths. The stellar data base covered 48 different types (O'Connell 1973) including 'super-metal-rich' stars and metal poor stars. The galaxies studied were the elliptical galaxies NGC 4374, NGC 4472 (M49) and NGC 4552 (M89). O'Connell found that M type giant stars dominated over M dwarf stars throughout the spectrum and excluded the possibility of a mass to light ratio greater than 30. His best models gave a $2 \lesssim M/L \lesssim 15$. The synthesis model used constraints which ensured continuity in the HR diagram and which placed limits on the relative numbers

of stars in various evolutionary stages. These constraints were derived from theoretical and empirical tracks of evolution in the giant and subgiant branches. The constraints for the evolved stars, however, had large uncertainties due to the absence of evolutionary tracks (particularly, the giant branch) which match well the tracks of well-observed old clusters in the Galaxy. The models yielded a small range of main sequence turnoffs (dependent on the relative rates of main sequence and subgiant evolution) implying that the bulk of the stars in the galaxies observed formed 8 to 11×10^9 years ago, with subsequent star formation at a low rate until about 4×10^9 years ago. There was no evidence of a significant contribution from population II stars whereas distinct enhancements of Na I and Mg I were found in the galaxies. O'Connell's main conclusions vis-a-vis contribution to the integrated light were: 20 to 30 per cent of the light in the V band from KO-3 giants, over 15 per cent of the near-infrared light from M giants. The model does not permit a satisfactory fit to both the continuum and absorption indices sensitive to luminosity in M stars. He also found that the inclusion of mainly normal (solar) abundance stars in the stellar data base used for the synthesis made it difficult to disentangle the effects of age and metallicity.

Gunn, Stryker and Tinsley (1981) used an evolutionary synthesis technique to derive population models for the galaxies NGC 545, 4472, 4486 (M87), 4486B, 4874, 4889, 6166 and M31. They used scanner data to cover 509 points in the spectrum between λ 3130Å to 10800Å with a resolution of 20Å in the region $\lambda < 5400\text{Å}$ and 40Å at longer wavelengths. The components chosen to fit the galaxy observations were certain populations in the HR diagram, such as theoretical isochrones for old populations, the entire solar neighbourhood young population etc., as opposed to groups of stars in small regions of the HR diagram. The basic conclusions were similar to earlier work: giant elliptical galaxies and the centre of M31 are dominated by an old metal-rich population (the light being mainly from strong-lined giant stars), with some hotter stars above the main-sequence turnoff point (as in Faber 1977 and O'Connell 1976). As opposed to O'Connell (1976, 1980) the colour at turnoff is redder, being $B-V = 0.80 \pm 0.05$, and, depending on the composition this leads to turn-off ages in the range 9 to 14×10^9 years. The question of the nature of the hot stars was not resolved, though the authors favoured blue stragglers and young stars over horizontal branch stars, since the metal rich population would produce too few of the latter.

Pickles (1985) performed differential population synthesis for 12 elliptical and five lenticular galaxies, all in the Fornax cluster of galaxies. His observations covered the range $\lambda 3600\text{\AA}$ to $10,000\text{\AA}$ with spectral resolutions of 10 to 20\AA . He used the technique of constrained minimisation to minimize residuals of the fit to observed galaxy spectral energy distributions by combinations of different types of stars from a library of 48 stellar groups. The data for the stellar groups did not, in all cases, have the resolution of 10 to 20\AA , especially beyond 8600\AA , where lower resolution data (50\AA bandpass) was used. He found the main sequence turn off groups to be quite young, indicating substantial star formation in all the early-type galaxies in the Fornax cluster for a period of 6 to 10×10^9 years after the epoch of globular cluster formation. The results generally indicate more of continuing star formation in the brighter galaxies. Three of the brighter ellipticals showed the presence of a significant hot star component, most likely due to early type upper main sequence stars, implying some current star formation. However, the evolutionary status of these hot blue stars was not absolutely certain: they could be upper main sequence stars or evolved stars on the horizontal branch. The best solutions showed about 40 to 50 per cent of the light in the visual

band (V) to be from G-K dwarfs in all ellipticals. The contribution from G-K giant stars decreased from about 50 per cent at V for the brightest elliptical galaxies to about 20 per cent for the faintest. It was not possible to get a unique proportion of M giant and dwarf stars which best fitted the near-infrared data. The mass to light ratio determined was thus rather uncertain. It is instructive to remark here that the late type dwarf-star-enriched models of Spinrad and Taylor (1971), discussed earlier, have not been corroborated by others. O'Connell (1974, 1976) found that M giant stars dominated the light from elliptical galaxies. The strength of the CO band at 2.3 mm in elliptical galaxies, which is a sensitive function of luminosity in a positive sense, indicates a giant dominated population (Frogel et al 1975, Baldwin et al 1973). On the other hand studies of indices reflecting the strength of the Wing-Ford (WF) band due to FeH at 9916\AA , which is significant only in dwarf stars of type M5 and later, revealed no detectable contribution from such stars in galaxies (Whitford 1977), thus ruling out very late-type dwarf dominated populations. The WF band was detected in higher resolution spectra of the nuclei of M31 and of M32 by Cohen (1978), who also studied the strengths of other luminosity sensitive features (the near-infrared doublet due to Na I, the Ca II triplet and TiO bands in the near-

infrared region); she did not, however, find any substantial dwarf enrichment in these galaxies.

Synthesis models for stellar populations in galaxies have been constructed by others, not discussed here in detail (Pritchett 1977, Aaronson et al 1978, Wyse 1985). Since the first ultraviolet observations of elliptical galaxies with the International Ultraviolet Explorer (IUE) Satellite, it became clear that a mix of a purely metal rich population of stars could not account for the high flux in the region λ 2000Å to 3300Å (Bruzual 1983). It does seem, however, that the basic problems remain in the interpretation of integrated spectra of early type galaxies i.e. the source of the excess light in the blue and the ultraviolet region of the spectrum, the age and metallicity of the dominant population of stars in these systems and the relative proportions of cool giant and dwarf stars.

I.3. Aims of Population Synthesis

The study of the evolution of galaxies (specifically, early-type 'normal' galaxies as discussed at the beginning of this Chapter), requires, as inputs from analyses of observations, the stellar content of galaxies at different epochs since their formation. The change in the stellar content can then be correlated with and interpreted in terms of current theories

of stellar evolution. The technique of population synthesis aims at determining, from observations, the number of stars in an absolute magnitude (luminosity) range dM_v around M_v , a spectral type range dS around S and a metallicity range dZ around Z , as a function of M_v , S and Z i.e. $N(M_v, S, Z)$. In the general case, the luminosity of a galaxy at any wavelength λ would then be

$$L_\lambda = \iiint_{Z S M_v} 10^{-0.4M_\lambda} N(M_v, S, Z) dM_v dS dZ$$

The above procedure, a static one, thus divides stars into various groups of luminosity, effective temperature and chemical composition and tries to obtain a best fit to the observed photometric properties of the galaxy in question using a mix of stars of different groups. The best fit, however, is strongly determined by constraints imposed on relative proportions of different kinds of stars, which are used to avoid non-unique solutions (Tinsley 1980).

The method of evolutionary population synthesis, on the other hand, uses the knowledge of stellar evolution to determine at any time, given a scenario of star formation (whether one time or continuous), the distribution of stars on the HR diagram. The observed photometric and spectral properties of this stellar

distribution are then compared with corresponding properties of the galaxy observed. In this method, the distribution of stars is thus consistent with stellar evolutionary requirements and no constraints are required in the fitting of the data. The major lacuna here, is that detailed evolutionary tracks are not available for all species of stars expected to be present in galaxies in significant numbers. Also, the models generally use various empirical forms of the function determining the formation of stars (the SFR or star formation rate) of different species (Tinsley 1980, Arimoto and Yoshii 1986, Renzini and Buzzoni 1986, Barbaro and Olivi 1986 and references therein). In the general case, if $f(m, t, Z)$ and $C(m, t, Z)$ denote the flux of a star (of mass, m , age t and chemical composition Z) and the birthrate of stars (of mass m and composition Z at time t) respectively, then the integrated flux of a galaxy (see Barbaro and Olivi, 1986) of age T is:

$$F_{\lambda}(T) = \int_0^T \int_{Z_1}^{Z_u} \int_{m_1}^{m_u} C(m, t, Z) f_{\lambda}(m, t, Z) dt dm dZ$$

where m_u , m_1 are upper and lower mass limits of stars and Z_u , Z_1 are upper and lower limits on the heavy element abundances in stars. Essentially, since f_{λ} and F_{λ} can be observed, various forms of $C(m, t, Z)$

can be used, in conjunction with stellar evolution theory to derive the distribution of stars in the HR diagram, whose integrated f_λ best matches F_λ for the galaxy.

I.4. Outline of this dissertation

This dissertation describes the observations, reductions and final analyses comprising a study of stellar populations in early type galaxies using the techniques of population synthesis. The plan of the dissertation is as follows:

The second chapter describes the telescopes and instrumentation used for observations at the Vainu Bappu Observatory, Kavalur (South India) and at the European Southern Observatory (Chile).

The third chapter discusses the considerations that went into the plan of observations, the observing procedures used and summarises information about the objects observed.

The fourth chapter describes, in some detail, the procedures used in reducing the data to a form amenable to analysis. The spectra of the stellar ingredients for population synthesis and of the galaxies are discussed and displayed.

The fifth chapter presents a brief description of the stellar and galaxy spectra with emphasis on spectral features particularly useful in spectral and luminosity classification. The techniques of population synthesis employed are also discussed, details of the actual synthesis runs performed are given and the results for the galaxies are presented.

The last chapter outlines the work done in the thesis and summarizes the principal results. Plans for future work to be undertaken are also discussed.

Chapter II

INSTRUMENTATION

The observational program for this dissertation was initially based on the usage of the 102-cm Zeiss reflecting telescope at the Vainu Bappu Observatory. A telescope of this aperture is perhaps, marginally small, for a program involving absorption line spectroscopy of galaxies, given the conventional photographic techniques of spectrum recording available at the observatory. Subsequently, attempts were made to obtain telescope time on larger telescopes at other observatories. A total of five nights were allotted for this work and another project on the 1.5 metre telescope of the European Southern Observatory at La Silla, Chile. The observational data used here thus consists of two distinct sets, one from the Vainu Bappu Observatory of the Indian Institute of Astrophysics and the other from the European Southern Observatory in Chile. The details of the instrumentation used in both cases are discussed below.

II.1. Instrumentation at the Vainu Bappu Observatory

The 102 cm Zeiss reflector telescope was, at the time this program was started, the largest telescope available with the Indian Institute of Astrophysics.

The telescope has two foci: the cassegrain focus with a focal ratio (aperture to focal length) of F/13 and the Coude focus with a focal ratio of about F/30.

The high resolution spectrographs and conventional photographic spectrum recording pre-empted the use of the Coude focus; all observations were carried out at the F/13 cassegrain focus. The image scale at this focus is 15.56 seconds of arc per millimeter.

The instruments available for observing spectral energy distributions at the F/13 focus were a single channel automated scanner and a cassegrain spectrograph, both built inhouse. The scanner based on an Ebert-Fastie configuration gave dispersions of $25\text{\AA}/\text{mm}$ and $12.5\text{\AA}/\text{mm}$ in the first and second orders respectively, using a grating of 600 $1/\text{mm}$ blazed at 7600\AA in the first order. There was no facility for simultaneous sky measurements and initial trials revealed that this was the main obstacle to using the scanner for spectrophotometry of galaxies requiring three to four hours of scanning time.

The only other instrument available was the cassegrain spectrograph, which was used for all the observations at the Vainu Bappu Observatory (VBO).

II.1.1. The Cassegrain Image Tube Spectrograph (CITS)

The cassegrain spectrograph, also called the cassegrain image tube spectrograph was built in house by the late Prof. M.K.V. Bappu and Mr. A. Charles. The plane of the slit of the spectrograph was at the F/13 focus of the telescope. The light from the telescope passed through the slit and onto a collimator mirror of focal length 648 mm. The light, made parallel by the collimator was incident on a plane reflectance grating which directed the light to the camera. The grating could be turned manually to observe different portions of the spectrum. The angle between the directions to the collimator and camera vis-a-vis the grating, was fixed i.e. the algebraic sum of the angles of incidence and diffraction was fixed, and was approximately 60 degrees. Figure 1 shows a schematic of the spectrograph.

The slit consisted of two polished and aluminised jaws, one of which was fixed while the other could be moved using a micrometer movement. A V-shaped decenter above the slit, also movable using a micrometer movement, enabled sampling of different widths (in a direction perpendicular to the dispersion) of spectrum between the arms of the 'V'. The spectrum of the wavelength comparison source was exposed in the area

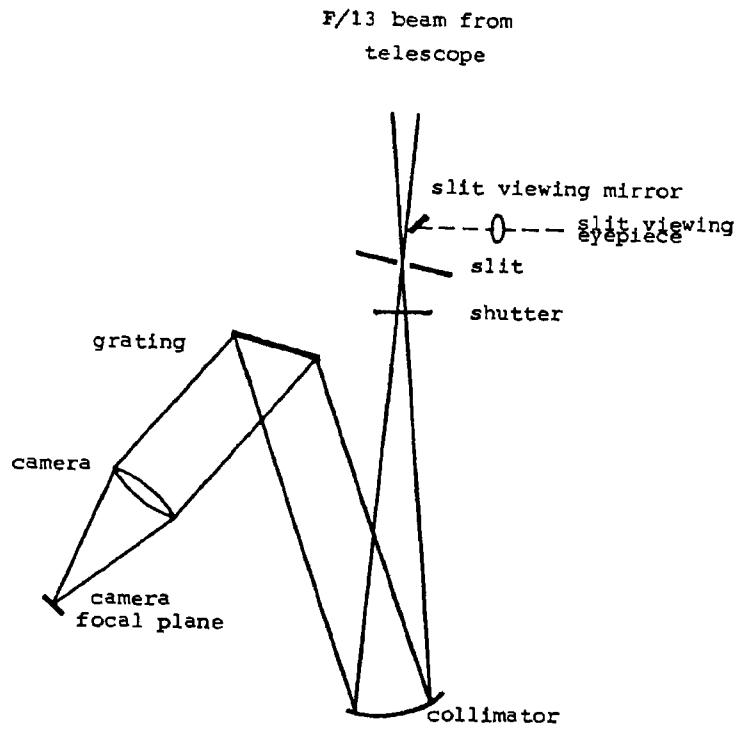


Figure 2.1 Schematic layout of the Cassegrain spectrograph used with the 102 cm telescope F/13 focus at the Vainu Bappu Observatory.

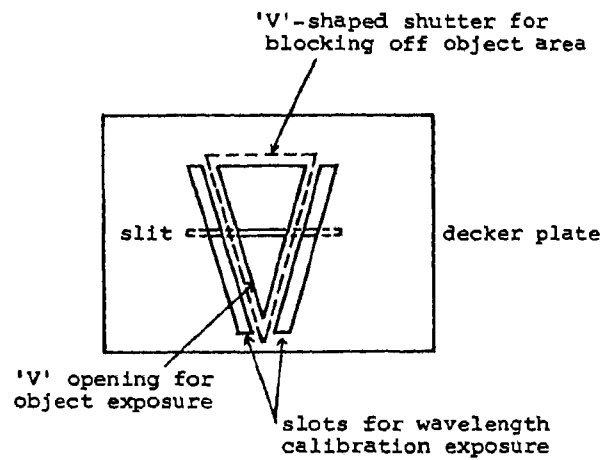


Figure 2.2 Decker plate and slit of the Cassegrain spectrograph used at the F/13 focus of the 102 cm reflector at Vainu Bappu Observatory.

outside the arms of the 'V', the latter being covered by a shutter during such exposures (See Figure 2). The slit plane was slightly tilted, so that objects reflected off the slit jaws could be monitored through an eye piece continuously and the telescope guided, during exposures.

Wavelength calibration exposures were done using a Neon Iron hollow cathode spectral lamp, whose light was directed onto the slit by positioning a small mirror. There was no arrangement to make the wavelength calibration light of the same focal ratio as the telescope beam. However, the slit plane was always evenly illuminated by the spectral lamp. Filters to prevent spectral order overlapping for the spectral lamp were placed directly in front of the lamp. The filter generally used was the Schott OG1 filter, in keeping with the grating used and the spectral region observed, as described below and in Chapter III.

Several cameras and gratings were available for use with the cassegrain spectrograph. Extensive trials were done using different combinations of gratings and cameras until the configuration adopted for the program was chosen. The main constraints were: the telescope aperture itself was marginally small for spectroscopy of galaxies using photographic

techniques and only a single stage, uncooled image intensifier tube was available; the ambient temperature, even in the winter months of December to February was high enough to cause problems with the image tube background for exposures of greater than four and a half to five hours. During the other months, it was not possible to expose for more than forty-five minutes to an hour due to the problems with background. Galaxy observations could thus be done only during the winter months.

The grating chosen finally for the observations was from Bausch and Lomb, having 400 grooves per millimetre and a blaze wavelength of 8452\AA in the first order. This grating had a good efficiency in the near infrared region of the spectrum and was well suited to the aim of observations in the near-infrared region.

There were three cameras with transmission optics available for use on the spectrograph. These had focal lengths of 178 mm (7-inches), 254 mm (10-inches) and 508 mm (20-inches). However, the trials showed that none of them were suited to the program of observations: they either required prohibitive exposure times or had problems with getting a good focus in the near-infrared region of the spectrum.

The camera finally used was a folded-schmidt camera utilising reflection optics and built in house

at the institute. The overall focal ratio of the camera was about $F/2.5$, with a focal length of around 5.5-inches (depending on the wavelength). The grating mentioned earlier along with the folded Schmidt (called the 6-inch Schmidt) provided the best configuration which could possibly be used for the program.

The image intensifier used was a VARO 8605, single stage, electrostatically focussed tube with fibre-optic extensions at the input and output ends of 40 mm diameter. The fibre-optic extension at the output end provided effective shielding, so that plates could be exposed in contact with the output face. The tube has an S-20 photocathode with useful response almost upto 8700\AA . At the output end, the P-20 phosphor screen emits mainly in the green region of the spectrum. The resolution of the image tube as a whole coupled with the response of the phosphor determined the emulsion which was to be used; these were the standard Kodak type IIa-D emulsions on glass.

II.1.2. Intensity Calibration

The cassegrain spectrograph, being small and compact due to considerations of weight at the $F/13$ focus of the 102 cm reflector did not have facilities for intensity calibration on the plate being exposed.

The intensity calibrations were done separately on a laboratory spectrograph (made by Messrs. Adam Hilger) employing a quartz lamp with a rotating sector plate in front of it, which gave strips of exposure with known intensity ratios. The calibration plates were placed in a portion at the focal plane corresponding to the green spectral region, in conformity with the emittance of the image tube phosphor output.

Since the plates used at the cassegrain spectrograph were small (38 mm square), and the Kodak IIa-D plates were considerably larger, the plate(s) used for intensity calibration and those used with the cassegrain spectrograph (to be calibrated using the former) were always from a single Kodak plate; the set of program plates and calibration plates were always developed and fixed together using the same photographic chemicals.

II.1.3. PDS Microdensitometer

All the photographic spectra were digitized using the PDS 1010 microdensitometer available at the Institute's headquarters at Bangalore. This is a standard instrument used widely in astronomy and will not be described here in detail. Briefly, a stable light source passes through the photographic plate and the transmitted light is measured by a photomultiplier

tube. The plate with the spectrum recorded on it is moved across the light beam and the photomultiplier output is sampled, digitized and stored on magnetic tape. The absolute positioning accuracy of the two dimensional traverse of the plate on which the photographic plate is held, is $\pm 5\mu\text{m}$, over an area of 254 mm x 254 mm, while the repeatability is $\pm 1\mu\text{m}$. The light beam passes through a source aperture, the photographic plate and sensor aperture before being detected by the photomultiplier. Different sizes of source and sensor aperture are available, as well as different magnifications in the optical imaging system, leading to a flexibility in choosing the area on the photographic plate which is represented by a single output value. The apertures and magnifications were adjusted so that each output value corresponded to the density in a rectangular area of $12.5\mu\text{m} \times 50\mu\text{m}$ on the photographic plate, the smaller dimension being along the direction of dispersion of the spectrum. This projected scanning aperture of $12.5\mu\text{m} \times 50\mu\text{m}$ was moved at $10\mu\text{m}$ steps from one end of the spectrum to the other. The wavelength calibration spectrum, the plate background levels as well as the object spectrum were scanned on each plate.

II.1.4. VAX 11/780 Computer System at VBO

The reduction of all the photographic spectra digitised using the PDS as well as part of the reduction of data obtained at the European Southern Observatory was done using the VAX 11/780 computer system at VBO. In particular, the high resolution Tektronix graphics terminal and graphics copier were used extensively for data reductions and plotting of the spectrograms.

II.2. Instrumentation used at the European Southern Observatory (ESO)

As mentioned at the beginning of this Chapter, some of observations were obtained using equipment at the ESO, in Chile, during April 1986. Description of this equipment is detailed in the various user/operator manuals published by ESO. The salient features and instrument parameters of particular interest to this program of observations is outlined below.

II.2.1. The ESO 1.5 m telescope

The ESO 1.5 m telescope was used for the observations of galaxies and standard stars. A total of five nights of observations were obtained for this project as well as another project from the Indian Institute of Astrophysics.

The 1.5 m telescope, though of a fairly old design (compared to the other telescopes at ESO, Chile) had sufficiently good tracking accuracy and stability to enable fairly efficient utilisation of the observing time. The cassegrain focus with a reduced focal ratio of F/7 (see below) was used. The availability of an intensified TV viewing system greatly eased the task of obtaining spectrograms of the galaxies. The only major limitation, with the spectrograph attached to the telescope, was that for objects with declination angle, $\delta \leq -45^\circ$, it is impossible to observe more than 30 minutes before the meridian with the telescope on the east side of the polar axis and more than 30 minutes after the meridian with the telescope on the west side of the polar axis. The image scale at the cassegrain focus, after conversion from F/15 to F/7 is 19.4 seconds of arc per millimetre.

II.2.2. The Boller & Chivers Spectrograph at the ESO 1.5 m telescope.

This spectrograph, in use at several major observatories world-wide, is a very stable instrument with several features which contribute to accurate observational data. The instrument will not be described here in detail; a schematic of the basic optical design is shown in Figure 3 (reproduced from

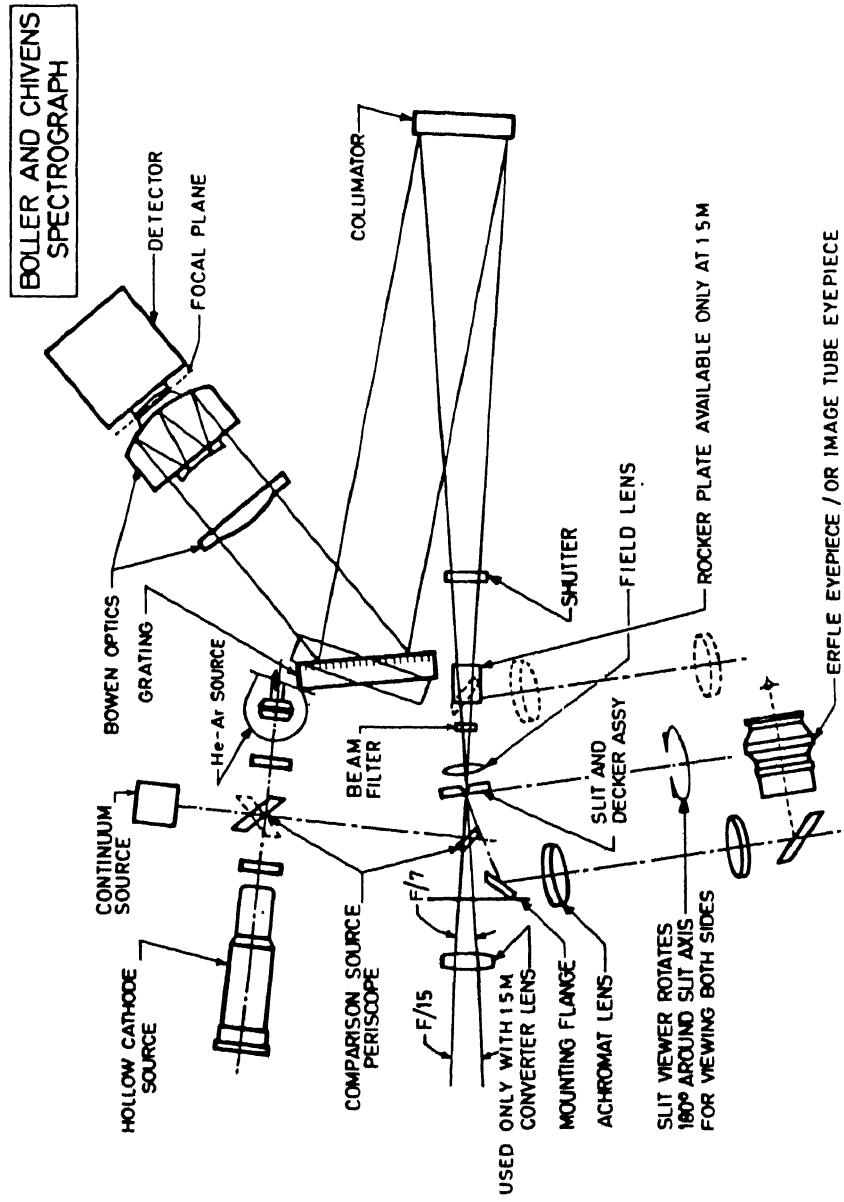


Figure 2.3. Schematic optical layout of the Boller and Chivens spectrograph.

the ESO users manual). The light from the telescope F/15 cassegrain beam is first converted to F/7 (for which the spectrograph was originally designed) by a convertor lens, then passes through the slit onto a collimator and then the spectrograph grating, and is finally imaged by a Bowen Schmidt camera onto the detector.

The slit consists of two polished and aluminised jaws forming a biparting slit that can be continuously varied from a width of 6 to 1200 μm . The image of the object, as reflected off the slit is picked up by an intensified (ISIT) TV camera and displayed on a monitor at the telescope control console. The field of view on this monitor is 3 x 2.2 arc minutes.

The spectrograph has different deckers for use with the different detectors available. The Reticon detector system was used for this program. The deckers for the Reticon have two apertures, one for the object of interest and the other for simultaneous sampling of the neighbouring sky. This mode is absolutely essential for observations of faint objects, since the sky is then monitored for as long as the object and any variations in the sky signal (superposed on the object) are also recorded separately. The two apertures allow light to fall on two portions of the slit

which are imaged finally by the camera onto the two Reticon arrays (see Section II.2.3).

The wavelength comparison source used was a Helium-Argon (He Ar) arc lamp with the appropriate optics to give the same beam geometry as the telescope. The wavelength calibration exposures were given before and after each object exposure so that checks could be performed to monitor any small wavelength shifts resulting from flexure at different positions of the telescope. The light from the He Ar lamp is also recorded simultaneously through both the apertures, for each of which wavelength calibration is done separately.

Several gratings are available for use with the Boller & Chivens spectrograph. The grating chosen for this program had 300 grooves per millimetre and first order blaze at 9100\AA . The dispersion of the spectrum at the plane of the detector was 228\AA per millimetre. In order to avoid contamination from light from the second order of the spectrum, a Schott OG 590 filter was used.

II.2.3. The Reticon Detector System

The detector used with the Boller & Chivens spectrograph, for this program of observations, is a

self scanned, linear photodiode array (type RL 1024C/17 from Messrs. Reticon Corporation) consisting of two parallel arrays of 1024 silicon photodiodes, each diode being 450 micrometers (μm) high and $25.4\ \mu\text{m}$ wide, with no dead space between diodes. The two arrays are separated by approximately 2.44 mm.

The Reticon has exceptionally good quantum efficiency (QE) in the red and near infrared region of the spectrum, the maximum QE being 80% between 7000 and $9000\ \text{\AA}$. Figure 4 shows the QE of the Reticon as well as some other commonly used photocathodes as a function of wavelength. Since the QE of the photocathodes of image intensifier tubes generally fall rapidly beyond $8000\ \text{\AA}$, the reticon (as used with the B & C spectrograph at ESO) is operated without an image intensifier to make full use of the sensitivity to wavelengths beyond $1\ \mu\text{m}$.

In order to reduce thermal noise, the Reticon is mounted inside a liquid nitrogen dewar operating at temperatures between -70°C and -130°C , depending on the desired sensitivity. The light from the spectrograph camera enters through a quartz window, behind which the Reticon is mounted. A temperature between -100°C and -90°C gives good sensitivity upto $10400\ \text{\AA}$; for longer wavelengths the temperature needs to be above -90°C .

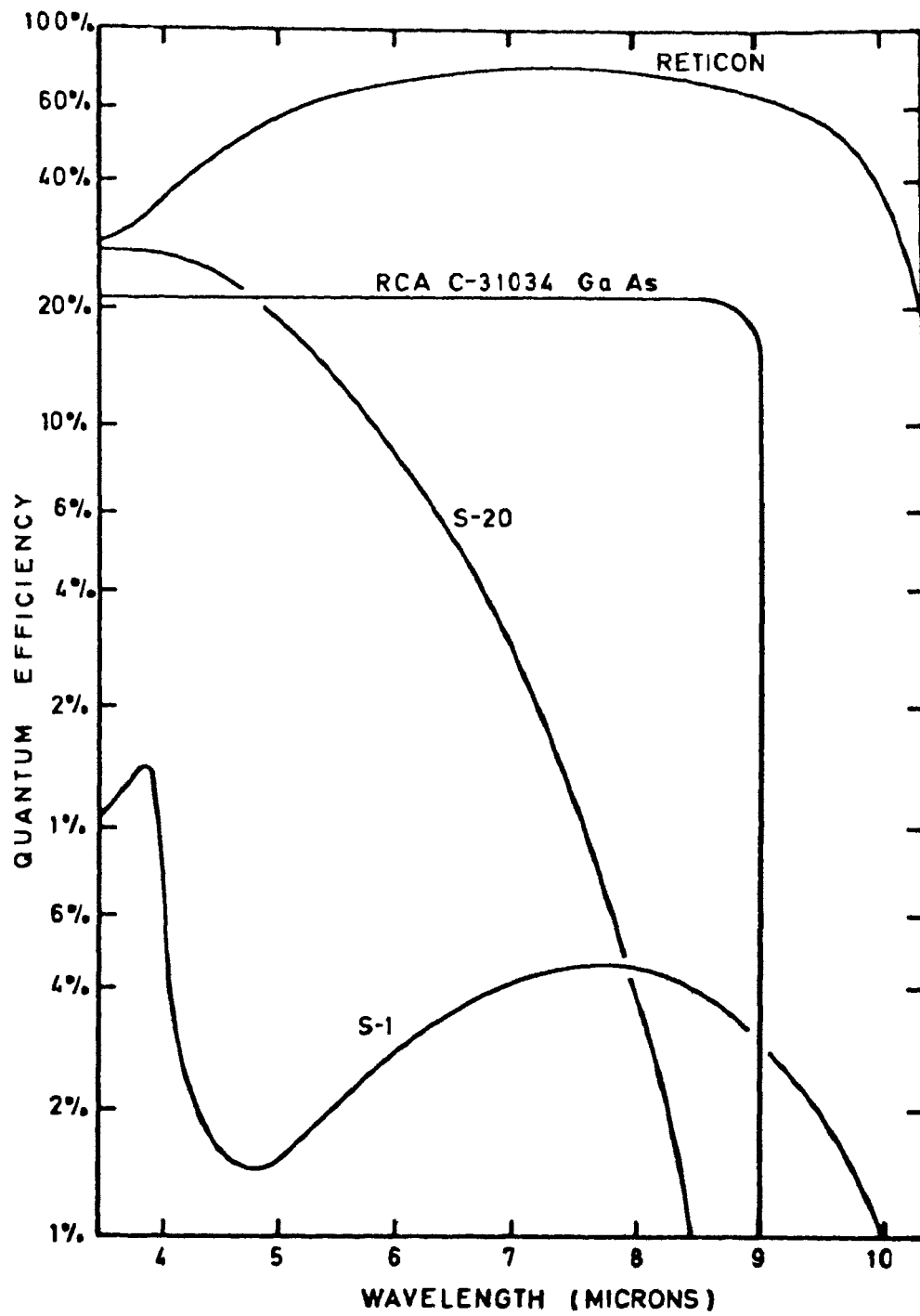


Figure 2.4. Quantum efficiency of the reticon array and several conventional photocathodes

We will not discuss the electronics system used for the control and operation of the Reticon except to say that the charge from each photodiode, which is proportional to the number of photons of light incident on it, is converted to a proportional voltage and digitised to an accuracy of 12 bits. This digital data is then transferred to a control computer and stored on disc and then on magnetic tape. The commands for operation of the Reticon are given at the control computer; observation-oriented commands are interpreted by the software into basic commands for the operation of the detector system. The software also takes care of proper formatting and organisation of the data as 'scans' corresponding to single exposures on each array of the Reticon. Time information, telescope and object information are all appended to the data files.

The resolution of the Reticon depends on the input signal level; however, unlike other detectors, the instrument profile in this set up does not have extended wings and the image (full width at half maximum) is very close to one pixel (one diode width). The dynamic range of the detector itself is very large and in the configuration used at ESO, saturation occurs at 4×10^6 counts. This corresponds to a 20% saturation level of the detector itself, at which level, departure from linearity is still less than 1%.

II.2.4. ESO Data Analysis Facility

There are several major computer systems for data reductions and analysis, at the ESO headquarters at Munich. The Hewlett Packard computer system running the ESO Imaging Handling and Analysis Package (IHAP) software was used for reducing the raw data to wavelength calibrated and flux calibrated spectra. The package has many conveniences permitting a large degree of flexibility in performing arithmetic on the data. A graphics terminal and plotter available at each data reduction station were very useful in examining intermediate results during the calibration process. The reduced data, after instrument dependent calibrations have been done, are finally put on magnetic tape.

Chapter III

OBSERVATIONS

Population synthesis of galaxies ideally requires observations of stars representing every spectral type and luminosity class on the HR diagram with each type having sub-types of normal (solar), deficient (metal-weak) and excess (metal-rich) abundances of the heavy elements. In principle, an average spectrum of each type (e.g. metal rich KO-2 giants or metal-weak F0 giants) should be formed from several observations of objects of that type.

In practice, however, the occurrence of certain stellar types such as the super-metal rich giants of type M now known to be present at the Galactic centre, carbon stars, Wolf-Rayet stars, in detectable numbers in galaxies had not been suspected till recently; components of stellar libraries for population synthesis, which are compiled from many observations of each type have usually not included stellar types thought to be of a minority class (i.e. relatively few in number) vis-a-vis contribution to the integrated light of galaxies. We shall discuss the effects of the completeness of stellar libraries in more detail in Chapter V.

Observations of galaxies and synthesis library stars should ideally be done with the same instrument setup giving identical spectral resolution for both. In practice, however, since the amount of observing time required for a complete synthesis library of stellar spectra is high, compilations from other sources are often used. Such external data can be used if it is of comparable spectral resolution and especially if available as absolute fluxes.

Here, we present the details of observations of the two independent data sets described in Chapter II. We describe the observations obtained with the ESO 1.5 m telescope first, since the data are of better quality and ultimately are reduced to absolute fluxes. The data recorded photographically at VBO are ultimately reduced to relative intensities and contain larger errors.

III.1. Observations at the ESO 1.5 m Telescope

An allotment of two nights of observing time was granted to this program in April 1986, on the 1.5 m ESO telescope at La Silla, Chile. Since the following three nights were also allotted to another program (requiring the same instrumentation) from the same institute, the total period of five nights could be shared among both programs in a manner permitting optimal observing efficiency for both.

III.1.2. Parameters of Observations

Spectroscopic observations of stars and galaxies were carried out using the Boller & Chivens spectrograph at the Cassegrain focus of the telescope. The general details of the instrument are given in Chapter II. A grating blazed at 9100\AA in the first order was used to obtain spectra covering the approximate wavelength range 5400\AA to 10400\AA in a single grating position.

All spectra were recorded through two apertures, with the object in one aperture and neighbouring sky in the other. The slit was aligned in the east-west direction and the apertures were 220 seconds of arc apart on the slit. The total observing time for each object was split into an even number of sub-intervals. Typically, during a sub-interval, the light from the object passed through the first aperture and that from the neighbouring sky, through the second one; in the next sub-interval the telescope was moved so that the object passed through the second aperture and the neighbouring sky on the opposite side of the object (as compared to the earlier sub-interval) passed through the first aperture. This sequence was repeated till sufficient signal was accumulated. At the end of each sub-interval, it was possible to display the accumulated counts to judge the signal level.

The above procedure of flipping the object from one aperture to the other was done in a manner to ensure that the total exposure time for the object through each aperture was equal; the same exposure was thus also recorded for the sky, simultaneously. The total sky exposure for each aperture was subtracted from the object exposure (with sky superimposed on it) for the same aperture. The reduction procedures described in Chapter IV explain the necessity for doing this. This procedure of simultaneous sky monitoring was followed for all objects except one galaxy, NGC 5128. For galaxy observations, the counts in the second aperture (called 'sky aperture') were compared with counts in a nearby field where no stars were seen despite a large integrating time of the TV acquisition camera. If the sky aperture counts (220 arc seconds east or west of the brightest part of the galaxy) were, on the average, the same as for the true sky field, they were taken as sky counts. This check was necessary since faint, outer regions of the galaxy under observation could contaminate the sky aperture. In the case of NGC 5128, this contamination was noticed and the two apertures were treated as independent observations of two portions of the galaxy. The sky was monitored separately before and after the galaxy exposure.

The size of the apertures along the direction of the slit was 20 seconds of arc, the size in the direction perpendicular to this being determined by the slit width. The slit width was chosen to optimise between spectral resolution, astronomical seeing and detector pixel size. As mentioned in Chapter II, the instrument profile of the Reticon as used with the Boller & Chivens spectrograph does not have extended wings and the full width at half maximum (FWHM) of the image is close to one pixel width. The slit width was kept at 130 microns, which, at the cassegrain $f/8$ scale of 19.4 seconds of arc per mm corresponds to 2.52 seconds of arc as the slit width. This slit width was adequate to compensate any light losses due to fluctuations in seeing, especially for the fainter stars.

The grating chosen was ESO Grating No.9/18 having a blaze angle of $8^{\circ} 38'$ and a blaze wavelength of 9100\AA in the first order. All observations covered the range 5400\AA to 10400\AA , centred at 7900\AA . The grating angle θ for this centre wavelength is about $7^{\circ} 30'$. The average dispersion at the detector plane was 228\AA per mm. The projected slit width ω and actual slit width W are related by

$$W = 4.5 \frac{\cos(\theta - 22.5)}{\cos(\theta + 22.5)} \omega$$

With $W = 130$ microns, ω is 25.9 microns; the projected slit was thus close to one pixel, corresponding to about 6\AA .

Wavelength calibration exposures were usually done immediately before and after each object exposure (for all stars and galaxies). A Helium-Argon calibration lamp was used to obtain spectrograms through both apertures simultaneously. To correct for small pixel-to-pixel variations in sensitivity of the Reticon, flat-field (FF) exposures using a quartz lamp were taken at the beginning and end of each observing night. Experience with this observing setup at ESO shows that, as long as there is no great change in the operating temperature of the Reticon, an average of flat field exposures at the beginning and end of the night is adequate for flat-field corrections. Records of the dark counts (with the shutter closed), had to be done for each exposure, as without this, records for the objects cannot be obtained.

III.1.3. Objects Observed

Since the amount of observing time available was short and keeping in view the spectral coverage, emphasis was laid on stellar observations of a few late-spectral-type stars with good signal-to noise ratio for the stellar library, in addition to galaxies.

III.1.3.1. Flux Standard Stars

Standard stars with known energy distributions were observed at airmasses covering the range of airmasses for the program stars and galaxies. Since absorption by the terrestrial atmosphere varies with airmass (proportional to the path length through the atmosphere), it was essential to have observations of flux calibration standards at around the same airmass as the program objects, to correct for this absorption. Due, again, to constraints of observing time it was not possible to observe flux standard stars with a range of brightnesses comparable to the program objects; the flux standards were chosen from the list of Taylor (1984). The calibrations of these standards are on the system of Hayes and Latham (1975) and include and extend the earlier calibrations (the most important of which is Breger 1976). An important criterion for the choice of the standards as calibrated by Taylor (1984) is that of a single uniform source covering the wavelength region from 3300\AA to 10800\AA . Calibrated magnitudes are given at a large number of points in the spectrum, covering the entire range.

The standard stars from this compilation that were observed are given in Table 3.1. The observations of the standards were repeated several times at

Table 3.1

Standard Stars Observed for Flux Calibration

| Star Name | HR No. | Spectral Type | V Magnitude |
|--------------|--------|------------------|----------------|
| η Hya | 3454 | B3 | 4.3 |
| θ Crt | 4468 | B9 | 4.7 |
| θ Vir | 4963 | A1 | 4.37 |
| 108 Vir | 5501 | B9 | 5.47 |
| 58 Aql | 7596 | A0 | 5.53 |

different airmasses, each night. Integrations of standards stars were done till a signal to noise (S/N) ratio of about 70 or higher was reached in the spectral region 9500\AA to 1 micron. For the configuration in which the Reticon is used, 500 counts correspond to a S/N ratio of about 100.

III.1.3.2. Synthesis Stellar Library Stars

An elaborate list of stars with well determined spectral and luminosity classes had been prepared for the observations. Since the spectral region of interest covered the yellow, red and near infrared wavelengths, the emphasis was on good signal to noise spectra of mainly late spectral type stars. The stars were selected mainly from the catalog of MK spectral classifications (Buscombe 1984) and the Catalog of Nearby Stars (Gliese 1969). Spectral types, photometric colours and magnitudes of these stars, as measured on standard systems were taken from various sources and these quantities will be discussed in more detail later.

Due to limitations of observing time, a few stars from the list could be observed and these are listed in table 3.2. The first column gives the star name, the second column gives the catalog number, when available, in the Yale catalog of Bright Stars

Table 3.2

Stars observed for the Stellar Flux Library

| Star Name | HR/HD number | Spectral Type | Apparent V magnitude | (R-I) _c |
|-----------------------------|---------------------|-------------------------|----------------------|--------------------|
| 1. | 2. | 3. | 4. | 5. |
| γ Pyx | HR 3518 HD 75691 | K3 III | 4.01 | 0.582 |
| C-26 | 4672 - | M7 I | 9.1 | - |
| R Leo | HR 3882 HD 84748 | M7 III | 5.07 | - |
| GL 453 | HD 103932 | K5V(G) | 6.96(G) | 0.545 |
| GL 296 | HD 66020 | K7V(G) | 9.62(G) | *0.768 |
| GL 488 | HD 111631 | M0.5 V E(G) | 8.51(G) | 0.838 |
| GL 526 | HD 119850 | M4 V E(G) M1.7 V (W) | 8.5(G) | *1.092 |
| GL 699 Barnard's Star | - | M5 V(G) M3.8 V (W) | 9.54(G) | 1.562 |
| ψ Vir | HD 112142 | M2.7 III | 4.80 | 1.177 |

(G) Catalog of nearby stars (Gliese 1969).

(W) Wing and Dean (1983).

* Colours from Gliese (1969) in the System of Kron (Kron et al 1953, 1957) converted to (R-I)_c using the transformations given by Bessel (1979).

(HR numbers-Hoffleit 1982) and the Henry Draper Catalog (HD numbers-Canon and Pickering 1918-24). The third column gives the spectral type which is from the MK catalog (Buscombe 1984), the Catalog of Bright Stars (Hoffleit 1982), the Catalog of Nearby Stars (Gliese 1969-superscript 'g') and those with superscript 'w' from Wing and Dean (1983). These latter authors have done spectral classification using photometric indices in the near infrared which are thought to be accurate for late spectral type stars. For some stars in Table 3.2, where the spectral types from different sources differ, all are indicated. The fourth column gives the apparent visual magnitude from the same sources as for spectral type. The fifth column gives the photometric R-I colour in the system of Kron-Cousins (Cousins 1980b and references therein). The $(R-I)_{KC}$ colours are from Cousins (1980a and b) for most of the stars; for some stars (superscript 'k' with $(R-I)_k$ colours in the Kron system (Kron et al 1953, 1957) taken from Gliese (1969), the $(R-I)_{kc}$ colours were derived using the transformations given in Cousins (1975).

The R-I colours tabulated in Table 3.2 are published colours; as described in Chapter IV these colours are synthesized from our spectroscopic observations as well as for the library of stellar spectra

which is taken from Pickles (1985). This library, which is described in more detail in later chapters is augmented, to some extent, by stellar data obtained in this program before being used for population synthesis.

III.1.3.3. Observations of Galaxies

The list of galaxies initially compiled for the program included early type (of types E and S0) objects of the following types: giant elliptical galaxies with no apparent signs of activity, normal elliptical (E) and S0 galaxies, bright elliptical galaxies with signs of activity and presence of dust/gas, and nuclei of spirals (thought to be similar to ellipticals). In the time available, it was possible to observe three galaxies. The properties of these galaxies are discussed below and also summarised in Table 3.3. Of particular interest is the effect of interstellar extinction within the Galaxy, in the direction of the observed galaxy. The effect of this extinction is wavelength dependant with the net result of making objects look redder - hence it is also called interstellar reddening. The interstellar reddening is often measured by the colour excess $E(B-V)$:

$$E(B-V) \equiv (B-V) - (B-V)_0$$

Table 3.3

Integrated parameters of the galaxies observed

| Galaxy | Type RMT Yerkes | Inte- grated magni- tude B_T^0 | Colour excess $E(B-V)$ | Velocity V_{sun} km/sec | Photometric colours | | | | | Photometric Magnitudes | | | | |
|-------------------|-----------------------|--|------------------------------|---------------------------------|---------------------|------|------|------|------|------------------------|-------|------|-------|-------|
| | | | | | U-V | B-V | V-R | V-K | J-H | H-K | V | K | M_V | M_K |
| 1. | 2. | 3. | 4. | 5. | 6. | 7. | 8. | 9. | 10. | 11. | 12. | 13. | 14. | 15. |
| NGC 4472 (M49) | E2 E2K | 9.10 | 0.0476 0.04(c) | 1001(a) | 3.32 | 0.69 | 0.21 | 8.99 | 5.70 | -22.7 | -26.0 | | | |
| NGC 3308 | SAB0 ⁻ | 12.80 | 0.0881 0.1166(p) | 3642(r) | 1.57 | 0.99 | 0.89 | 3.11 | 0.68 | 0.20 | 12.56 | 9.48 | -21.8 | -24.9 |
| NGC 5128 | SOpec Ep ? | 7.40 | 0.1214 | 541(s) | | | | | | | | | | |

Notes:

- Column (2) : Revised Morphological Type from RC2; Yerkes type from Morgan (1958)
- Column (3) : from RC2
- Column (4) : Colour excess from RC2 derived using $E(B-V) = AB/(R+1)$ and $R = 3.2$. Other sources: (c) O'Connell (1976); (p) Persson, Frogel and Aaronson (1979)
- Column (5) : Heliocentric velocity: (a) the best value from Palumbo, Tanzella-Nitti and Vettolani (1983); (r) Richter (1987); (s) Sadler (1984)
- Columns (6)-11: at $\log A/D(0) = -0.6$ from Persson, Frogel and Aaronson (1979)
- Columns (12-15): at $\log A/D(0) = -0.3$ from Persson, Frogel and Aaronson (1979).

where B , V are magnitudes in the B and V filter bands and the colour $(B-V)_0$ is the intrinsic colour of the object. The extinction in the visual band, A_V , that in the blue band A_B and the colour excess are related by:

$$A_V = RE(B-V)$$

$$A_B = (R+1)E(B-V)$$

$$A_V = A_B R / (R+1)$$

where R is an observationally determined constant.

The values of $E(B-V)$ and/or A_V in different directions due to extinction in the Galaxy can be determined by various models such as the Whitford reddening law (Whitford 1958), the de Vancouleurs model for reddening (de Vancouleurs et al, 1976, hereafter called RC2), the Sandage model (Sandage 1973). The values of $E(B-V)$ in Table 3.3 from different sources are explained in the notes to the table. The use of reddening values in the reduction of spectra and their importance for synthesis will be discussed in Chapters IV and V.

Photometric colours for the galaxies where available are also given in the table. The infra-red and optical photometry as well as the magnitudes are from Persson et al (1979), unless otherwise noted. Since galaxies are seen projected against the sky, whereas

their actual orientations differ, it is standard practice to derive "face-on" optical diameters $D(0)$ (see RC2 for a description of the procedures). Photometry is done using a variety of apertures and hence, for purposes of comparison, photometric magnitudes are usually reduced to a standard value of the ratio of the aperture A to the face-on diameter $D(0)$.

The values of the heliocentric velocity, v_{sun} of the galaxies in km/sec are also given in Table 3.3. The values are from different sources as marked in the table. The recently compiled catalog of radial velocities of galaxies by Palumbo et al (1983) has velocities from different sources with errors indicated where available. For NGC 4472 we have taken the value with the lowest error from this catalog. For the other galaxies we have adopted velocities from the other sources indicated in the table.

NGC 4472

NGC 4472 (M49) is the brightest giant elliptical (gE2) in the Virgo I "E" cloud of galaxies, at a distance of 13.6 Mpc (de Vaucouleurs 1975). Following the colour-magnitude relationship for early-type galaxies, it is also the reddest of the group. It has been detected in the radio region, though the total emission is several orders of magnitude weaker than a

typical radio galaxy (Ekers and Kotanyi 1977). The recent discovery of X-ray emission from this galaxy came as a surprise since its gas content was estimated to be low, based on HI measurements (Thonnard 1983). The X-ray observations imply that about $10^{10} M_{\odot}$ of hot gas is residing in the halo of the galaxy, and is flowing inward as it cools (Thomas 1986). The gas distribution is extended beyond the optical image of the galaxy. However, no H-alpha filaments are seen as in NGC 1275, another galaxy with a cooling flow, implying that the rate of star formation in the cooling flow is rather low.

NGC 4472 has been studied well spectroscopically and photometrically. It has been included in several investigations of stellar population synthesis in the past. In the present study, the spectrograph aperture was centred on the galaxy.

NGC 3308

This is a late-type elliptical exhibiting signs of transition to the lenticular class of galaxies. A member of Abell 1060 cluster of galaxies in Hydra, it is the farthest (~ 36 Mpc) and faintest of the three galaxies investigated here. NGC 3308 has not been studied well in the past, the available information being limited to radial velocities and multiaperture

photometry. Present observations are centred on the galaxy.

NGC 5128

Also known as Centaurus A, this is the nearest of the giant radio galaxies. It is a member of the Centaurus group of galaxies at an estimated distance of 4.0 Mpc (de Vaucouleurs 1975). Due to its proximity, nuclear activity and peculiar morphology, the galaxy has been a target for many observational and theoretical investigations (see Ebeneter and Balick 1983 for a review). The optical structure is dominated by two components (Dufour et al 1979).

1. An elliptical component of similar colour and luminosity distribution as a giant E2 galaxy.

2. A highly inclined disk component containing a young metal-rich stellar population, gas and dust in the equatorial region of the galaxy.

Deep, large-scale photographs subjected to unsharp masking technique (Malin, Quinn and Graham 1983) reveal a system of rings in the outer extensions of the elliptical component. NGC 5128 houses an active nucleus from which a pair of radio jets emanate. Though the energetic phenomena and star-formation in the galaxy are well-studied, no attempt has been made so far

towards synthesizing the stellar populations of the ellipsoidal component. The region of the ellipsoidal component observed here avoids the dust lanes and star-forming regions (Figure 3.1).

III.2. Observations carried out at VBO.

Observations of several galaxies and many standard stars covering different spectral types and luminosities were carried out during the period January 1982 to December 1985. The observations for this study were tried mainly during the winter months, for reasons mentioned earlier in this chapter.

As described in Chapter IV, the reductions of the photographic spectra revealed that the data set was not homogeneous and not of a quality that could be used for the aims set forth in this study. We give below a list of galaxies observed with the 1 metre telescope at VBO. At the time of writing this dissertation, a new Universal Astronomical Grating Spectrograph from Messrs. Carl Zeiss - Jena is available for use at the 1-metre telescope. The observations carried out in the initial phases of this study were all with the Cassegrain Image Tube spectrograph built in house at the Institute.

The spectrograms of the galaxies were obtained with a reciprocal dispersion of around $220\text{\AA}/\text{mm}$ with a slit 150 to 225 microns wide (depending on the

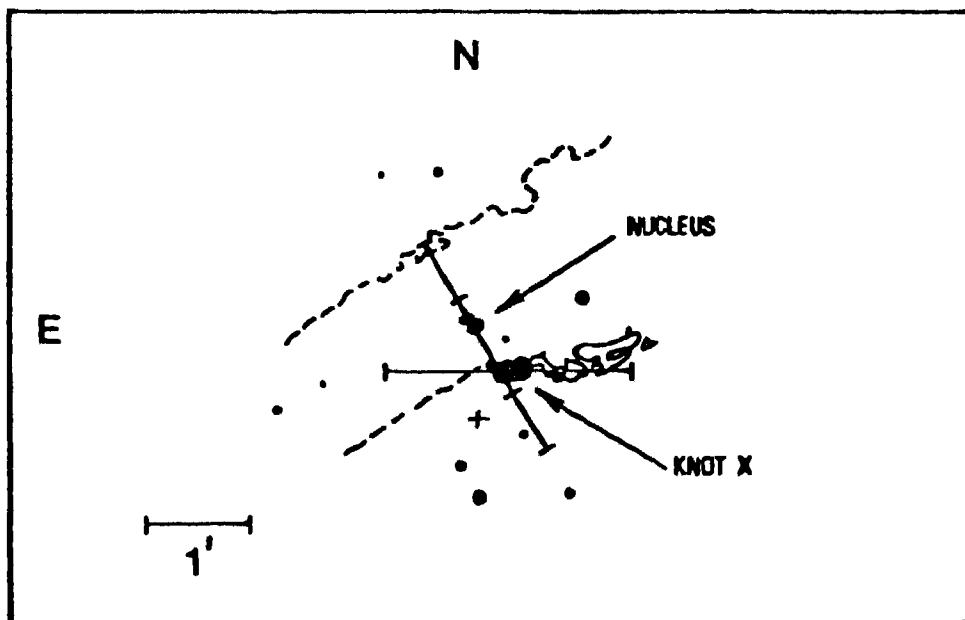
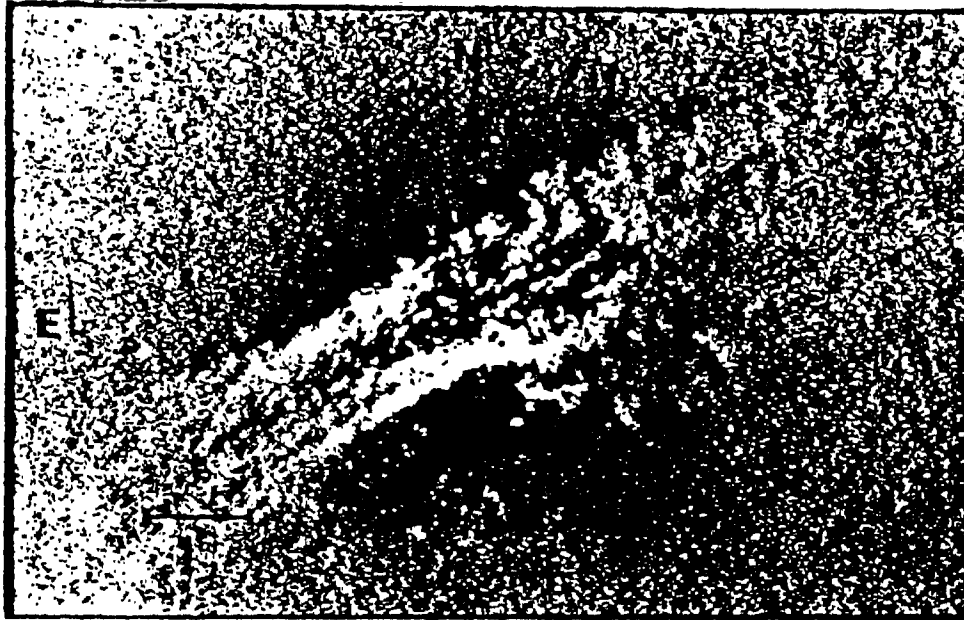


Figure 3.1. A photograph of NGC 5128 and schematic diagram of the nucleus and dark lanes (reproduced from Phillips 1981). The position of the spectrograph aperture is shown as '+' on the diagram.

brightness of the galaxy. Typical exposure times for galaxies were about 4 hours.

Galaxies Observed

| | |
|---------------|----------|
| NGC 224 (M31) | NGC 2903 |
| NGC 1398 | NGC 3031 |
| NGC 1808 | NGC 3034 |
| NGC 2841 | NGC 4472 |

Chapter IV

DATA REDUCTIONS AND PRESENTATION OF DATA

In this Chapter we give the details of the reduction procedures followed in bringing the raw data to a form amenable to analysis. The data obtained at ESO were reduced to absolute fluxes before being used in population synthesis. These spectra are presented here. The data obtained at VBO over the period 1982 to 1984 suffers from a lack of uniformity in instrument settings, due to major changes made in that period. These are discussed in the later part of this Chapter.

IV.1. Reductions of Spectra Obtained at ESO

The raw data obtained from the Reticon system on magnetic tape was reduced using the ESO IHAP software at the ESO headquarters in Munich (FRG). The raw data is stored as image files in the same format as for the Image Dissector Scanner (IDS), which is also a detector system for use with the Boller & Chivens spectrograph.

The scans of the spectrum are stored as scan lines in the image file. The two apertures of the Reticon being called A and B, the scans through

aperture A (corresponding to the sub-intervals of integration line referred to in Chapter III) are stored in scan lines of odd number and those through aperture B in scan lines of even number. The scan lines from line 7 upward contain data pairs (for A and B) for the individual sub-intervals. Scan lines 1 and 2 contain the sum of the integrations for the object in aperture A and sky in aperture B, respectively. Scan lines 3 and 4 contain the sum of the integrations for the sky in aperture A and the object in aperture B. Each image file has a header block where details of the integration time, telescope position, time of observation and other comments are stored.

The reduction procedure consists of several steps:

1. Examining the scan lines and making sure that lines 1 to 4 contain the sequence of integrations as described above. Further steps in the reduction procedure require this format and in cases where the second aperture was not the true sky observation (such as for NGC 5128), the separate sky observations and object observations have to be processed independantly and then put in a format suitable for the reduction procedure.
2. Determining wavelength shifts during each night and drifts in flat-field exposures.
3. Wavelength calibration.
4. Sky subtraction.

5. Flat-field correction.
6. Determining the instrument response curve
7. Final reduction to fluxes.

IV.1.2. Data Formats

Observations for all objects except NGC 5128 were made in the prescribed manner, with the light from the object being measured through one aperture while sky was monitored through the other, followed by switching the object to the second aperture in the subsequent integration. This procedure ensured that scan lines 1 to 4 were in the correct order.

In the case of NGC 5128, there were three data files. The first file had counts for the 'nucleus' of the galaxy in aperture A for a total time of 1 hour (two integrations of 30 minutes each), stored in scan line 1; similarly the counts for a point 220 seconds of arc east of the nucleus, through aperture B, were in scan line 2. The third file was similar to the first one, with a total integration of one hour. The second file had the sky exposure of 30 minute through aperture A in scan line 1 and that through aperture B in scan line 2. In subsequent steps of reduction, where sky subtraction was done, this was taken into account.

IV.1.3. Shifts in Wavelength and Flat field exposures

It is possible that small shifts in the point of incidence, on the Reticon, of light of a given wavelength can occur, due to flexure in the instrument at different positions of the telescope. These shifts, if not accounted for, lead to erroneous wavelength calibration of the spectra. Since flat field exposures are used to determine and calibrate out the variation in sensitivity over the Reticon, it is also necessary to see if they shift with position of the telescope.

Wavelength calibration exposures using the Helium Argon lamp (He Ar) had been taken before and after each object exposure. These two He Ar spectra were superposed on each other on the graphic terminal and it was found that there was essentially no shift to within one pixel, in the position of the comparison lines. There was, however, a shift in position of the lines for aperture A, as compared to aperture B.

Similarly, the three or four flat field exposures taken each night, one taken in the evening, one in the morning and one or two in between, were superposed on each other and no shift to within one pixel, was found. During this examination, it was seen that the response of the Reticon was not identical for the two apertures. A small change in the sensitivity between evening and

morning for a given aperture was seen, amounting to about 2.5 per cent between pixels 1 to 100, about 1.6 to 1 per cent from around pixel 100 to around pixel 400 and thereafter decreasing to negligible values. Pixel 1 was the blue end of the spectrum.

IV.1.4. Wavelength Calibration

The Helium-Argon calibration lamp used for wavelength calibration had spectral lines well-spaced over the entire region of observation except between 5100Å and 5500Å and between 9800Å and 10470Å. A typical HeAr exposure is shown in Figure 4.1. The standard wavelength calibration procedure in the IHAP software was used and is described below. After checking for wavelength shifts, wavelength calibration was done for one exposure; for subsequent objects in the same night a new wavelength calibration was done only if a shift of the HeAr lines was noticed as compared to the calibration exposure for the previous exposure. For most of the exposures it was found that a new calibration was not required.

The HeAr spectrum was first displayed on the graphic terminal and a few unblended, clear lines were identified throughout the spectrum. This was done by entering the approximate wavelength for each line and locating it with the graphics cursor. This procedure

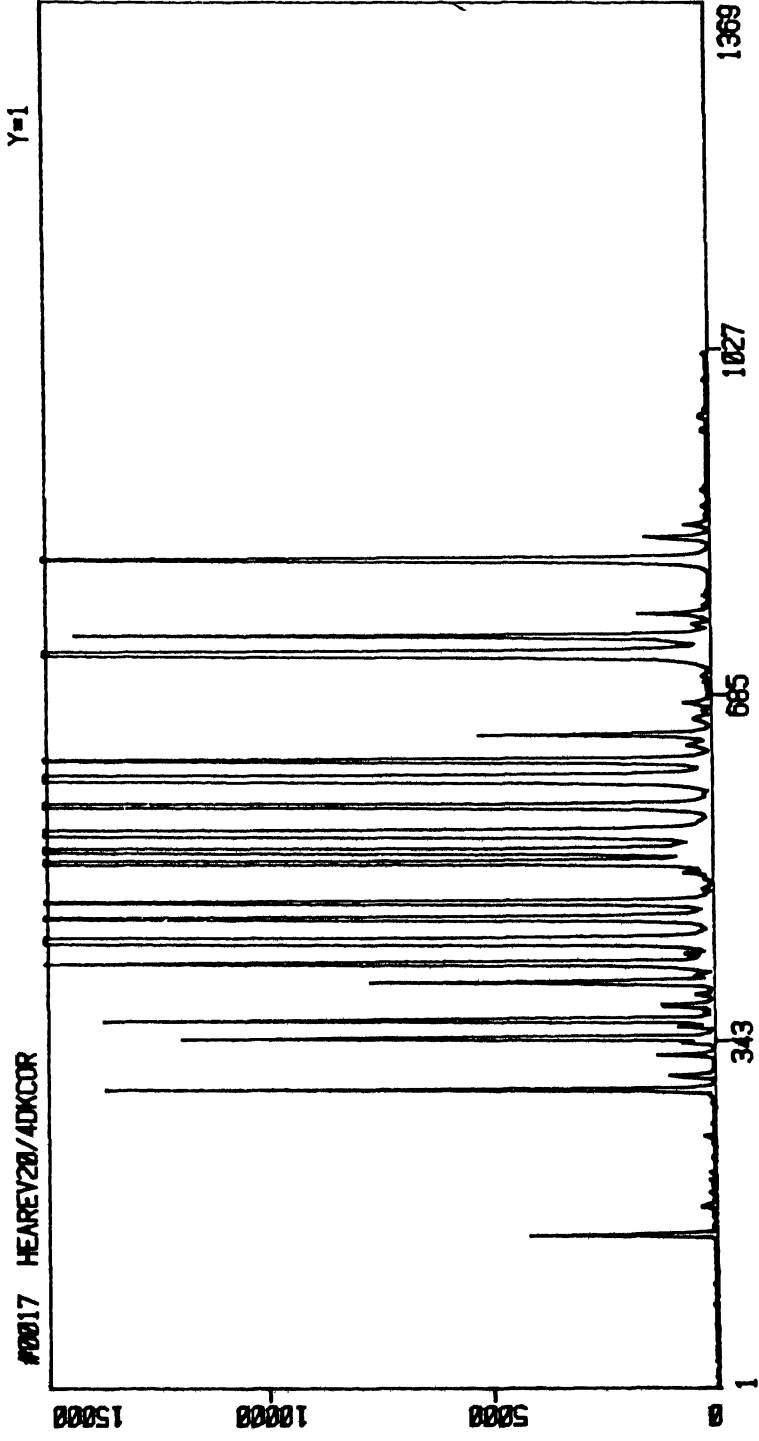


Figure 4.1. Helium Argon spectrum obtained with the reticon.

creates a table of pixel values and the associated wavelengths. A least-squares fit was done to the data in this table and, initially, a linear relation was fitted and displayed as a line with the entered values marked above and below it. These points should define a smooth curve; points far removed from the trend were removed using an editing facility, and the fit was recalculated. This approximate fit of pixel versus wavelength was used in an automatic line search procedure.

The automatic line search and identification procedure searches the data for the exposure, detects spectral lines and associates them with a stored table of known wavelengths for the calibration source. The table of known wavelengths can be created but for the HeAr source it was already available in the system. The detection of spectral lines in the data requires a window to be specified, within which a line will be detected; an optimum value for this is double the full width at half maximum of a typical spectral line. Another parameter specifies the algorithm to be used for line detection; the algorithm used involved a gaussian fit to the points defining a line within the window. The window is scanned along the entire spectrum and pixel values for the centroids of the detected lines are stored. Using the approximate fit done initially

and linear interpolation, the nearest wavelengths from the stored table of wavelengths are found. The pixel position, wavelength and approximate intensity of the lines located are displayed; lines in the table that are not found in the spectrum are also indicated. After this, the procedure does a least squares polynomial fit relating the wavelength (λ) and $\Delta\lambda$, where the latter is the difference in wavelength of the line located in the table and that determined from the initial linear fit. The polynomial fit is displayed along with all lines identified. At this stage again obviously bad points, such as faint lines not expected to be present with a good signal-to-noise or lines in crowded regions which may be mis-identified, can be removed and the entire search and fit procedure repeated. The procedure allows the degree of the polynomial to be specified. Iterations of the search and fit procedure are repeated until a satisfactory fit is found. The coefficients of the fit are then stored in a special file and used to calibrate other data files. Figure 4.2 shows a typical fit for an HeAr exposure. The dashed line represents the initial linear relation, the squares are the initial rough identifications of lines. The polynomial fit and the lines found in the search and fitted are also shown. In this case a polynomial of degree five was

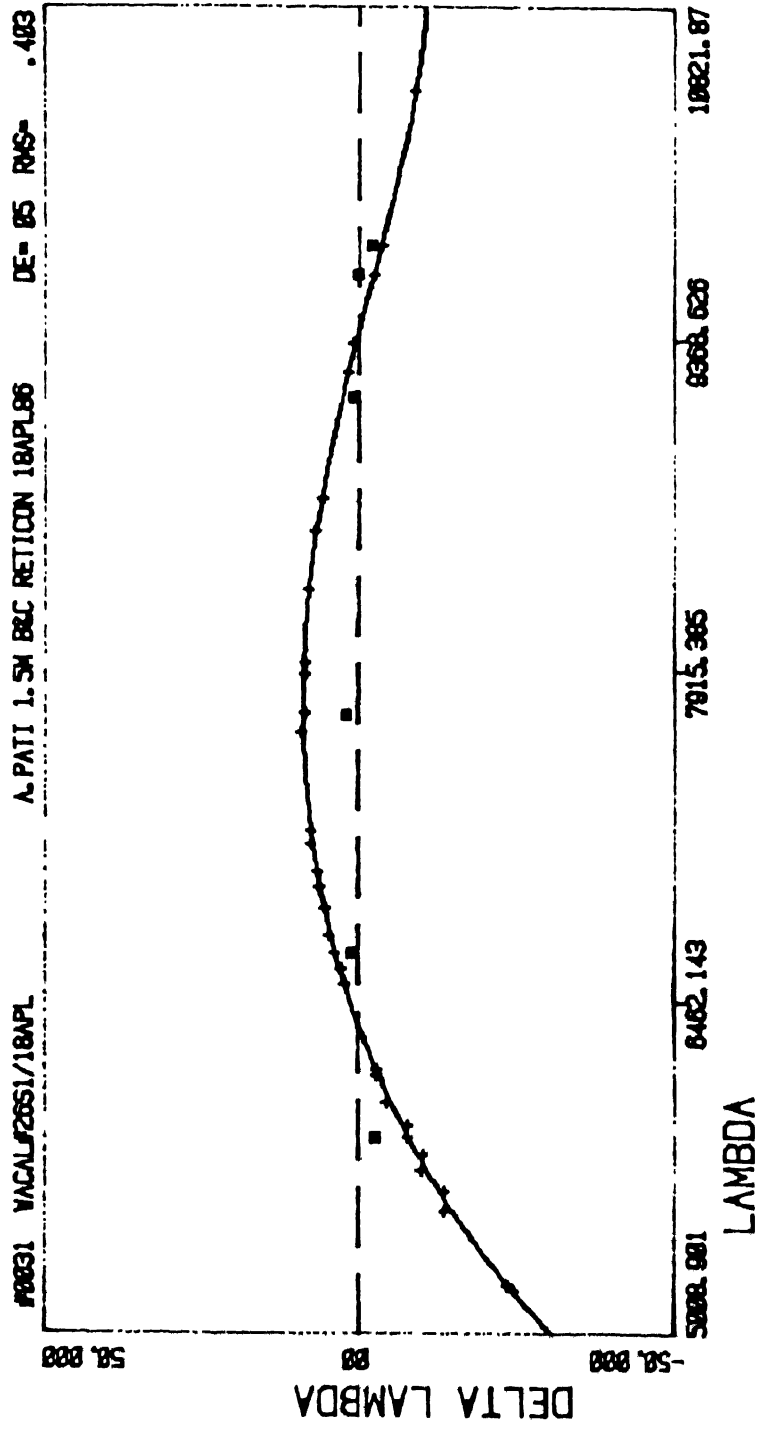


Figure 4.2. Typical fit obtained with the wavelength calibration procedure in IHAP.

used. The maximum error between the wavelength given by the polynomial fit and the actual wavelength in any calibration was about 2.5 angstroms.

The wavelength calibration procedure was followed and the files of coefficients were created, separately for aperture A and B. For each object observed, once the wavelength coefficient files for the HeAr exposure to be used were available, the wavelength calibration was done. This could be done with a single command, where the data file and the two coefficient files (for the two apertures) were indicated. The data file itself contained counts for the object with the sky subtracted out and flat field corrected, as described below. The wavelength calibration command allowed the specification of the starting wavelength and rebinned the data to a linear scale with a step size that could be specified. The rebinning was done using linear interpolation. All data were rebinned to a step size of 2 angstroms.

IV.1.5. Sky Subtraction

Since the sky was monitored simultaneously with the object, subtraction of the sky counts was done quite easily. The sky counts for aperture A were subtracted from the counts for the object (plus sky super imposed) observed through aperture A; the same was done for

aperture B. This was accomplished by a single command which presumes the sequence of object and sky counts in scan lines 1 to 4 in Section IV.1. The result is a new data file with the sky subtracted counts for apertures A and B in scan lines 1 and 2. This procedure effectively removes contamination due to night sky emission, unless excessively large and rapid variations in the emission occur. The absorption of radiation in the atmosphere, however, cannot be corrected in this way and such corrections for absorption are dealt with later. The 'dark' counts for the system, arising from noise in the electronics is also subtracted out along with the sky counts, since it is present in both apertures.

In the sole case of the galaxy NGC 5128 the sky subtraction could not be done with the standard procedure, since the object and sky counts were not in the same data file in the required format. The exposure for NGC 5128 was in two instalments (each an independant exposure) of one hour each, with a sky exposure of 30 minutes in between them. The two exposures of the galaxy were summed up to give a total of 2 hours for each of apertures A and B. The sky exposure for each aperture was scaled up to match the 2 hour galaxy exposure and then subtracted from the latter. The final result was in a data file with sky

corrected counts for apertures A and B in scan lines 1 and 2, respectively. Subsequent reductions for this file could then be done as for the other object files.

IV.1.6. Flat Field Correction

The procedure of flat field correction removes the effect of variation of sensitivity of the detector with pixel location from the data. The flat field exposure essentially measures the relative response of the detector, given a uniform source of illumination. Figure 4.3 shows the counts for a flat field exposure for both apertures; the dark noise (stored in scan lines 7 and 8 of the raw data file) has been subtracted from the data. The flat field response shows two components, with high spatial frequencies probably due to irregular pixel-to-pixel variation and low spatial frequencies due to slowly varying sensitivity over the wavelength range of the exposure.

The most convenient procedure was to construct a flat field correction file for the high spatial frequencies and to implicitly allow the procedure for construction of the instrument response curve to take care of the low frequency variation (see Section IV.1.7). Hence, a copy was made of the flat field data file; the flat field data in the copy were smoothed heavily using a running unweighted mean over a window 50 to 60

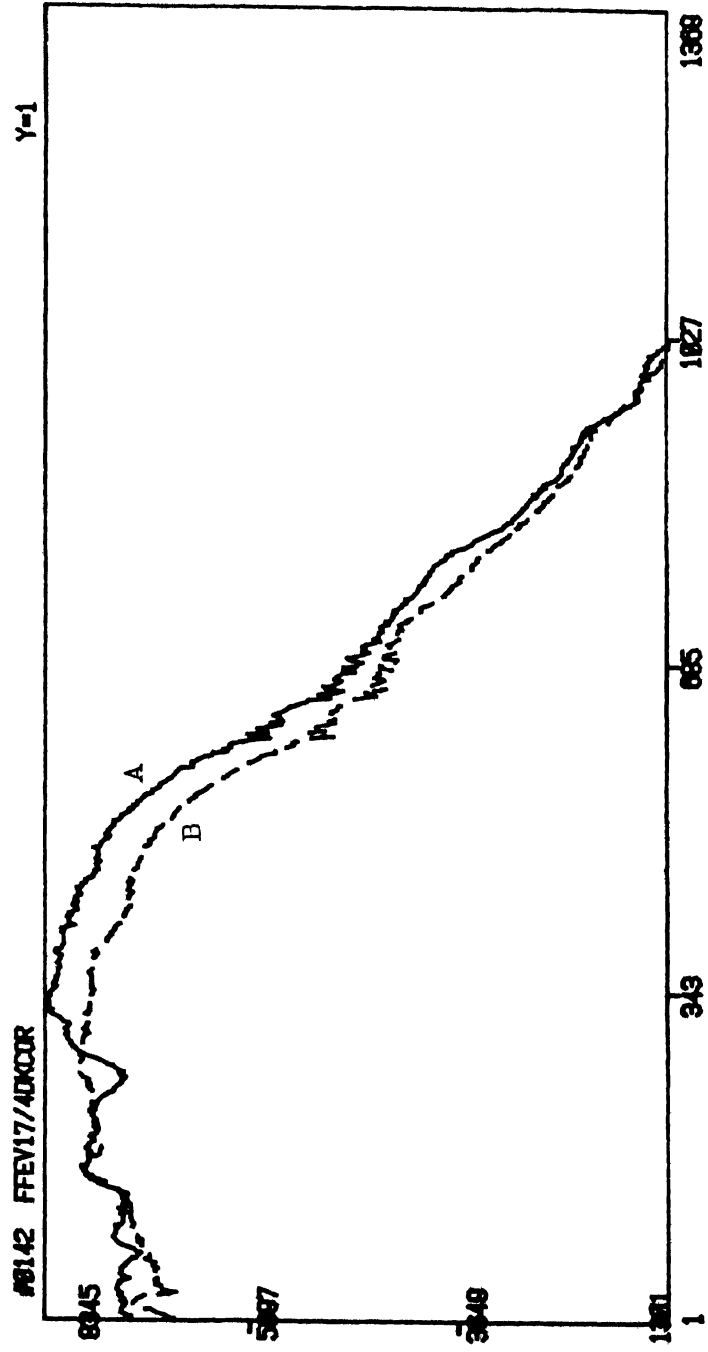


Figure 4.3. Dark corrected flat field exposure for both apertures of the reticon.

pixels wide. This was done independently for each aperture. The original flat field exposure was then divided by the smoothed exposure, giving a flat field exposure containing only the high spatial frequencies. Figure 4.4 shows the result for one aperture of a flat field exposure. This final flat field again has only two scan lines, the first for aperture A and the second for aperture B. The object exposures were to be divided by this flat field data, to correct for the high spatial frequency variation.

IV.1.7. Instrument response curve

The spectrum obtained from the instrument are in the form of counts put out by the analog to digital conversion process. It is essential to know what these counts correspond to, in terms of the energy incident on the earth. The determination of the instrument response curve permits this. The observations of flux standard stars, for which the energy incident on the earth (outside the atmosphere) is known, are used for this purpose.

The flux standard stars are themselves calibrated using the absolute calibration of the star α Lyra. The system of calibration adopted here is that of Hayes and Latham (1975), according to which the monochromatic flux reaching the earth's atmosphere from α Lyra at

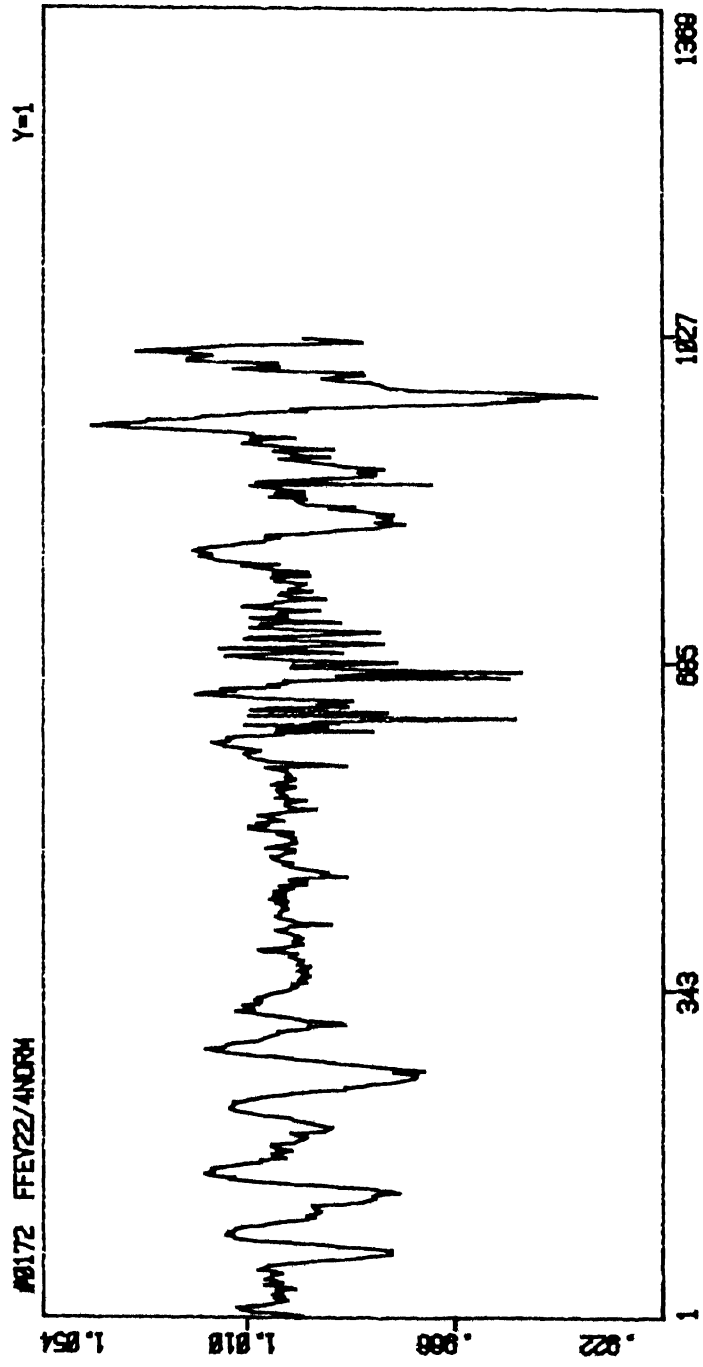


Figure 4.4. High spatial frequency response derived from a flat-field exposure for one aperture.

the wavelength 5556\AA is:

$$F_{\lambda} = 3.39 \times 10^{-9} \text{ ergs cm}^{-2} \text{ sec}^{-1} \text{\AA}^{-1} \quad \text{or}$$

$$F_{\nu} = 3.50 \times 10^{-20} \text{ ergs cm}^{-2} \text{ sec}^{-1} \text{ Hz}^{-1}$$

where $F_{\lambda} = F_{\nu} c/\lambda^2$, c being the velocity of light.

The magnitude per unit frequency at the frequency is given by

$$m_{\nu} = -2.5 \log F_{\nu} + 48.64$$

where the constant derives from assigning the flux for α Lyra at 5556\AA to a magnitude of 0.0.

The flux standards observed here are from Taylor (1984), where the magnitudes are given for the entire range 3300 to 10800\AA . These magnitudes were first converted to fluxes and then stored in a tabular form as required by the IHAP software. The procedure for obtaining the response curve is described below:

For each object in the program, an observation of a flux standard star at a similar airmass, at around the same time (i.e. immediately before or after) was chosen for flux calibration. As far as possible this was done to avoid uncertainty due to differences in telescope position and sky variability. The standard star data was corrected for sky emission using the sky subtraction procedure. The resulting data was then

divided by the flat field data, treating each aperture separately. The flat field corrected data were wavelength calibrated and rebinned to a linear wavelength scale using the wavelength coefficient files for the two apertures, following the procedure outlined in Section IV.1.4.

The flux standard star was then corrected for atmospheric extinction. Atmospheric extinction is a measure of the extent to which the atmosphere absorbs or scatters energy at different wavelengths; the observed energy distribution has to be corrected for this. The average values of extinction in magnitudes for the ESO site at La Silla, compiled over several years, was available in the IHAP system and these values were used. Table 4.1 lists these extinction values, in magnitudes, at different wavelengths per unit airmass. These values were converted to the airmass for the observation of the standard star and the correction applied. The IHAP software has a single command for the entire procedure of extinction correction.

The flux table for the standard star contains in successive columns, the central wavelength, the flux values and the window around the central wavelength over which the flux is taken. The flux calibration command generates a ratio of the integrated values of

Table 4.1

EXTINCTION VALUES AT ESO, La Silla

| Wave-length (Å) | Extinction (magnitudes) | Wave-length (Å) | Extinction (magnitudes) |
|--------------------|----------------------------|--------------------|----------------------------|
| 3100 | 1.530 | 5600 | 0.107 |
| 3200 | 0.943 | 5800 | 0.102 |
| 3300 | 0.720 | 6000 | 0.097 |
| 3400 | 0.606 | 6200 | 0.083 |
| 3500 | 0.529 | 6400 | 0.070 |
| 3600 | 0.467 | 6600 | 0.057 |
| 3700 | 0.418 | 6800 | 0.049 |
| 3800 | 0.374 | 7000 | 0.042 |
| 3900 | 0.337 | 7200 | 0.036 |
| 4000 | 0.304 | 7400 | 0.032 |
| 4100 | 0.275 | 7600 | 0.028 |
| 4200 | 0.250 | 7800 | 0.025 |
| 4300 | 0.227 | 8000 | 0.023 |
| 4400 | 0.207 | 8200 | 0.021 |
| 4500 | 0.191 | 8400 | 0.019 |
| 4600 | 0.175 | 8600 | 0.018 |
| 4700 | 0.162 | 8800 | 0.017 |
| 4800 | 0.152 | 9000 | 0.015 |
| 4900 | 0.141 | 9500 | 0.015 |
| 5000 | 0.135 | 10000 | 0.015 |
| 5200 | 0.123 | 10500 | 0.015 |
| 5400 | 0.115 | 11000 | 0.015 |

the standard star over the window specified to the flux in the table for all wavelength points of the table present in the observation. A spline fit is made to generate a smooth curve fitting the points; it was important at this stage, to ensure that there were no sudden jumps in the curve, by controlling the parameters of the spline fit. A single array of points was finally generated for each aperture, using the coefficients of the fit and the same starting wavelength and step for rebinning as used in the wavelength calibration procedure. Figure 4.5 shows the typical response curves obtained for the two apertures.

IV.1.8. Conversion of spectra of fluxes

After comparing the airmasses and times of observation (during a given night) of flux standard stars, synthesis library stars and galaxies, a choice was made of which standard stars were to be used for flux calibration of the various program objects. Though standard star observations were made at airmasses close to that for the program objects, in some cases these could not be used since the sky had varied by the time the standard was observed after the object observation; the moon was also present for part of the night and it was preferable to have both standard star and program object in either the dark part or the moonlit part. Table 4.2 lists the

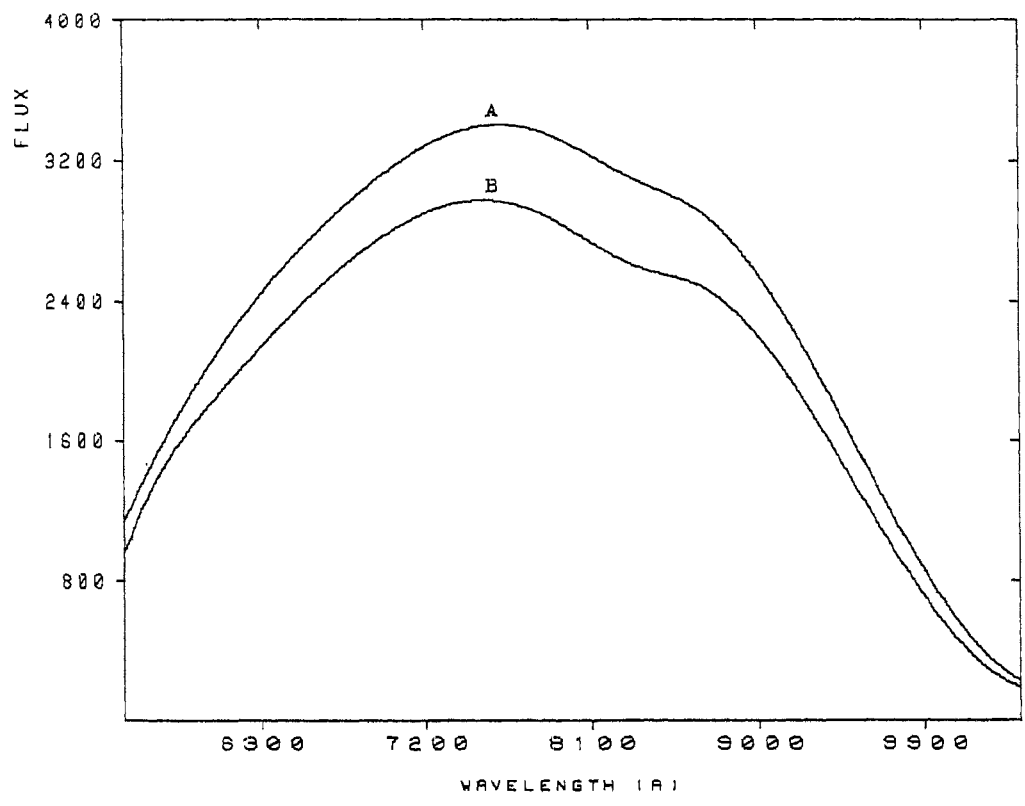


Figure 4.5. Instrument response curves for the two apertures

Table 4.2

AIRMASSES OF OBJECTS OBSERVED AND STANDARD STARS

| Object | Mean Air- mass of observa- tion | Flux standard used | Mean Airmass of standard observation |
|--------------|--|--------------------------|--|
| γ Pyx | 1.001 | η Hya | 1.245 |
| C-26 4672 | 1.087 | η Hya | 1.245 |
| R Leo | 1.320 | η Hya | 1.245 |
| NGC 3308 | 1.059 | η Hya | 1.245 |
| GL 453 | 1.014 | θ Crt | 1.118 |
| *NGC 5128 | 1.318 | θ Crt | 1.118 |
| GL 296 | 1.277 | η Hya | 1.193 |
| NGC 4472 | 1.525 | θ Vir | 1.413 |
| HD 112142 | 1.516 | θ Vir | 1.413 |
| GL 488 | 1.779 | θ Vir | 1.413 |
| GL 526 | 1.862 | θ Vir | 1.413 |
| GL 699 | 1.229 | 58 Aql | 1.295 |

* Mean airmass for second observation which was at a larger airmass.

airmasses for the program stars and galaxies and those for the standard stars used for flux calibration. The standard star observations were chosen keeping in mind both the matching of airmasses as well as sky conditions. In several cases, we see in Table 4.2 that the airmasses do not match closely enough. This would introduce some errors in the flux calibration, but the fact that the spectra are ultimately normalised to 5556\AA before being used in synthesis, reduces the effect of these errors.

For the program objects, the wavelength calibration, rebinning the linear wavelength scale, division by flat field response, division by the instrument response curve (generated for the chosen standard star) for the two apertures separately and correction for extinction were all done as part of a single batch job on the computer. The final output when multiplied by the ratio of exposure time of the standard star to that of the program object yielded the flux in $\text{ergs cm}^{-2} \text{sec}^{-1}$ per wavelength step (2\AA). For use in population synthesis, this last multiplication by the ratio of exposure times was not required since the spectra were to be normalised to a value of 100 at 5556\AA .

Though the wavelength range of the raw data was from around 5250\AA to about 10400\AA , the data were usually trimmed at the two ends of the spectrum where irregular

variations in the data were seen. The wavelength range of the flux calibrated spectra was 5539\AA to 10393\AA with a step of 2\AA per pixel. During the wavelength calibration procedure, the data was oversampled (the observed resolution was 6\AA per pixel), so that operations involving smoothing, shifting the data to correct for small zero-point wavelength shifts rebinning the data with a different start wavelength to correct for the redshift of galaxies, would not degrade the resolution.

IV.1.9. Errors in flux calibration

Observations of synthesis library standard stars and galaxies, should ideally be repeated several times and averaged to get the data to be used for synthesis. Due to the small amount of observing time available, it was not possible to do this. The synthesis standard stars and galaxies were observed once each.

The standard stars from Taylor (1984), were observed several times each night at different telescope positions at airmasses upto 1.9. We calculated M_y in Hayes-Latham (1975) system for the standard star observations at 5556\AA and 10256\AA . We then corrected the values of M_y from Taylor (1975) for the zero-point difference in calibration and obtained the differences in M_y in the sense M_y (Taylor 1975) - M_y (this work) for both points 5556\AA and 10256\AA .

We find that the mean difference at 5556\AA is -0.067 magnitudes, with the standard deviation of the mean being 0.042 magnitudes. Similarly, the mean difference at 10256\AA is $+0.092$ magnitudes, with the standard deviation of the mean being 0.031 magnitudes. The implication of these errors would apparently be that our observations yield systematically fainter magnitudes in the visual region of the spectrum and systematically brighter magnitudes in the near-infrared region of the spectrum. The effects of these systematic differences will be discussed in Chapter V.

IV.2. Further reductions and formatting for population synthesis.

To perform population synthesis, as explained earlier, a library of stellar spectra covering stars of various spectral types, luminosity classes and abundances are required. Since the compilation of such a library takes a lot of observing time and since the observing/^{time}available for this project was less, such compilations by others had to be used, to which the stellar data observed in this program were added.

The stellar synthesis library used was that compiled by Pickles (1985) using observations from the 1.9m telescope at Mount Stromlo Observatory and the 3.9m Anglo Australian Telescope (AAT), and an earlier

compilation of lower resolution (50\AA) data by Straizys and Sviderskiene (1972 - hereafter referred to as Vilnius Standard Spectra, since these were observed at the Vilnius Observatory).

The stellar library of Pickles (1985), hereafter referred to as SLP, includes 49 standard stellar types covering the wavelength range 3600\AA to 10000\AA . Most of the observations used to compile the SLP had a spectral resolution of 10 to 17\AA ; the flux calibrated spectra have a mean standard deviation in photometric magnitudes of 0.062 mag for the wavelength region 3600 to 3800\AA , 0.031 mag for the region 3800 to 6000\AA and 0.026 mag for the region 6000 to 10000\AA . The flux calibrated spectra corrected to remove atmospheric absorption bands and normalised to a value of 100 at 5450\AA were obtained on magnetic tape. The data obtained for this thesis has a superior resolution and extends farther to the infrared. Since the SLP library was required for synthesis, the data had to be truncated at 10000\AA , and then added to the library. We describe below the further reductions performed to make the galaxy and SLP library compatible with each other.

All reductions at this stage were done using the STARLINK software package installed on the VAX 11/780 system at VBO; specifically, the package SPICA was used

for all the processing of spectral data. The flux calibrated data from ESO were brought to VBO on magnetic tape in FITS format, which made it easier to read them using SPICA.

IV.2.1. Removal of sky absorption bands

The data in the SLP library had been corrected for removal of sky absorption bands. The sky subtraction procedure outlined in Section IV.1.5 does not correct for molecular absorption of radiation in the earth's atmosphere. There are several strong absorption band systems due to atmospheric O_2 and H_2O scattered throughout the spectral range of the observations, the strongest ones being the B-band of O_2 at 6867\AA , the A-band due to O_2 at 7594\AA and the strong vibration rotation systems of H_2O in the region 7130 to 7300\AA , 8130 to 8370\AA and 8950 to about 9850\AA .

If a hot star of spectral type O, early B, or better still a hot white dwarf star, is observed at around the same airmass as the program object, the spectrum of the former can be used to generate the fractional depression below the spectral continuum caused by the atmospheric absorption bands throughout the spectrum. The spectra of hot stars contain few, easily identifiable spectral lines of mainly hydrogen and helium, which can be masked out quite easily. The

procedure adopted here is described below.

The standard star η Hya, of spectral type B3, which had been observed at different airmasses each night, was used for creating atmospheric fractional absorption files (AFA files). The star θ Crt of spectral type B9 was also used to create average AFA files. First, a mask file was created identifying areas affected by atmospheric absorption. The high resolution atlases of the sun by Moore et al (1966) and Babcock and Moore (1947) were scanned to see the regions where absorption was significant. The mask consisted of windows containing the absorption bands, all points within the mask windows being set to a value of one and portions outside the windows being zero. The mask windows excluded all regions which had stellar lines (for the early type stars) and which did not have significant atmospheric absorption bands. The window in the region 9000 to 9850 \AA did have strong lines in the Paschen series of hydrogen and this point is discussed later.

A continuum was fitted to the early type star spectrum; a spline fitting technique was used to fit the continuum in parts, which were then joined together. Figure 4.6 shows the spectrum of the star θ Crt along with the fitted continuum and the location of the window in the mask file for atmosphere absorption bands.

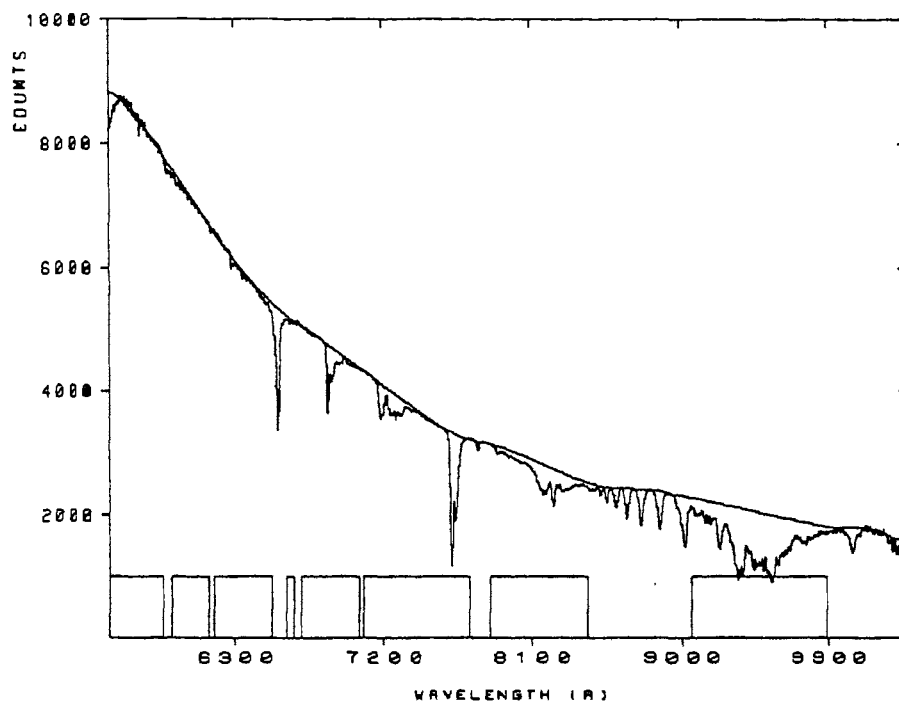


Figure 4.6. The spectrum of θ Crt, the spline continuum and location of windows for atmospheric absorption bands

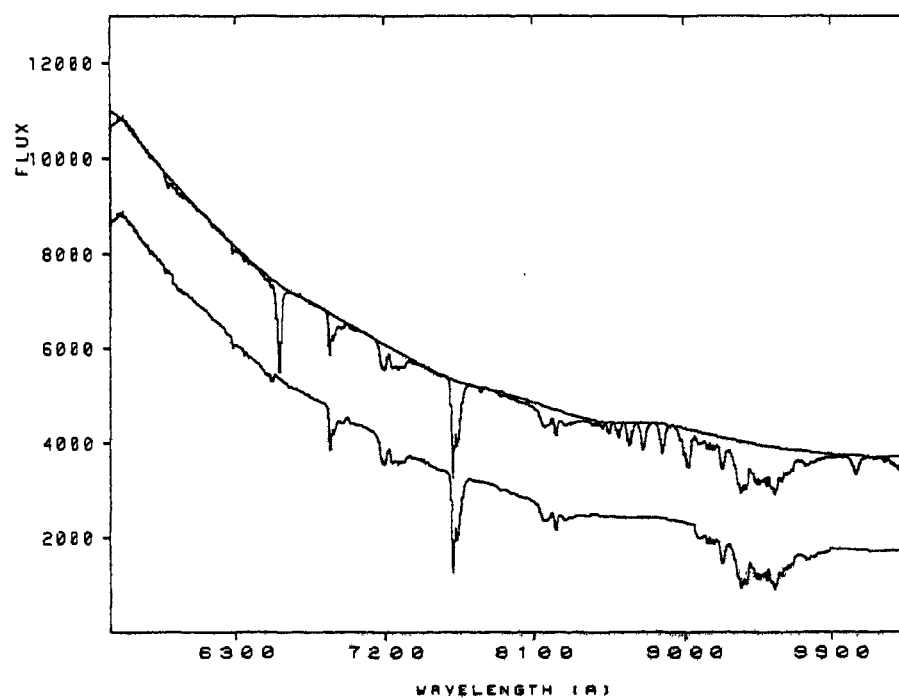


Figure 4.7. Spectrum of θ Crt, the spline continuum and (bottom) the spectrum containing only atmospheric absorption bands.

Dividing the spectrum by the continuum would give the fractional absorption at each pixel; the regions with stellar lines had to be excluded. A new star spectrum was required with the original spectrum within the windows and the spline continuum outside them. An inverse mask file was generated which was zero in the regions where the mask file was one and vice versa. Multiplying the original spectrum by the mask file and the continuum by the inverse mask and adding the two together produced the desired new spectrum. Figure 4.7 shows the original spectrum, the spline continuum and the new spectrum containing mainly atmospheric absorption bands for the star θ Crt. The upper spectrum has been shifted up for convenience of presentation. Dividing the new spectrum by the continuum file produced the fractional depression caused by atmospheric absorption at each pixel. This we shall call the 'ratio file'.

Dividing an object spectrum by the ratio file would push up the counts at the atmospheric absorptions and remove the absorptions, ideally, if the airmass of the early type star observation and the object observation to be corrected were the same. Since this was not the case, the ratio had to be corrected for the airmass. The change in intensity due to absorption in the atmosphere can be given by

$$I_{\text{obs}} = I_0 e^{-kx} \quad \dots (4.1)$$

where x is the airmass, k is a constant representing the coefficient of absorption, I_{obs} is the intensity observed and I_0 the incident intensity above the atmosphere. This equation can be rewritten as

$$\frac{I_{\text{obs}}}{I_0} = 10^{cx}, \text{ where } c \text{ is a constant } \dots (4.2)$$

If x_s is the airmass of observation of the standard star and x_p that for the program star then

$$\left(\frac{I_{\text{obs}}}{I_0} \right)_{\text{std. star}}^{1/x_s} = (10^{cx_s})^{1/x_s} = 10^c \quad \dots (4.3)$$

which effectively determines the constant, and

$$\left(\frac{I_{\text{obs}}}{I_0} \right)_{\text{program star}} = (10^c)^{x_p} = 10^{cx_p} \quad \dots (4.4)$$

Hence, assuming there is no absorption in the regions outside the windows, we have for the window regions containing absorption for the program star

$$I_0 = \frac{I_{\text{obsv}}}{10^{cx_p}} \quad \dots (4.5)$$

Equation 4.3 essentially converts the ratio file data in the mask window regions to unit airmass, assuming

again that the continuum represents I_0 , which is reasonably valid since the data were extinction corrected. The product of the original early type star spectrum and the mask file was hence raised to the power of the reciprocal of the airmass. The result was then raised to the power of the airmass of observation of the program star, the product of the continuum and inverse mask (essentially with value 1) was added to this and the resulting file divided into the observation of the program star, as in equation 4.5, to give the corrected spectrum.

In the window covering the region 8950 to 9900Å, two strong lines of the Paschen series of hydrogen, P8 at 9545.8Å and P9 at 9229.02Å, which are present in early type stars create 'emission' lines in the program object spectra when the above procedure is followed. This problem was eliminated by fitting a local continuum to the dips at the positions of these lines in the ratio file. The dips were replaced by the local continuum.

This procedure for removal of atmospheric absorption bands was followed for all objects observed. Figures 4.8 and 4.9 illustrate the results of this correction for the star GL 488 and the galaxy NGC 4472, respectively. The 9200Å region, especially for long

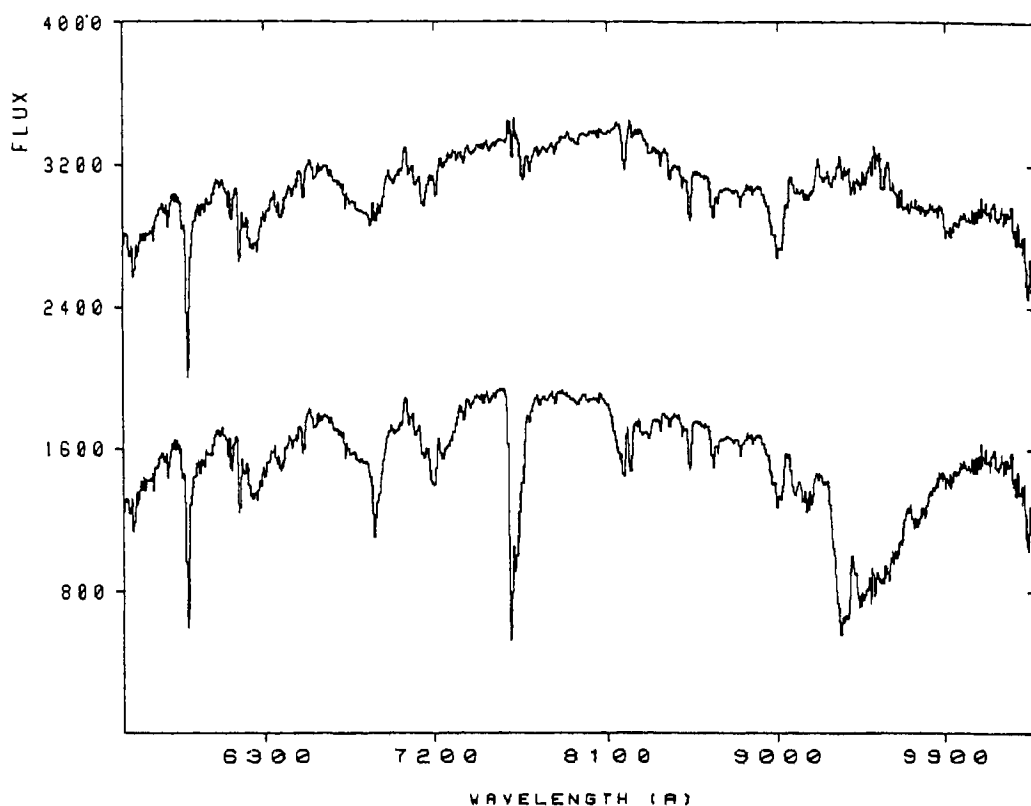


Figure 4.8. Flux calibrated spectrum of GL 488 and (top) the same spectrum after removal of atmospheric absorption bands.

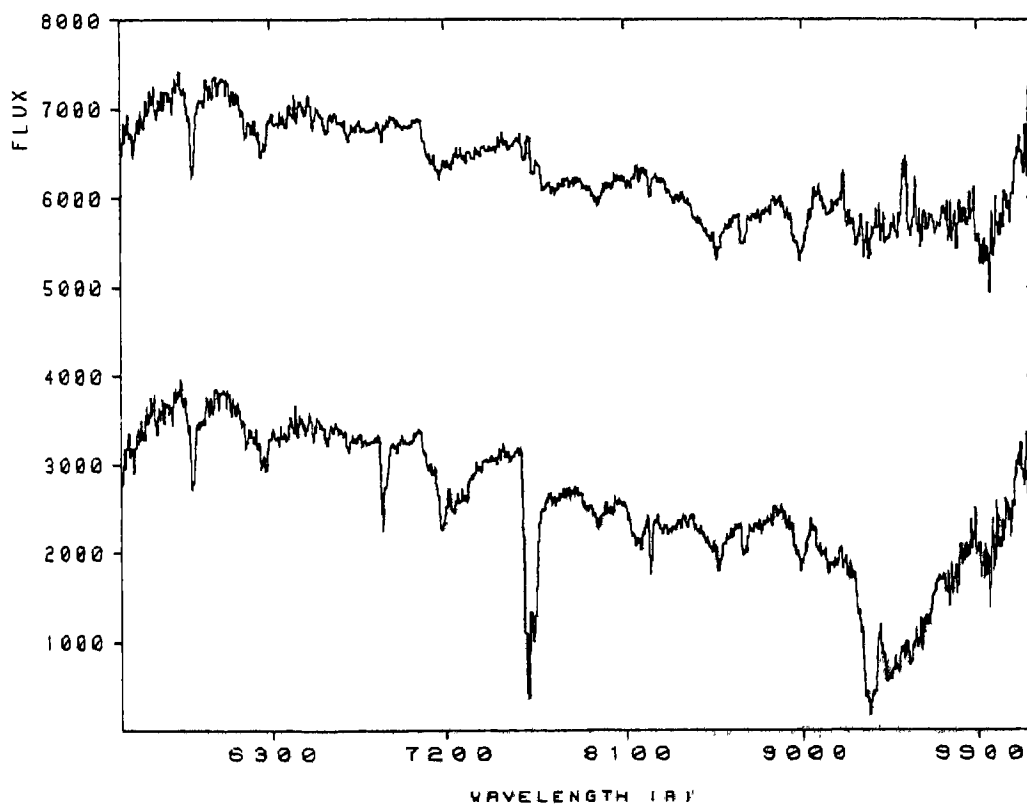


Figure 4.9. Flux calibrated spectrum of NGC 4472 and (top) after removal of atmospheric absorption bands.

galaxy exposures cannot be corrected very well. Care was taken to ensure that there were no relative shifts in wavelength scale between the early type star and the program objects.

IV.2.2. Residual wavelength correction and rebinning of star spectra for synthesis

The spectra of the stars observed for inclusion in the stellar library were examined carefully at the full resolution of the Tektronix graphics terminal at VBO, for small zero point shifts in wavelength. The cursor was placed at the line centres (usually the absorption line minimum points) of known lines in the spectrum and the wavelengths were determined. At times, for symmetric lines, a gaussian profile fitting technique was also used to determine the wavelengths. The wavelengths were compared with the known wavelengths for these lines; at the resolution of the observations, shifts due to velocity of motion of the stars are expected to be negligible. In some cases, where small shifts were found (usually the equivalent of less than one pixel), the data were shifted with respect to the wavelength scale using a sinc interpolation algorithm available in the SPICA package.

After corrections for redshifts to the spectra (discussed later) of galaxies, all spectra were examined to determine the exact wavelength range to be used for population synthesis. This range was from 5543⁰Å

to 10000\AA . Since the resolution of the observations was 6\AA , it was decided that synthesis would be done to exploit this resolution for the galaxy spectra.

The spectra in the SLP were in pixels of 3\AA and those for the stars observed here in pixels of 2\AA . All the spectra were rebinned to a linear scale with a pixel size corresponding to 1\AA . After this, it was seen that the centres of pixels in the SLP data were integral wavelengths whereas for the data observed here, they were half-integral wavelengths. The latter data were made to have integral wavelengths at pixel centres, using an interpolation technique. This shift of 0.5\AA does not make any substantial difference, given the resolution of 6\AA . The final set of spectra from both sources were rebinned to 6\AA per pixel, giving 743 pixels covering the wavelength range 5542.5\AA to 10000.5\AA , from the left side edge of pixel 1 to the right side edge of pixel 743. The SLP data as received on tape was normalised to a value of 100 in the wavelength region 5450 to 5500\AA . The 6\AA data set (including the SLP data) were renormalised to a value of 100 at pixel containing the wavelength 5556\AA . The SLP data have not been corrected for reddening, since each stellar group contains a range of objects with a spread in $(V-R)_c$ colour; dereddening the data would have only increased this range (Pickles 1985a). The observations

of stars obtained in this study were also not corrected for reddening, since they were to be used to augment the SLP library.

IV.2.3. Parameters of stellar group spectra

The parameters of the stellar groups in the SLP library are given in Table 4.3; these are reproduced from Pickles (1985a). The photometric colours were measured from the flux calibrated spectra by convolving the filter transmission functions for the UBV system called the Johnson system (see Blanco et al 1968) and the VRI system known as the Kron-Cousins system (Cousins 1980). The filter transmissions for the former system were obtained from Buser (1978) and that for the latter from Bessell (1983-R and I filters only). The standard method was used by Pickles (1985a) to derive the magnitudes and colours. Using the same notation as in Section IV.1.8, the magnitude through a given filter is

$$\text{Magnitude} = \text{constant} - 2.5 \log \langle F_\nu \rangle - 48.60 \quad (4.6)$$

where the flux per unit frequency through the filter is given by

$$\langle F_\nu \rangle = \frac{\int_0^{b_0} F(\nu) R(\nu) d\nu}{\int_0^{b_0} R(\nu) d\nu} = \frac{\int_0^{\infty} F(\lambda) R(\lambda) d\lambda}{\int_0^{\infty} R(\lambda) \frac{c}{\lambda^2} d\lambda}$$

Table 4.3

Parameters of stellar groups in the standard synthesis library of Pickles (1985a)

| Group No. | Name | Measured (Pickles 1985a) | | | Measured (this work) (R-I) _c | Updated Group (R-I) _c | Assigned (Pickles 1985a) | | | Assigned (this work) M _v | |
|---------------|-------|--------------------------|--------------------|--------------------|---|----------------------------------|--------------------------|----------------|------------------|-------------------------------------|-------|
| | | B-V | (V-R) _c | (R-I) _c | | | log T _e | M _v | M/M ₀ | | Fe/H |
| 1. | 2. | 3. | 4. | 5. | 6. | 7. | 8. | 9. | 10. | 11. | 12. |
| <u>Dwarfs</u> | | | | | | | | | | | |
| 1 | 07-9 | -0.32 | -0.16 | -0.14 | -0.147 | -0.147 | 4.53 | -5.1 | 30 | Solar | -5.1 |
| 2 | B1-3 | -0.18 | -0.09 | -0.13 | -0.133 | -0.105* | 4.23 | -1.9 | 10 | " | -2.4 |
| 3 | B4-5 | -0.14 | -0.05 | (0.01) | 0.013 | 0.013 | 4.14 | -0.8 | 6 | " | -1.2 |
| 4 | B6-9 | 0.0 | (0.06) | -0.03 | -0.028 | -0.028 | 3.98 | 0.4 | 4 | " | -0.25 |
| 5 | A0-3 | 0.05 | 0.01 | 0.04 | 0.045 | 0.045 | 3.95 | 1.2 | 3 | " | 0.83 |
| 6 | A4-6 | (0.34) | 0.09 | 0.14 | 0.134 | 0.134 | 3.89 | 2.2 | 2 | " | 1.47 |
| 7 | A7-F1 | 0.27 | 0.18 | 0.23 | 0.231 | 0.231 | 3.87 | 3.0 | 1.5 | " | 2.93 |
| 8 | F2-4 | 0.41 | 0.21 | 0.26 | 0.256 | 0.256 | 3.82 | 3.5 | 1.4 | " | 3.28 |
| 9 | F5-6 | 0.49 | 0.26 | 0.25 | 0.253 | 0.253 | 3.80 | 3.8 | 1.3 | " | 3.94 |
| 10 | F7-8 | 0.55 | 0.34 | 0.30 | 0.296 | 0.296 | 3.78 | 4.2 | 1.1 | " | 3.88 |
| 11 | G0-4 | 0.64 | 0.35 | 0.37 | 0.366 | 0.366 | 3.76 | 4.5 | 1.05 | " | 3.93 |
| 12 | G5-8 | 0.70 | 0.37 | 0.37 | 0.370 | 0.370 | 3.75 | 4.9 | 1.0 | " | 4.46 |
| 13 | K0-1 | 0.76 | 0.45 | 0.39 | 0.394 | 0.394 | 3.72 | 5.6 | 0.8 | " | 5.91 |
| 14 | K2-3 | 0.98 | 0.56 | 0.50 | 0.498 | 0.498 | 3.68 | 6.5 | 0.7 | " | 6.89 |
| 15 | K4-7 | 1.13 | 0.68 | 0.61 | 0.611 | 0.625* | 3.65 | 7.3 | 0.6 | " | 8.2 |
| 16 | M0-2 | 1.39 | 0.90 | 1.03 | 1.024 | 0.938* | 3.58 | 9.2 | 0.5 | " | 9.74 |
| 17 | M3 | 1.51 | 1.07 | 1.32 | 1.315 | 1.315 | 3.55 | 10.8 | 0.3 | " | 11.55 |
| 18 | M4 | 1.60 | 1.25 | 1.57 | 1.550 | 1.577* | 3.52 | 13.0 | 0.2 | " | 13.02 |
| 19 | M5-6 | 1.60 | 1.27 | 1.71 | 1.695 | 1.651 | 3.50 | 14.0 | 0.15 | " | 14.27 |

Table 4.3 contd.

| 1. | 2. | 3. | 4. | 5. | 6. | 7. | 8. | 9. | 10. | 11. | 12. |
|-------------------------|----------|------|------|------|--------|--------|-------|------|-----|-------|-------|
| 20 | Early G | 0.71 | 0.32 | 0.38 | 0.376 | 0.376 | 3.76 | 4.1 | 1.1 | Solar | 3.79 |
| 21 | Mid G | 0.76 | 0.39 | 0.39 | 0.386 | 0.386 | 3.735 | 3.8 | 1.1 | " | 3.80 |
| 22 | Late G | 0.84 | 0.47 | 0.47 | 0.465 | 0.465 | 3.71 | 4.0 | 1.1 | " | 3.89 |
| <u>Sub-Giants</u> | | | | | | | | | | | |
| 23 | B | 0.0 | 0.05 | 0.04 | 0.041 | 0.041 | 3.98 | -0.6 | 1.1 | Solar | -0.6 |
| 24 | Early A | 0.19 | 0.07 | 0.08 | 0.083 | 0.083 | 3.90 | 0.7 | 1.1 | " | 0.7 |
| 25 | A7-F0 | 0.32 | 0.16 | 0.19 | 0.196 | 0.196 | 3.85 | 0.3 | 1.1 | " | 1.5 |
| 26 | Late F | 0.42 | 0.28 | 0.26 | 0.263 | 0.263 | 3.81 | 0.2 | 1.1 | " | 1.6 |
| 27 | G5-9 | 0.91 | 0.48 | 0.44 | 0.441 | 0.441 | 3.69 | 4.1 | 1.1 | " | 3.37 |
| <u>Normal Giants</u> | | | | | | | | | | | |
| 28 | K0-1 | 0.98 | 0.52 | 0.47 | 0.467 | 0.467 | 3.68 | 3.6 | 1.1 | " | 2.04 |
| 29 | K2 | 1.11 | 0.57 | 0.53 | 0.526 | 0.526 | 3.66 | 2.5 | 1.1 | " | 0.9 |
| 30 | K3 | 1.19 | 0.64 | 0.57 | 0.555 | 0.555 | 3.63 | 1.2 | 1.1 | " | 0.38 |
| 31 | K4 | 1.56 | 0.73 | 0.64 | 0.631* | 0.631* | 3.60 | 0.3 | 1.1 | " | -0.31 |
| 32 | K5 | 1.44 | 0.77 | 0.78 | 0.781 | 0.781 | 3.59 | 0.0 | 1.1 | " | -0.56 |
| 33 | M0-2 | 1.57 | 0.87 | 0.95 | 0.943 | 0.943 | 3.56 | -0.7 | 1.1 | " | -0.77 |
| 34 | M3 | 1.61 | 1.02 | 1.19 | 1.138* | 1.138* | 3.52 | -1.3 | 1.1 | " | -1.2 |
| 35 | M4 | 1.54 | 1.14 | 1.49 | 1.487 | 1.487 | 3.49 | -1.3 | 1.1 | " | -1.09 |
| 36 | M5 | 1.56 | 1.27 | 1.68 | 1.684 | 1.684 | 3.48 | -1.3 | 1.1 | " | -1.3 |
| 37 | M6 | 1.43 | 1.50 | 1.94 | 1.916 | 1.916 | 3.47 | -1.3 | 1.1 | " | -1.3 |
| <u>Metal-Rich Giant</u> | | | | | | | | | | | |
| 38 | mr G5-K0 | 0.89 | 0.51 | 0.43 | 0.432 | 0.432 | 3.69 | 4.3 | 1.2 | 0.3 | 4.22 |
| 39 | mr K1-2 | 1.10 | 0.58 | 0.52 | 0.524 | 0.524 | 3.66 | 3.7 | 1.2 | 0.3 | 1.83 |
| 40 | mr K3 | 1.25 | 0.61 | 0.57 | 0.568 | 0.568 | 3.63 | 2.0 | 1.2 | 0.2 | 1.38 |

$F(\nu)$ is in $\text{ergs cm}^{-2} \text{ sec}^{-1} \text{ Hz}^{-1}$

$F(\lambda)$ is in $\text{ergs cm}^{-2} \text{ sec}^{-1} \text{ \AA}^{-1}$

$R(\nu)$ and $R(\lambda)$ specify the filter transmission at values of the frequency ν and wavelength λ

The discretised form of the above is

$$\langle F_\nu \rangle = \frac{\sum F_i R_i}{\sum R_i \frac{c}{\lambda^2}} \quad \begin{array}{l} \text{ergs cm}^{-2} \text{ sec}^{-1} \text{ through the} \\ \text{filter} \end{array} \quad \dots \quad (4.7)$$

The constants in the magnitude definitions were derived (by Pickles) using a calibration on the Vilnius Standard Spectra (VSS). The colours derived for the VSS stellar types were compared with values given by Buser (1978) for UBV and by Cousins (1981) for VRI; with the constants determined, the colours for the 47 stellar types in the VSS were found to fit very well in the range $-0.16 < (V-R)_c < 1.2$ (spectral types O to M4), with the latest type M stars showing significant residuals. Since Pickles did not observe all the late type group stars to the red limit (8900\AA) of the R and I filters, he created a truncated filter set with the R and I filters cutting off at 8250\AA . The colours derived using the truncated set were again fitted to the true $(V-R)_c$ and $(R-I)_c$ colours and a well fitting linear relation was found, which could be used to derive measured $(V-R)_c$ and $(R-I)_c$ colours. The mean

standard deviations derived from the fits were 0.011 mag for $(V-R)_c$ and 0.007 mag for $(R-I)_c$.

The stars observed in this work were to be added to the SLP library; it was thus necessary to derive colours from the spectra, to decide the stellar group to which they would be added. The wavelength region covered by the observations here permitted the derivation of the $(R-I)_c$ colours only. The $(R-I)_c$ colours were calculated by us for the SLP spectra, using the R and I filter definitions from Bessel (1983). Since the SLP spectra available to us were normalised spectra, the filter magnitudes could not be calculated. The $(R-I)$ colour is given by

$$(R-I) = \text{constant} + 2.5 \log \langle F_\nu^n \rangle_I - 2.5 \log \langle F_\nu^n \rangle_R \quad \dots (4.8)$$

where $\langle F_\nu^n \rangle_R$ and $\langle F_\nu^n \rangle_I$ are calculated using the normalised spectra and equation (4.7). The constant in equation (4.8) was determined by comparison of the $(R-I)$ colours with those measured by Pickles (1985). The $(R-I)_c$ colours measured by Pickles and calculated here for the stellar types in the SLP library are given in Table 4.3. The values agree quite well and it was clear that the method of calculating colours using 4.8 could be used for the observations in this program.

The $(R-I)_c$ colours were calculated for the stars observed here. Table 4.4 lists the stars observed and available $(R-I)_c$ colours as well as the colours calculated here. Assignment of the stars to groups was done on the basis of comparison of calculated colour and the group colour in Table 4.3. Some of the group $(R-I)_c$ colours incorporate a large range; in such cases a comparison of the calculated colour was made with the catalog colour (sources are indicated in Table 3.2) for the individual star as well as catalog colours (Cousins 1981) for standard stellar types. The spectral types of the stars are given in Table 3.2. The case of GL 699 (Barnard's star) merits more discussion. The catalog colour of 1.562 (Gliese 1969) for this star, as well as the mean stellar type colour of 1.552 (Cousins, 1981) would place this star in the M5-6 dwarf group. The colour calculated for this SLP group is 1.695 and that for the star itself is 1.605. The star would seem to lie in between groups 18 (M4 dwarf) and 19 (M5-6 dwarfs). An examination of the spectrum (Figure 4.10) showed it to be of a type intermediate between the spectra of the two groups. The spectral classification by Wing and Dean (1983) assigns a type of M3.8. It was finally decided to average the spectrum with those of groups 18 as well as 19.

Table 4.4

(R-I)_c Colours of Stars Observed

| Star Name | Catalog (R-I) _c | Calcula- ted (R-I) _c | Standard Stellar group assigned (number as in Table 4.3) |
|-----------|-------------------------------|---------------------------------------|---|
| γ Pyx | 0.582 | 0.617 | 31 |
| GL 453 | 0.545 | 0.560 | 15 |
| GL 296 | 0.768 | 0.672 | 15 |
| GL 488 | 0.838 | 0.812 | 16 |
| GL 526 | 1.092 | 1.045 | 16 |
| HD 112142 | 1.177 | 1.138 | 34 |
| GL 699 | 1.562 | 1.605 | 18, 19 |
| R Leo | - | 2.685 | - |
| γ Hya | | -0.08 | 2 |
| θ Crt | | -0.016 | 3 |
| θ Vir | | 0.02 | 5 |
| 58 Aql | | 0.093 | 6 |

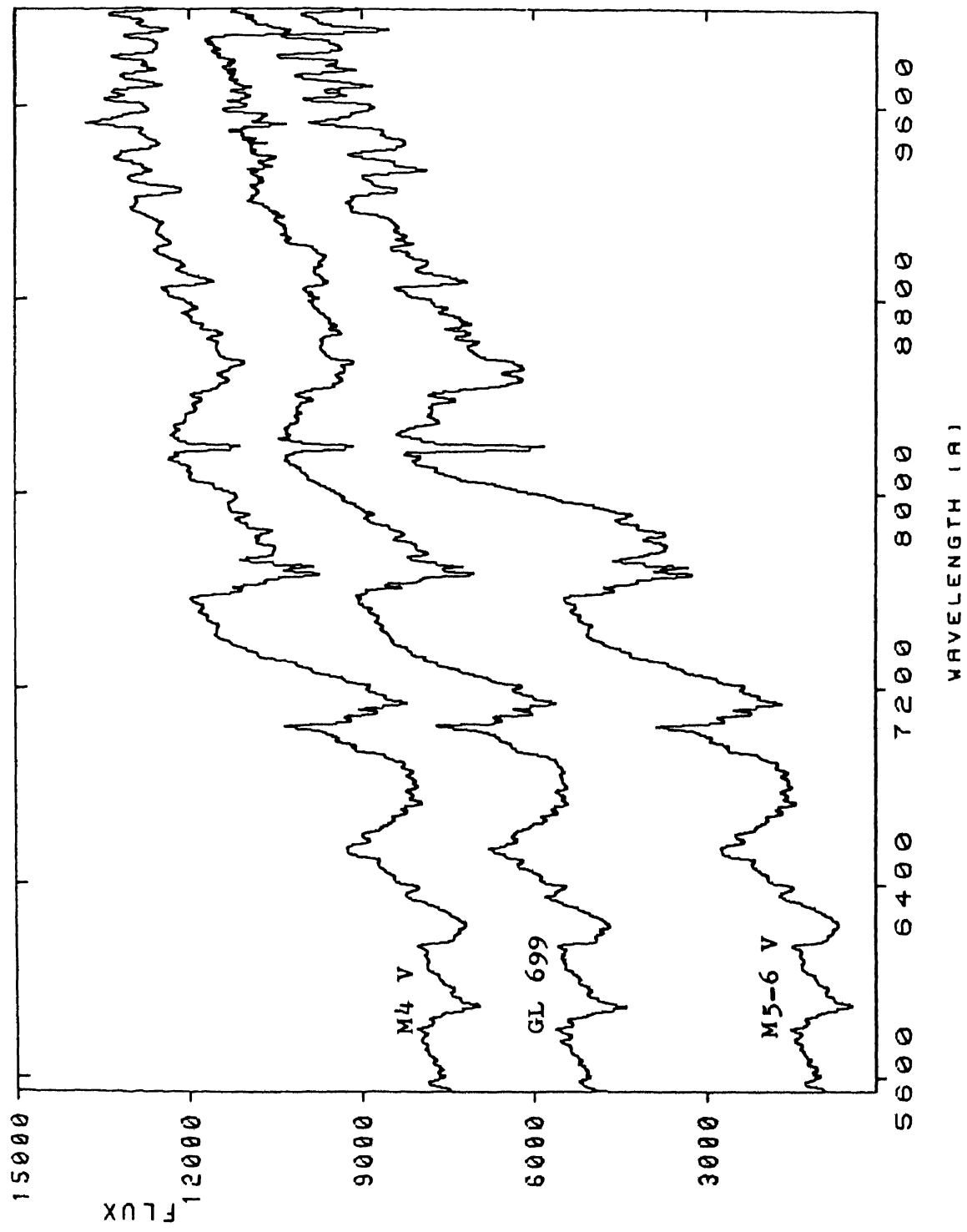


Figure 4.10. Spectrum of a mean M4 dwarf (top), GL 699 (middle), mean M5-6 dwarf (bottom).

IV.2.4. Augmented Stellar Library for Synthesis

The spectra of the stars observed here, as well as the spectra of the groups to which they are assigned as taken from the SLP data, are shown in Figures 4.11a to g. In some cases (Figures 4.11a, b, c, g), the spectrum of the star observed in this program (middle spectrum) was averaged with the group spectrum from SLP. The averaged spectra (showed on top) were then taken as representing the group in the augmented stellar library (hereafter called ASL). In other cases (Figures 4.11d, e and f), the spectra obtained in this study (top) were judged to be superior to the existing one in the SLP (bottom) and were taken to represent the group in the ASL. All the spectra in Figure 4.10 and Figure 4.11 are normalised to a value of 100 at 5556\AA ; the counts plotted are scaled up by 100 for convenience of display. The spectra are also shifted up or down, to avoid overlapping.

The spectra of the groups in the ASL are plotted in Figures 4.12a to 4.12o. All spectra are normalised to a value of 100 at 5556\AA ; the plotted values are scaled up and shifted relative to each other for convenience of plotting. Prominent spectral features are marked in the plots. In Table 4.3 and in the plots of spectra, the group names indicate the spectral type range i.e. M0-2 indicates spectral types M0 to M2.

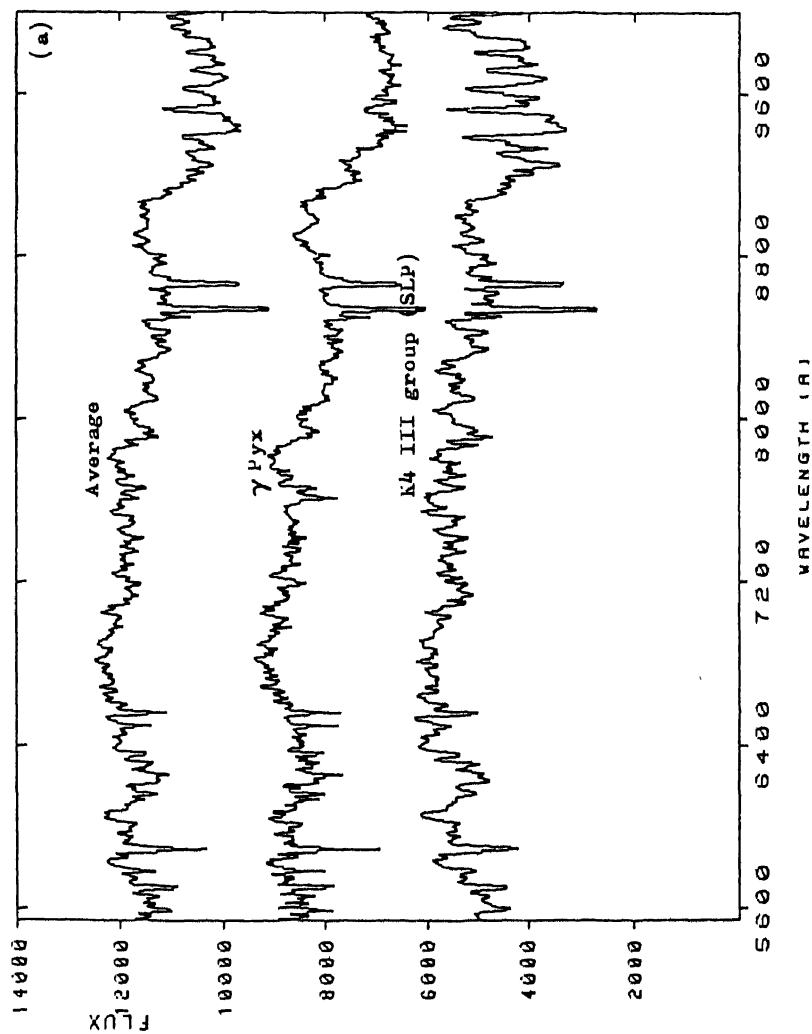


Figure 4.11. Stellar group spectra from the library of Pickles (1985a, denoted SLP and shown at bottom). The spectra obtained in the current program for the same group (middle or top) are also shown above the corresponding group spectra. Third spectrum (top most) when present is the average of the two.

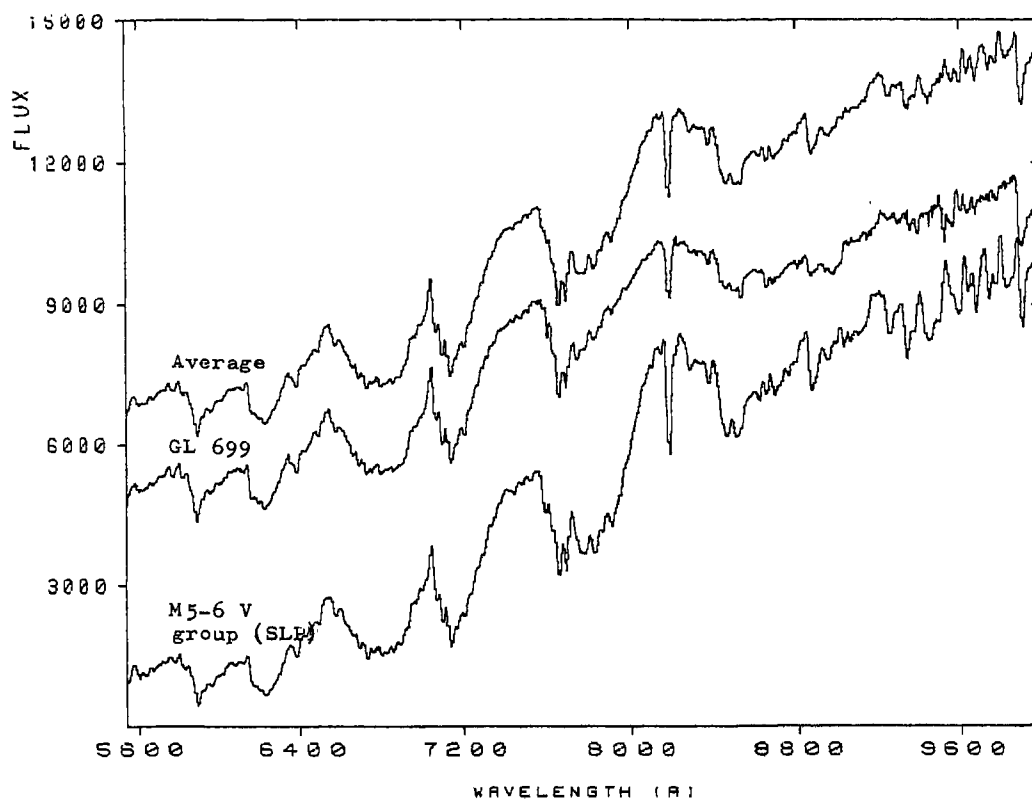


Figure 4.11(b).

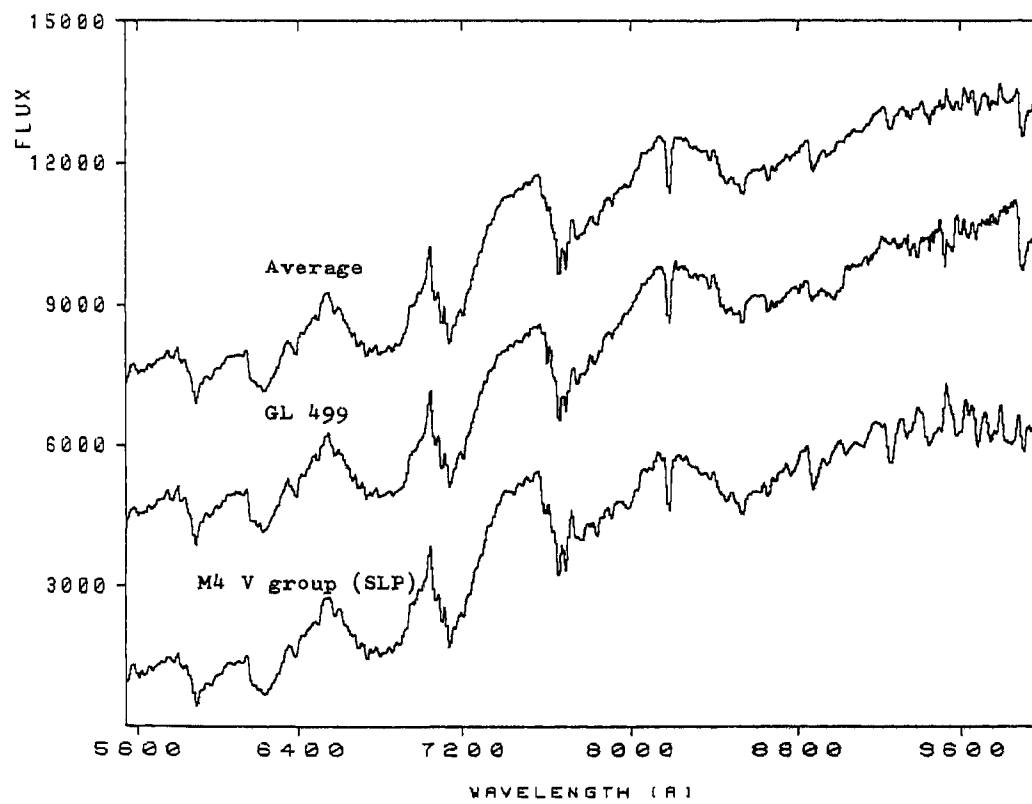


Figure 4.11(c)

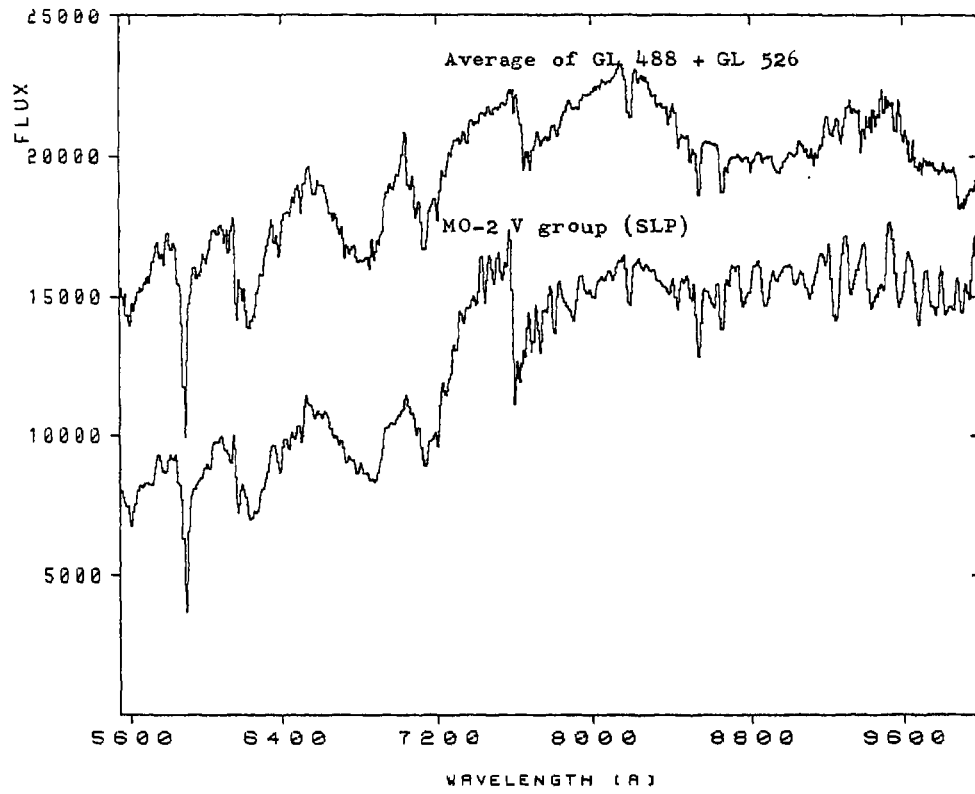


Figure 4.11(d)

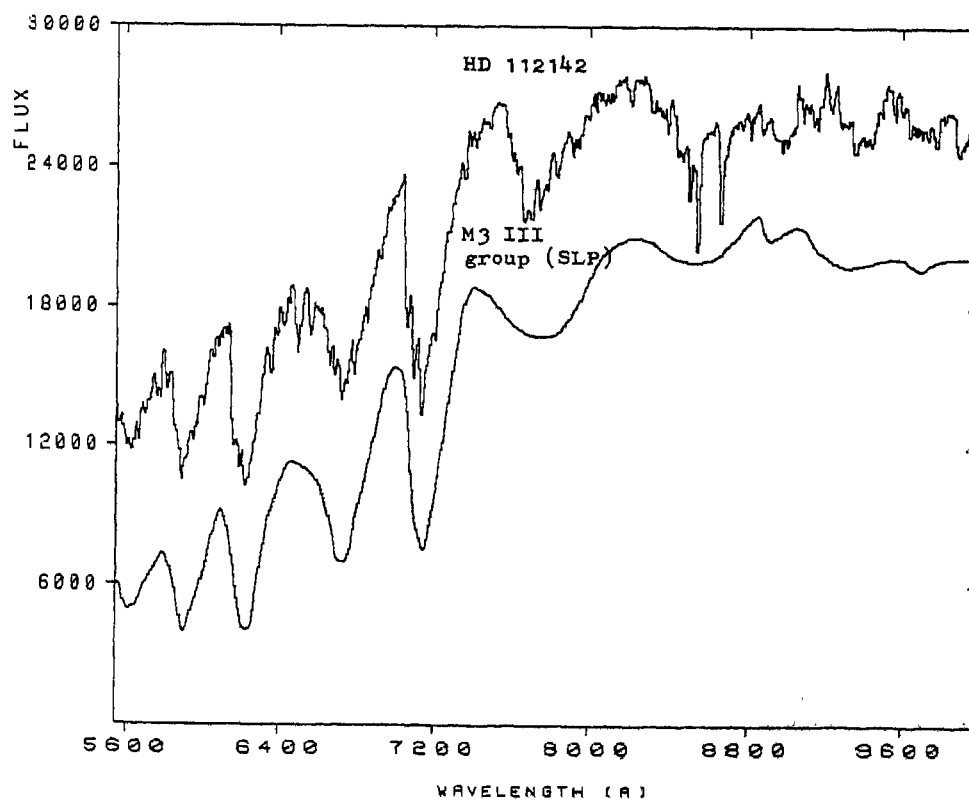


Figure 4.11(e)

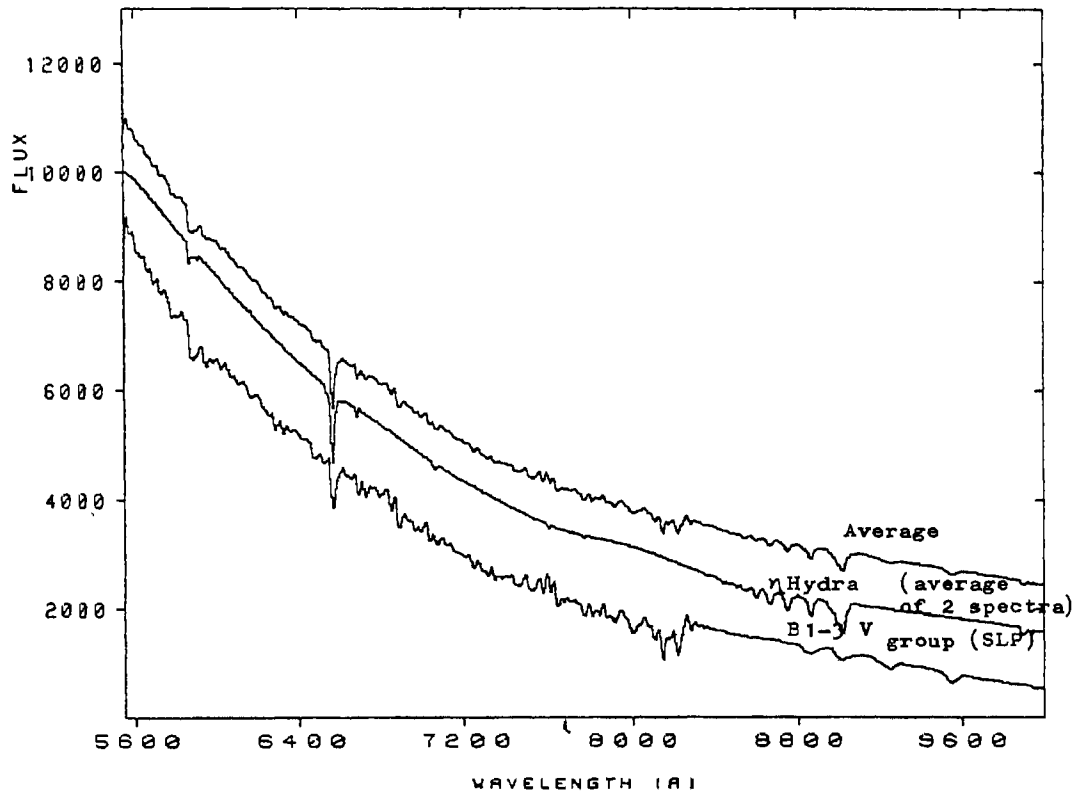


Figure 4.11(g)

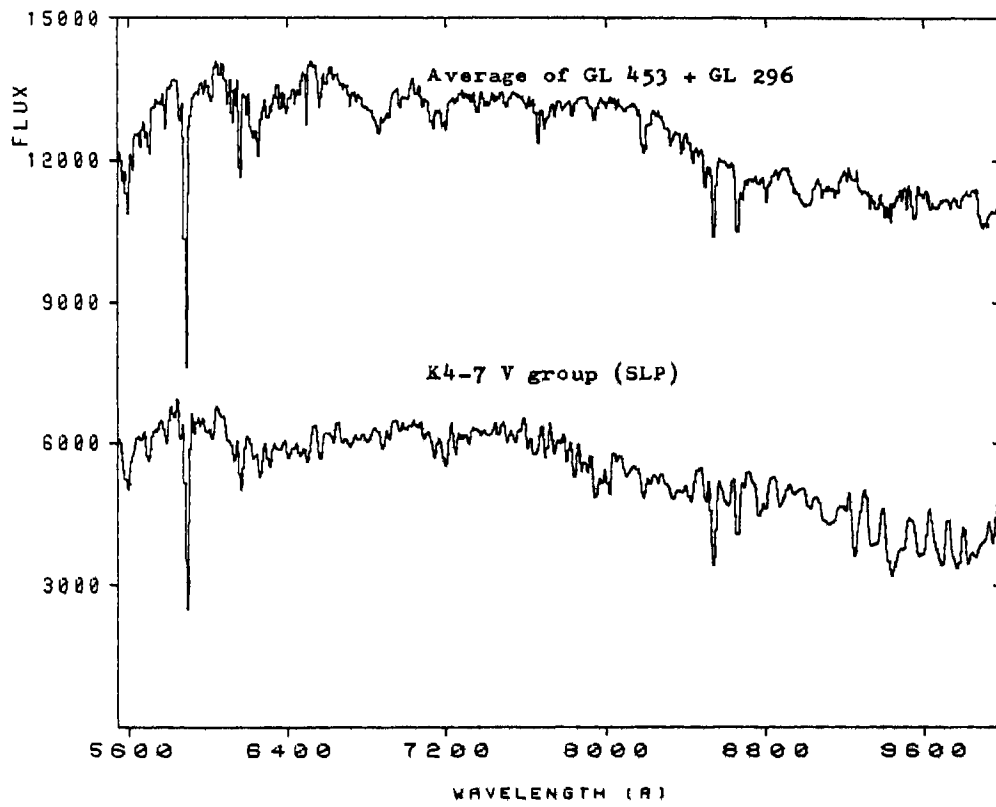


Figure 4.11(f)

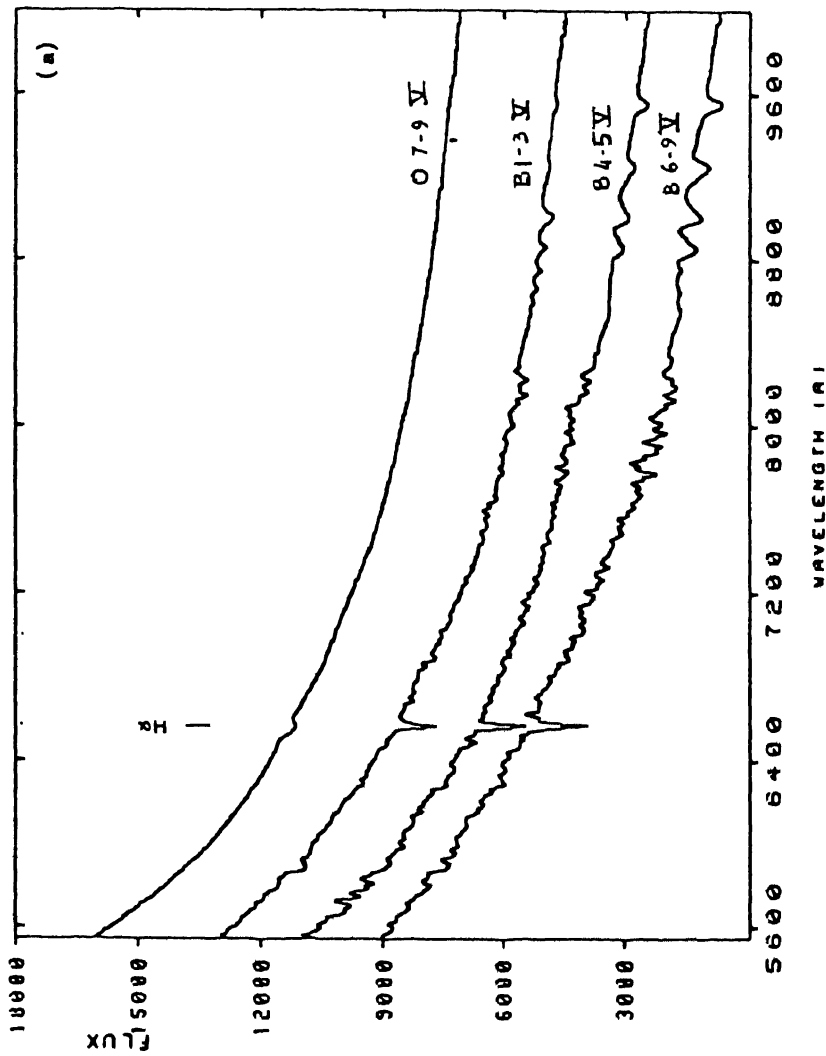


Figure 4.12. Spectra of the entire augmented stellar library, normalized to a value of 100 at $\lambda 5556\text{\AA}$. The numbers are scaled by a factor of $\times 10^2$ and individual spectra are shifted with respect to each other for convenience of plotting.

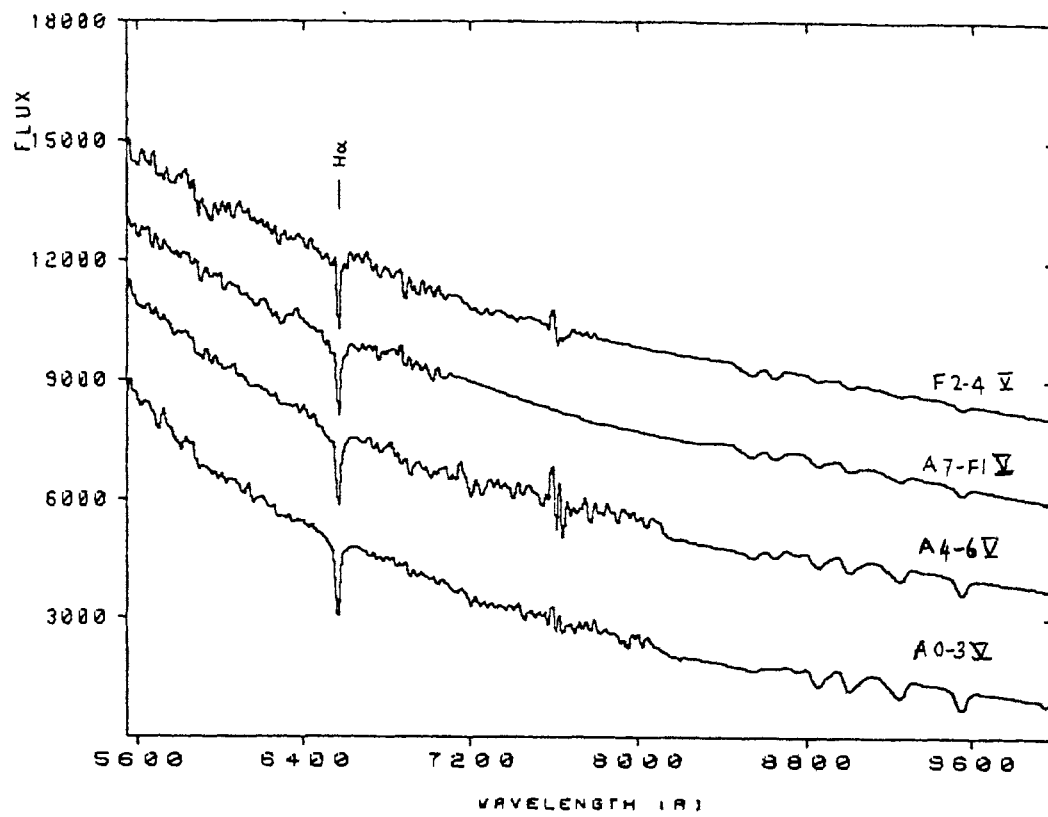


Figure 4.12(b)

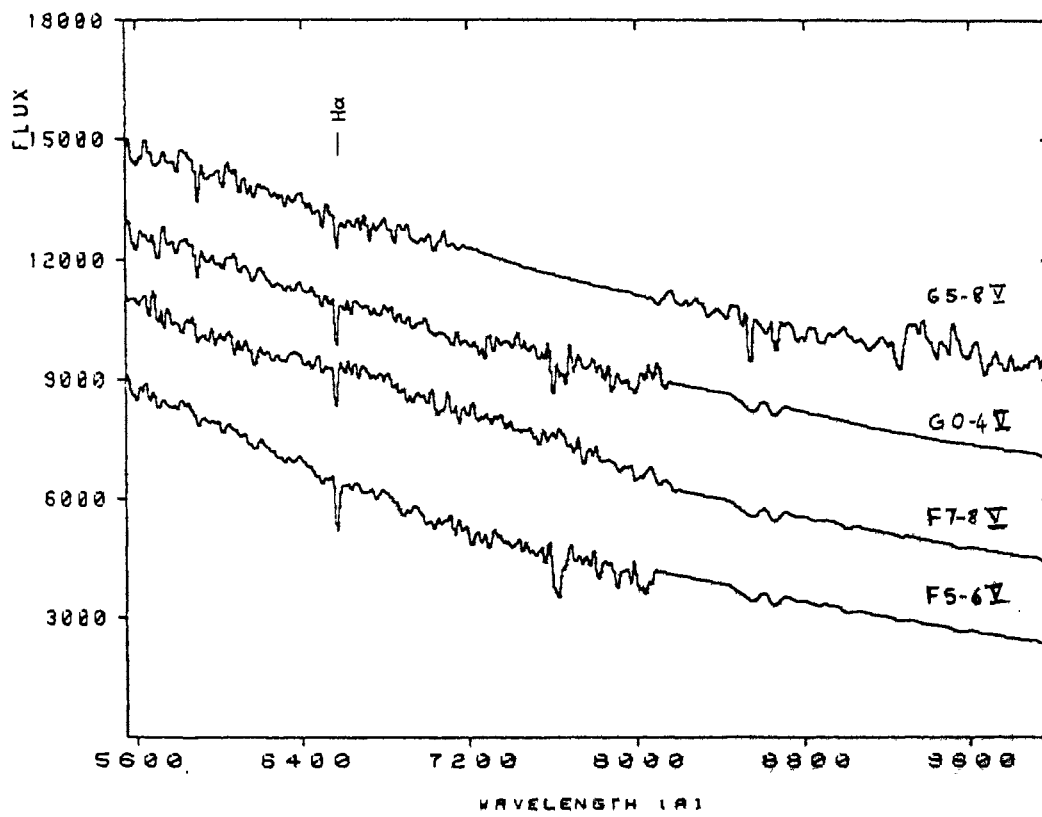


Figure 4.12(c)

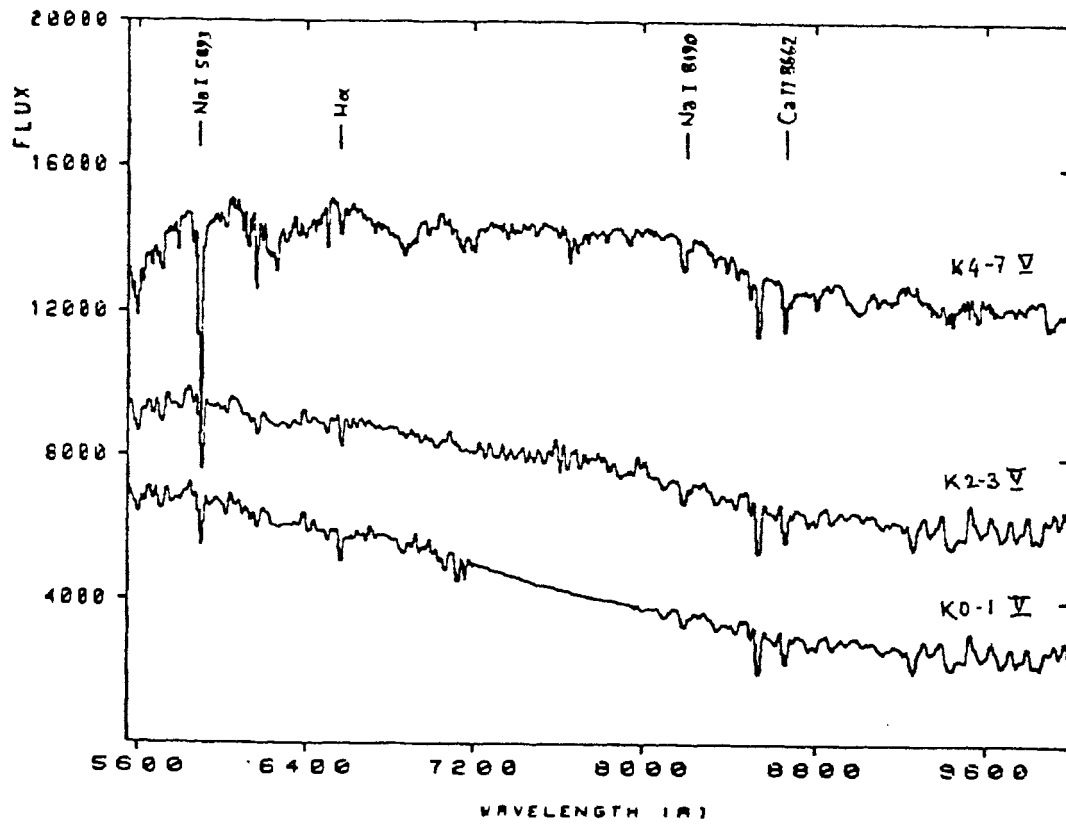


Figure 4.12(d)

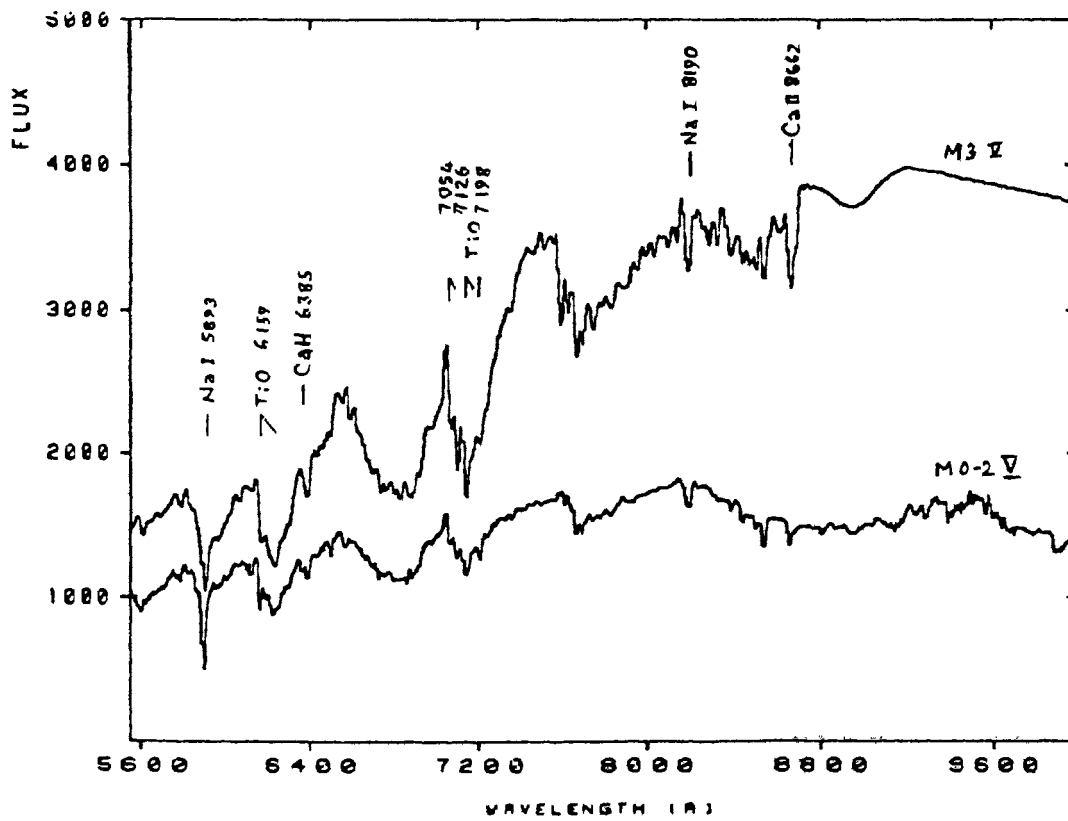


Figure 4.12(e)

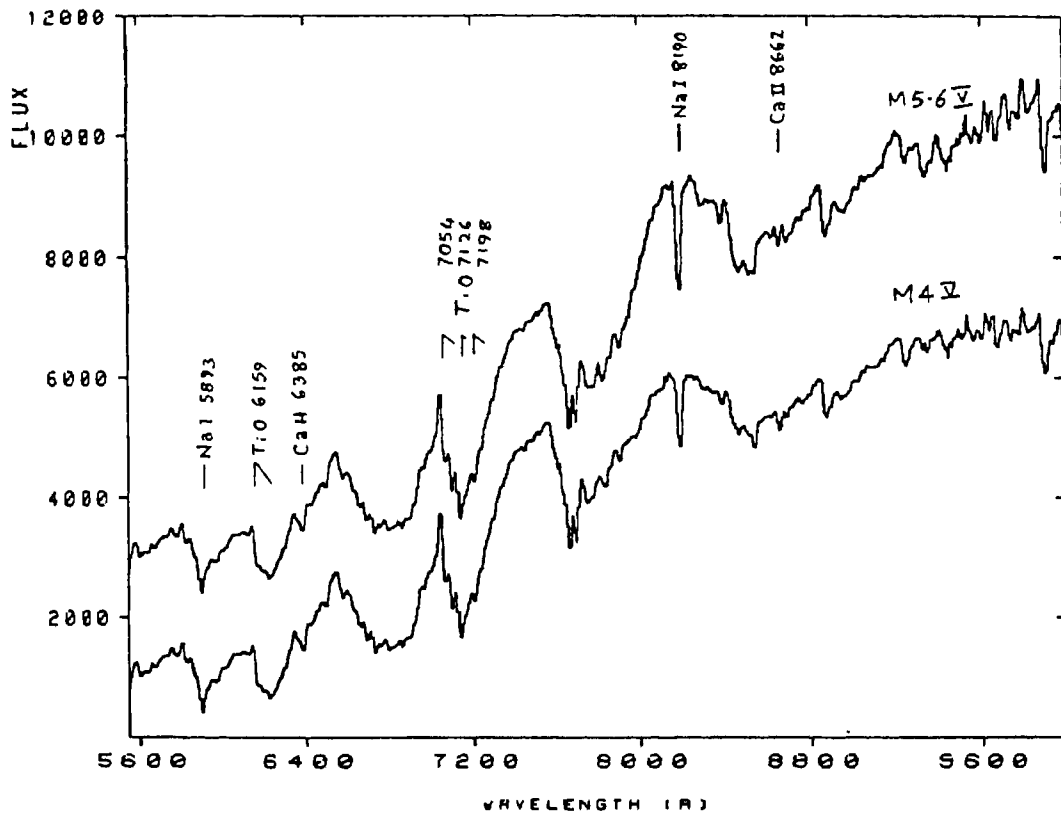


Figure 4.12(f)

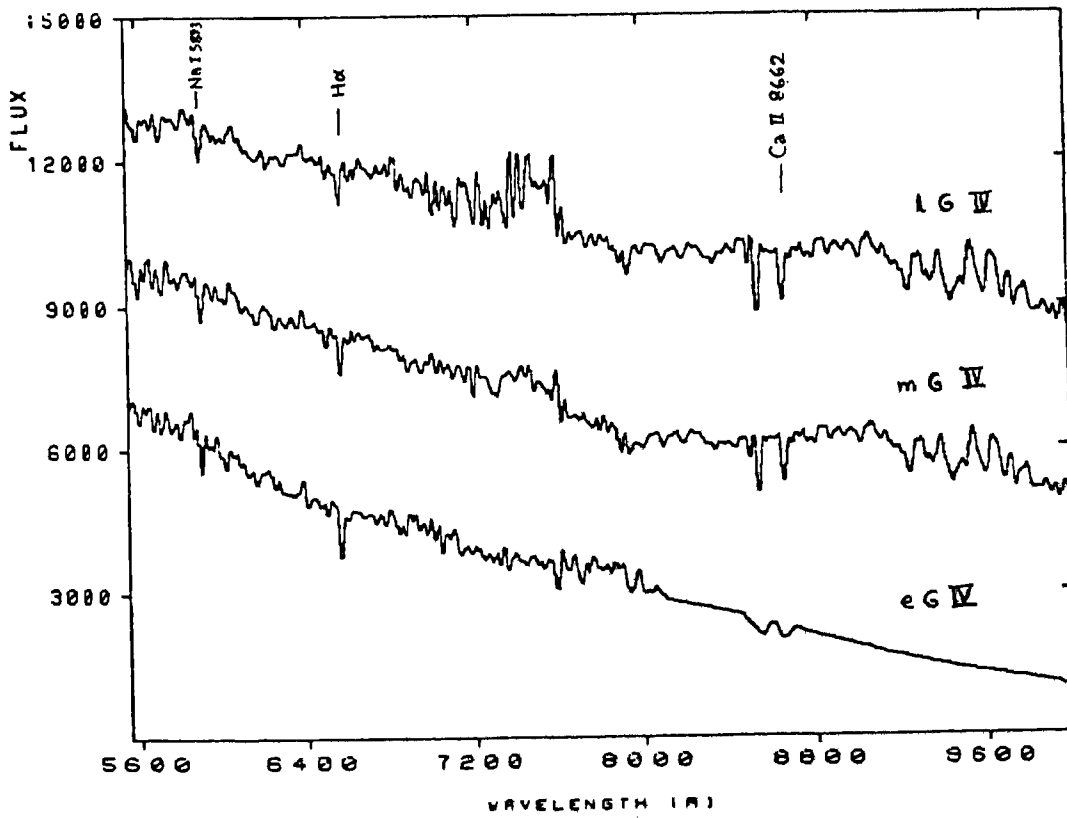


Figure 4.12(g)

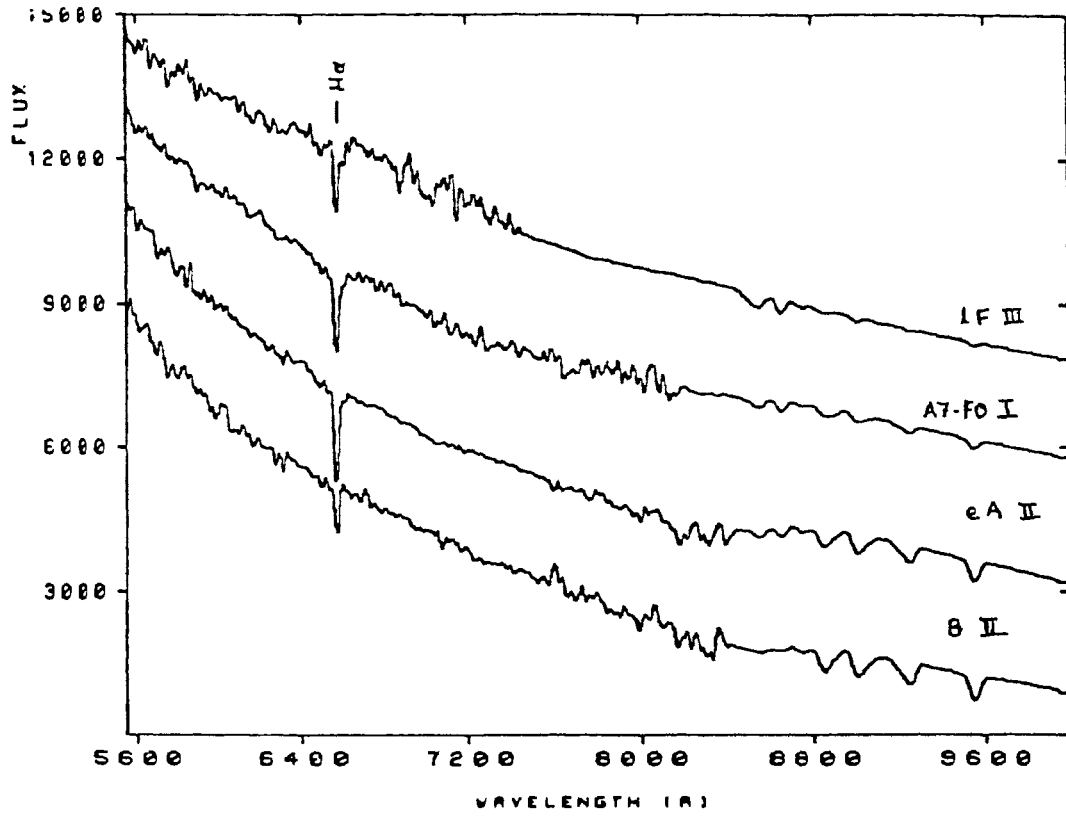


Figure 4.12(h)

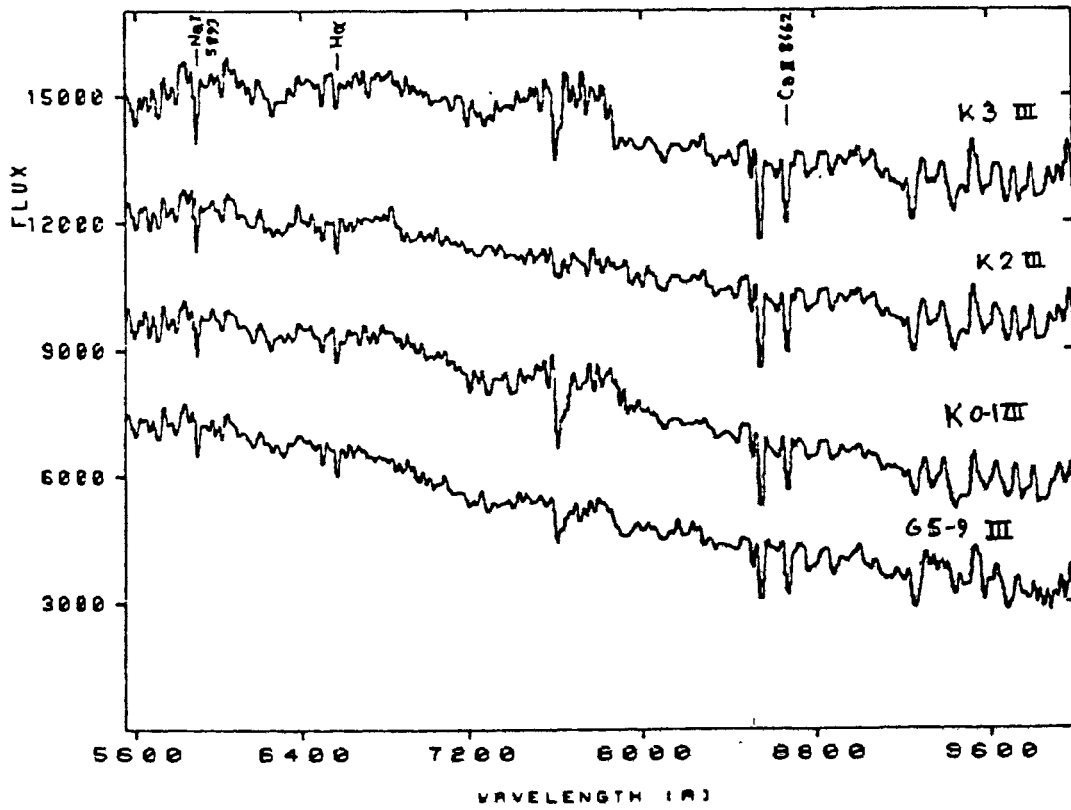


Figure 4.12(i)

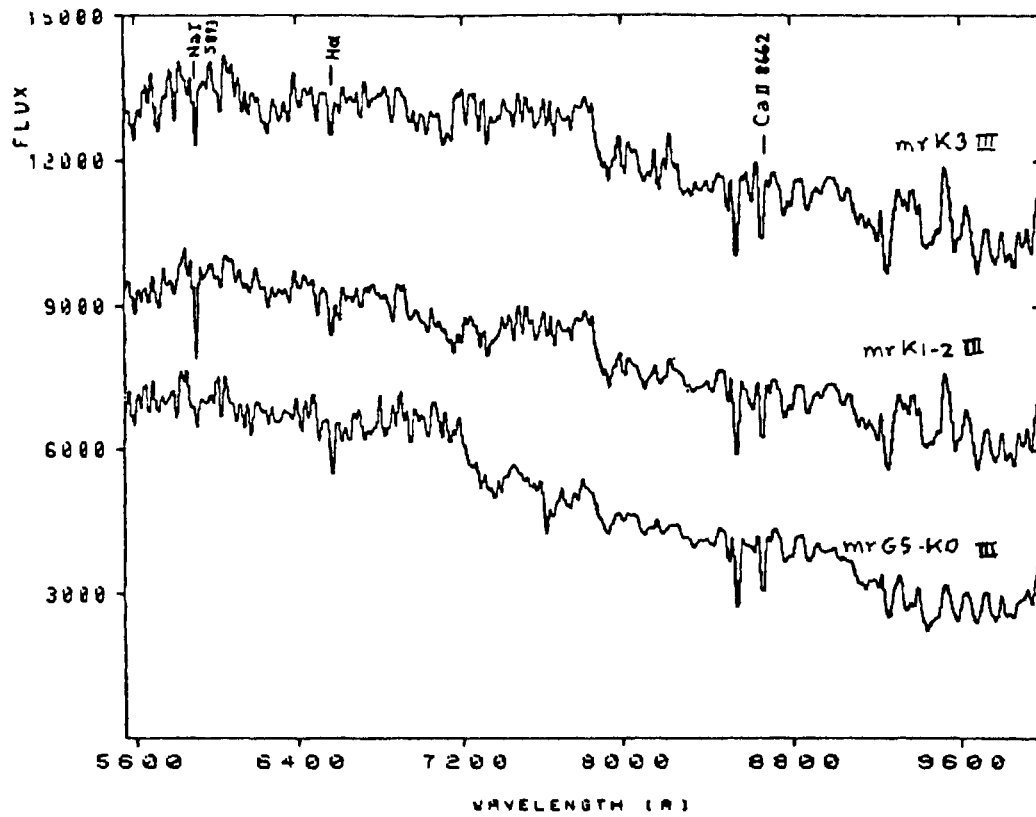


Figure 4.12(j)

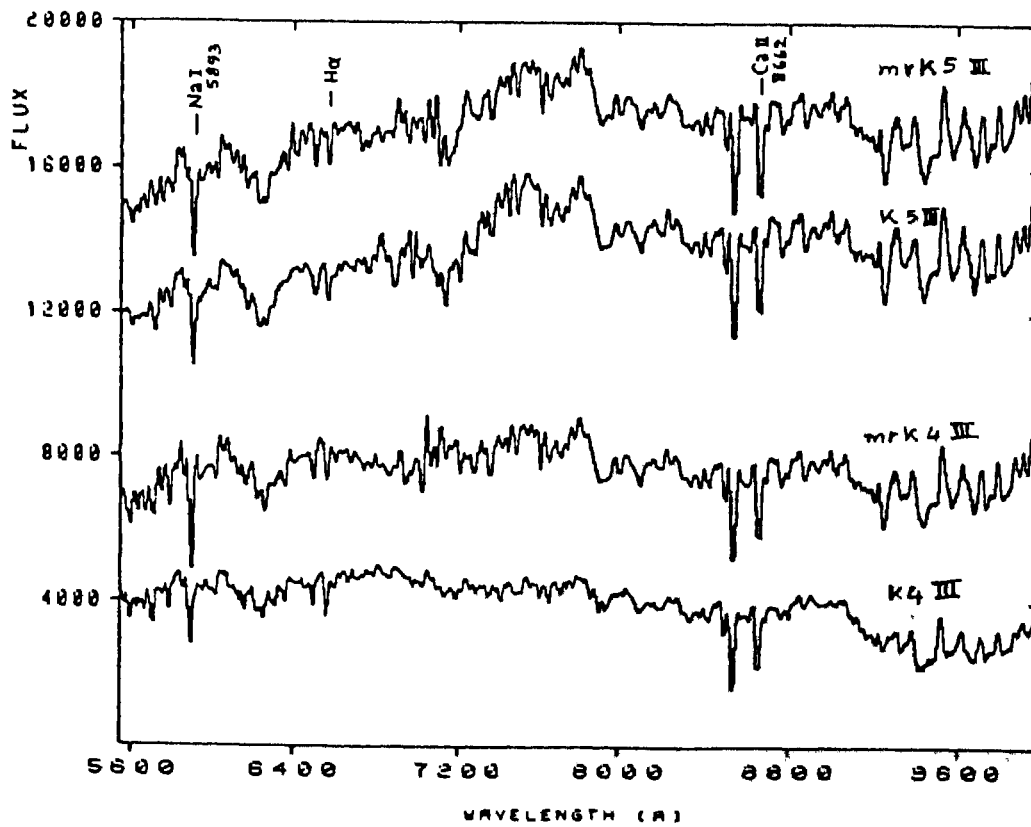


Figure 4.12(k)

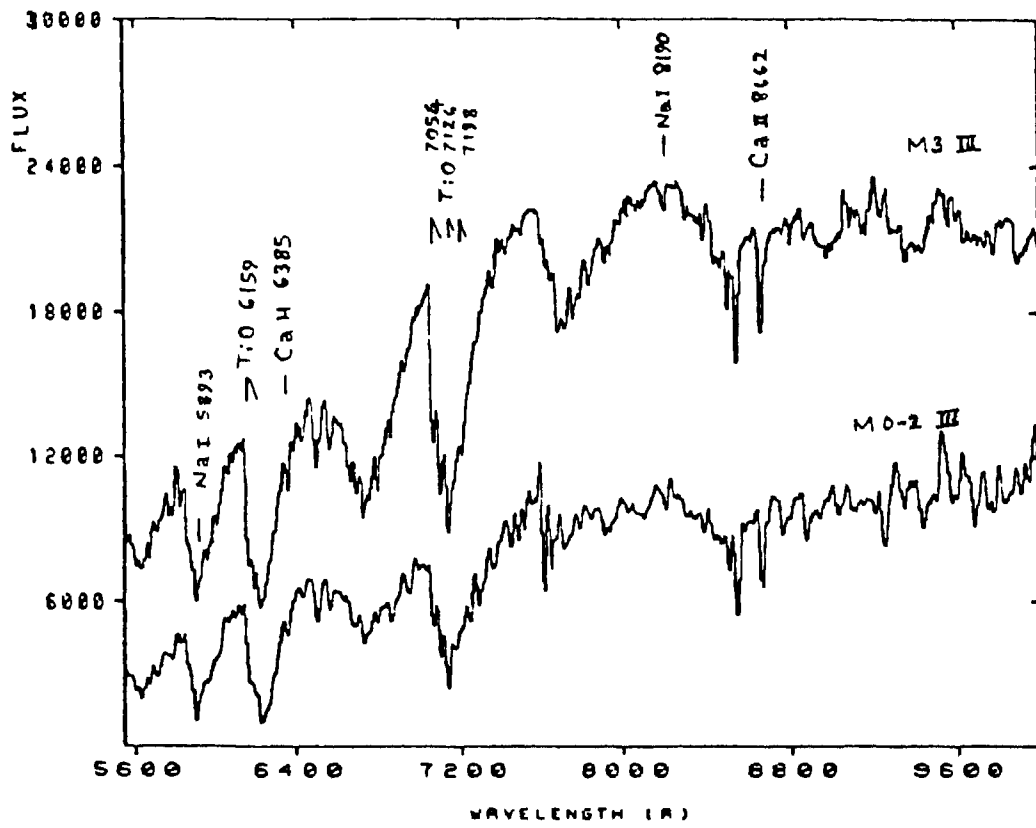


Figure 4.12(1)

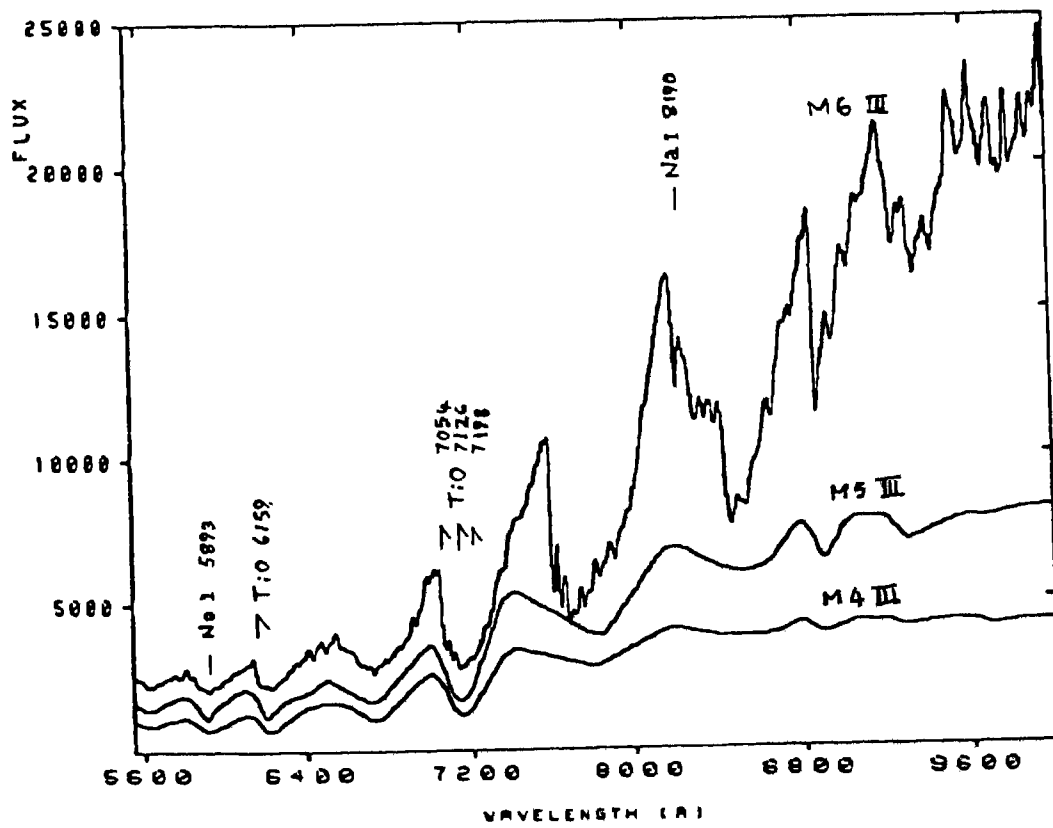


Figure 4.12(m)

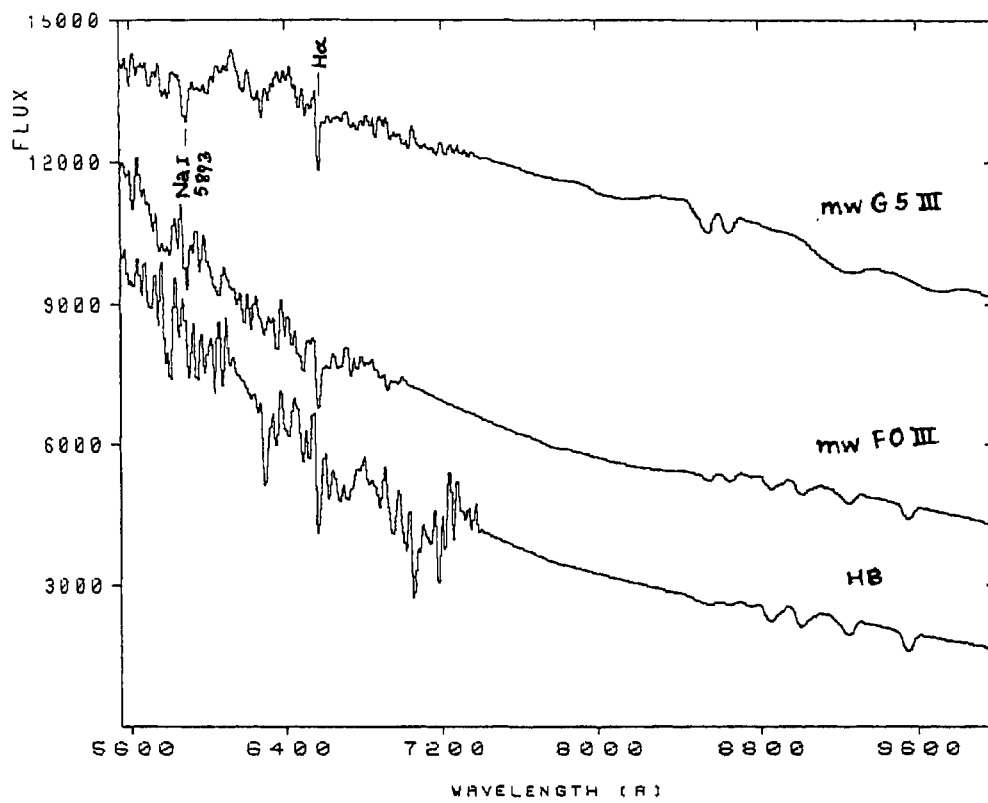


Figure 4.12(n)

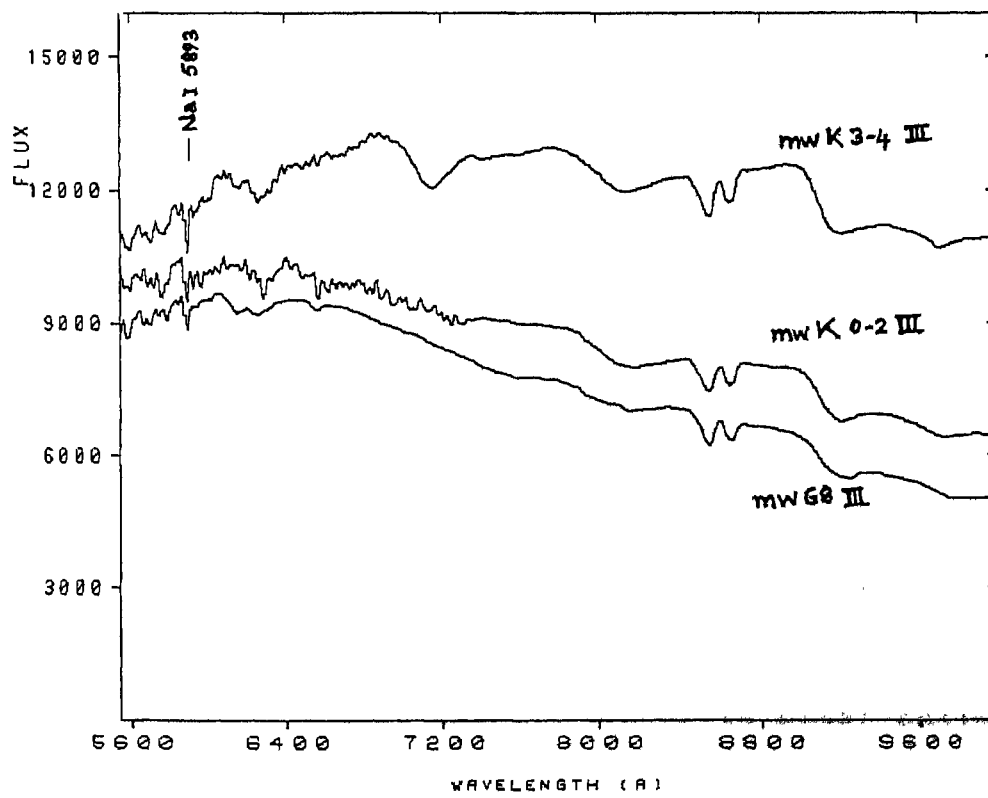


Figure 4.12(o)

The usual symbols for dwarf (V), giant (III), sub-giant (IV) stars are used; the prefixes 'mr' and 'mw' refer to metal rich and metal weak classes and 'e', 'm' and 'l' refer to early, middle and late spectral sub-classes. The $(R-I)_c$ colours of the ASL are given in the column 7.

IV.2.5. Reddening Correction for Galaxy Spectra

The flux calibrated spectra of the galaxies had to be corrected for foreground reddening before being shifted to rest-frame wavelengths. The values of the colour excess, $E(B-V)$, used to correct for reddening were taken from RC2. The correction was applied using the relation given by Seaton (1979) which is incorporated in a correction procedure in the SPICA software package. The choice ^{of} colour excess from RC2 was mainly based on the criterion of a uniform source for all three galaxies. The $E(B-V)$ values from RC2 as well as other sources are given in Table 3.3.

The expression given by Seaton (1979) allows the computation of the extinction in magnitudes A_λ , using

$$X(x) = A_\lambda / E(B-V)$$

where $x = 1/\lambda$ with λ in microns and $X(x)$ is interpolated between a set of tabulated values. The data are corrected for A_λ on a pixel to pixel basis.

IV.2.6. Shifting to rest frame wavelength, rebinning,
normalising of galaxy spectra.

The procedure for wavelength calibration (Section IV.1.4) produced spectra binned to a linear wavelength scale specified by the start wavelength, WSTART and the wavelength increment per pixel WINC. The wavelength of pixel n is then given by

$$\lambda_n = \text{WSTART} + (n - 0.5) \text{WINC}$$

The factor of 0.5 is used since WSTART refers to the left side edge of the first pixel. The effect of the velocities of recession of galaxies is to shift wavelengths redwards such that

$$\lambda = \lambda_0 (1 + Z)$$

where λ_0 is the rest frame wavelength and $Z = \frac{v}{c}$, v being the velocity of recession and c , the velocity of light. Comparing the above two equations, we get

$$\begin{aligned} \text{WSTART} &= (\text{WSTART})_0 (1 + Z) \quad \text{and} \\ \text{WINC} &= (\text{WINC})_0 (1 + Z) \end{aligned}$$

where the subscript 0 refers to the rest wavelength case.

The procedure for shifting to rest wavelengths thus amounted to calculating $(\text{WSTART})_0$ and $(\text{WINC})_0$.

and setting these values in the spectrum data files. The velocity of recession for the galaxies adopted were: NGC 3308, $v = 3642$ km/sec (Richter 1987), NGC 4472, $v = 947$ km/sec (mean of values in Palumbo et al 1983), NGC 5128, $v = 541$ km/sec (Sadler 1984).

The spectra of the galaxies, after shifting to rest frame wavelengths, were examined for small residual errors in wavelength, by obtaining the wavelengths of identifiable features. Small shifts of a maximum of one pixel were required to match the rest wavelengths of the lines. The spectra were then rebinned to 1\AA pixels and the wavelength range 5543 to 10000\AA extracted. The final spectra, in bins of 6\AA as for the stellar spectra, were normalised at 5556\AA . Figures 4, 13a, b and c show these spectra for NGC 3308, NGC 4472 and NGC 5128, respectively. Some of the principal spectral features are marked.

IV.3. Photographic Data

During the process of reduction of the photographic data, it was found that the data were not all of uniform quality and did not constitute a homogeneous set. The relative intensities from spectra of the same star taken a year apart, showed upto 27% variation in some cases.

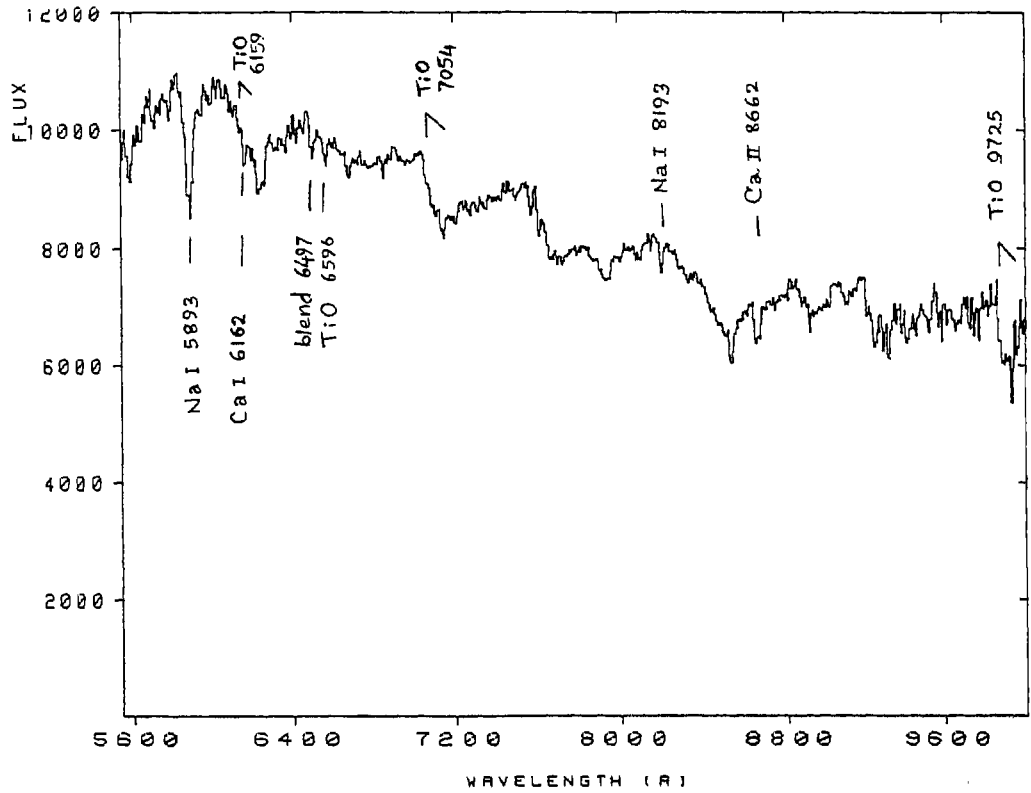


Figure 4.13a. The observed spectrum of NGC 4472 in bins of 6\AA , reduced to rest frame wavelength and normalized to 100 at $\lambda 5556\text{\AA}$ (a further scale factor of $\times 10^2$ is applied for convenience of plotting.)

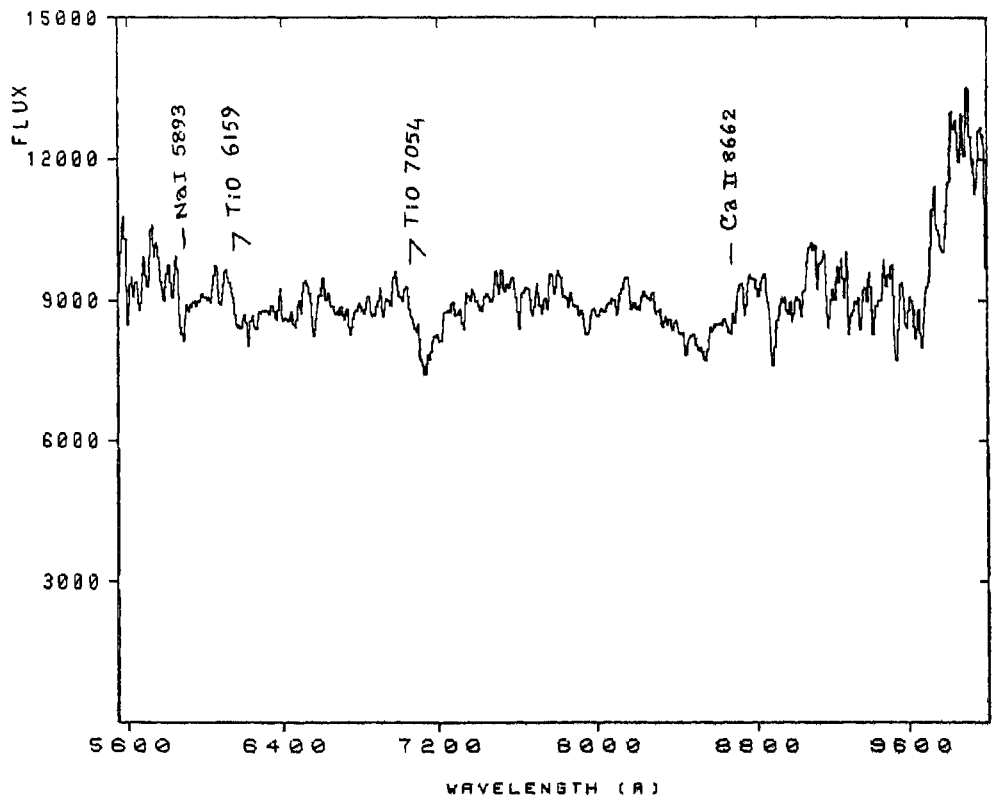


Figure 4.13b. The observed spectrum of NGC 3308 in bins of 6\AA , reduced to rest frame wavelength and normalized to 100 at $\lambda 5556\text{\AA}$ (a further scale factor of $\times 10^2$ is applied for convenience of plotting).

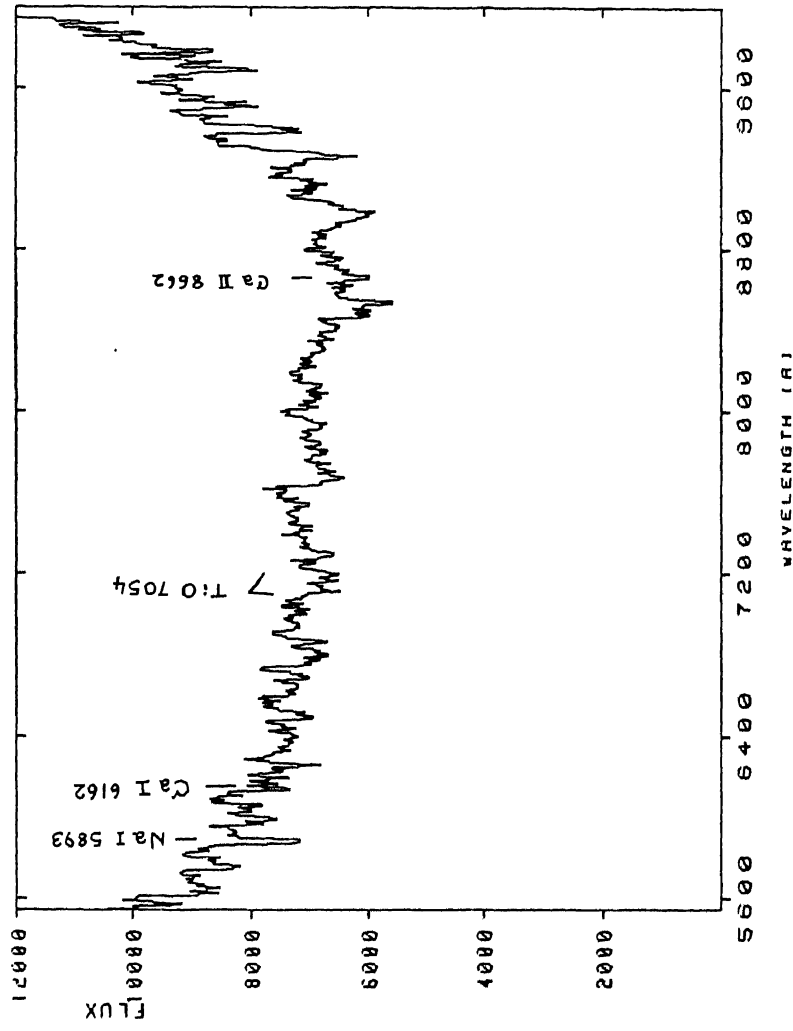


Figure 4.13c. The observed spectrum of NGC 5128 in bins of 6Å, reduced to rest frame wavelength and normalized to 100 at $\lambda 556\text{\AA}$ (a further scale factor of $\times 10^2$ is applied for convenience of plotting). Weak emission lines of H α and [NII] $\lambda\lambda 6548, 6584$ have been removed.

This variation, seen in some cases, may be due to several reasons. Uneven background fog on the photographic plates caused by improper storage during shipment is one strong possibility. The plates are imported from Eastman Kodak and often, goods imported into India are left lying in customs warehouses for upto one month or more before the consignee is informed. Since the image tube was uncooled, there was no control over the variation of background. Though scans of the background were taken using the PDS, it was seen that an average over scans on either side of the spectrum was not good enough to correct for background at the location of the spectrum.

During the period when the spectra were acquired (1982 to 1985), several changes had been made to the Image Tube Spectrograph. The image tube itself was replaced once. These changes make it very difficult to keep track of sources of error in the data, especially when a large collection of spectra of uniformly good quality are required for the stellar library, in addition to those for the galaxies.

The usable spectra are not enough in number to do any kind of analysis vis-a-vis study of stellar populations in galaxies. Therefore, it was decided to omit the photographic data from this dissertation. The

exercise of observations and reduction of the data did, however, provide valuable experience in the area of spectroscopy, especially of faint objects.

Chapter V

ANALYSIS AND SYNTHESIS MODELS

In this chapter, the data reduced to its final form as described in Chapter IV, are interpreted and correlated to derive some information on the nature of the stellar content of the galaxies observed. First, a study of the spectra of the synthesis library stars and galaxies is presented, where the behaviour of different spectral features is discussed. Next, the stellar populations in the galaxies observed are derived using the technique of population synthesis.

V.1. Spectra, Spectral lines and indices

In the early work on the interpretation of galaxy spectra (e.g. Morgan and Mayall 1957), the appearance of the spectrum of a galaxy i.e. the overall shape of distribution of energy and the strength of absorption lines due to various species, was used to judge the dominant stellar population(s) present in it: the spectrum was compared with stellar spectra and an equivalent spectral type was assigned to the galaxy depending on the wavelength region observed (mainly the blue region). This process, in more quantitative terms, is still very useful in analysing the stellar content of galaxies.

The spectra of stars which will be used for interpreting the galaxy spectra (the augmented stellar library or ASL) are plotted in Figures 4.12a to 4.12 o, with some of the prominent spectral features marked. The spectra of the galaxies are plotted in Figures 4.13a to 4.13c.

The scheme of stellar spectral classification is based on the fact that the strength of absorption lines in the spectrum is dependant on the effective temperature, gravity and abundances of the elements in stars. The change in strength of spectral lines, individually and relative to one another is used to determine the spectral type (temperature), and the luminosity (surface gravity). In this section we study the behaviour of some spectral features in the galaxies observed in the light of their behaviour in the stellar types making up the ASL.

The spectral features studied are listed in Table 5.1a. The central wavelength of the line or molecular band, the atomic or molecular species and the definitions of the spectral indices calculated are given in the table. The spectral indices are calculated in the manner done by O'Connell (1973). The continuum flux per unit wavelength at the feature of interest is linearly interpolated from two points in

Table 5.18

Spectral features and definitions of indices

| Wavelength Å | Species | Index-Name | Index Definition | | | | | |
|-----------------|-----------------------------|------------|---|---------------------------------|---|--|---|---|
| | | | Feature wave- length λ_2 (Å) | Feature band- pass (Å) | Conti- num wave- length λ_1 (Å) | Conti- num band- pass for λ_1 (Å) | Conti- num wave- length λ_3 (Å) | Continuum bandpass for λ_3 (Å) |
| 5711 | MgI | MgI-5711 | 5711 | 6 | 5696 | 6 | 5731 | 6 |
| 5890, 5896 | NaI | NaI-5893 | 5893 | 30 | 5836 | 12 | 6040 | 12 |
| 6162 | CaI | CaI-6162 | 6162 | 12 | 6075 | 6 | 6330 | 6 |
| 6362 | Blend of atomic lines | At.B1-6362 | 6362 | 12 | 6349 | 6 | 6422 | 6 |
| 6385 | CaH | CaH-6385 | 6385 | 12 | 6349 | 6 | 6422 | 6 |
| 7126 | TiO | TiO-7126 | 7126 | 24 | 7045 | 12 | 7550 | 12 |
| 7198 | TiO | TiO-7198 | 7198 | 24 | 7045 | 12 | 7550 | 12 |
| 7699 | KI | KI-7699 | 7699 | 12 | 7555 | 12 | 8165 | 12 |
| 7929 | VO | VO-7929 | 7929 | 30 | 7560 | 18 | 7995 | 18 |
| 8183, 8195 | NaI | NaI-ir | 8190 | 12 | 8165 | 12 | 8410 | 12 |
| 8662 | CaII | CaII-8662 | 8662 | 24 | 8585 | 24 | 8710 | 24 |
| 9916 | FeH | WF-77 | 9916 | 6 | 9866 | 6 | 9966 | 6 |
| 9918 | TiO | TiO-9918 | 9910 | 24 | 9880 | 12 | 9975 | 12 |

the continuum on either side. The ratio of the flux at the feature to that of the interpolated continuum flux, converted to magnitudes is the feature index. If λ_1 and λ_3 are the wavelengths of the continuum points and λ_2 is the wavelength of the feature ($\lambda_3 > \lambda_2 > \lambda_1$), then the index I is defined by

$$I = -2.5 \log \left[\frac{F_\lambda(\lambda_2)}{F_\lambda(\lambda_1) + \left\{ F_\lambda(\lambda_3) - F_\lambda(\lambda_1) \frac{(\lambda_2 - \lambda_1)}{(\lambda_3 - \lambda_1)} \right\}} \right].$$

Indices representing absorption features defined in this way are quite insensitive to the amount of interstellar reddening and the form of the reddening law, especially if the continuum points closely bracket the feature.

The Wing-Ford band due to FeH at 9916\AA , used for separation of giant and dwarf stars beyond spectral type M5, has an index as defined in Whitford (1977). Here, again, continuum points on either side of the feature are used and the index is defined

$$\text{WF 77} = -2.5 \log \left[\frac{2F_\lambda(9916\text{\AA})}{F_\lambda(9866\text{\AA}) + F_\lambda(9966\text{\AA})} \right].$$

The behaviour of the indices calculated, with $(R-I)_c$ colour (which indicates the spectral type) is shown in Figures 5.1a to 5.1m. The explanation of the

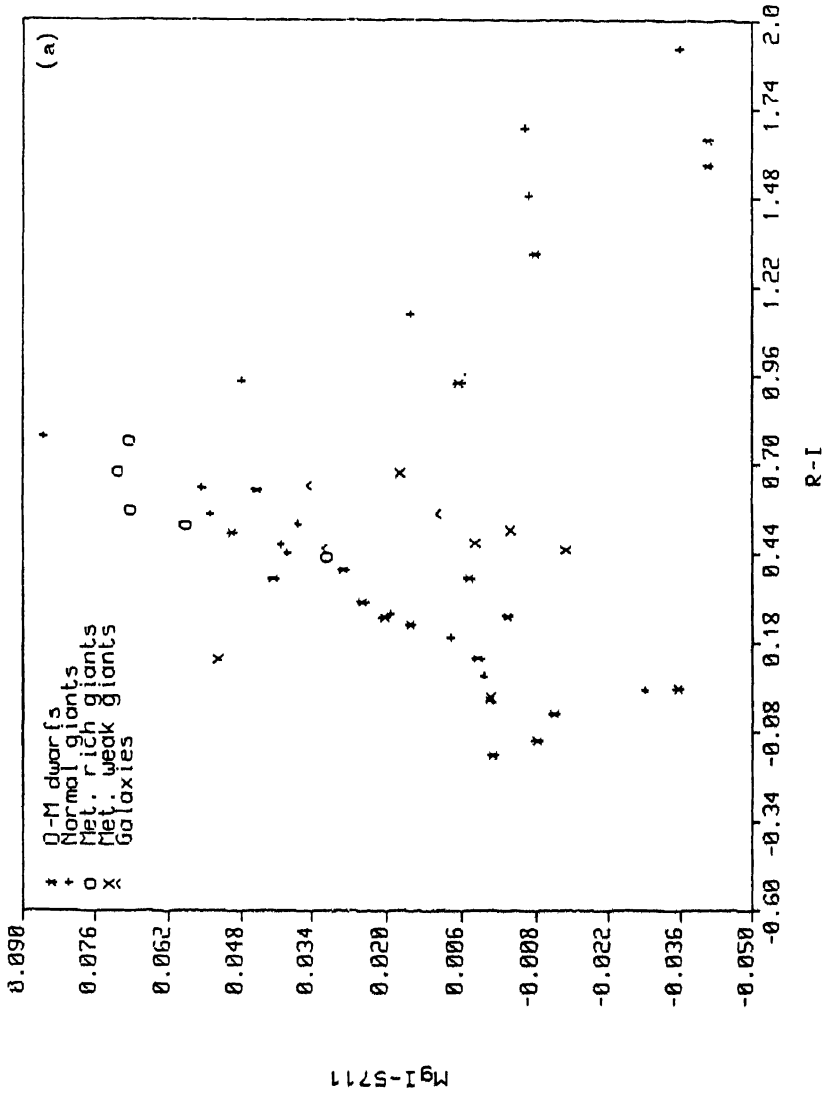


Figure 5.1. Variations of computed line indices with $(R-I)_c$ colour.

symbols is in the figures. All stellar types (except the subgiant groups 20, 21 and 22) and the galaxies observed are indicated.

The $(R-I)_c$ colours for the galaxies were calculated in the same manner as for the stars (Section IV.2.3) and the values are listed in Table 5.1b. It must be emphasized that these colours represent the portion of the galaxy whose light passes through the slit.

The programs written for calculating the indices and plotting them, read the index definitions as well as the stellar spectra from files which can be updated quite easily. New indices are hence quite simple to define and are calculated for all stellar types at one time. The plotting routines permit definition of sets of stellar types (e.g. dwarfs, giants) for overplotting with different symbols.

The behaviour of some of the spectral indices is briefly discussed below:

Na I

The Na I-5893 index covers the D resonance lines of Sodium (Na I 5890.0, 5896.9). This feature is a well-known temperature and luminosity discriminant among late-type stars (O'Connell 1973, Pickles 1985a) and permits strong separation between giant and dwarf

Table 5.1b

Calculated $(R-I)_c$ colours of observed galaxies

| Galaxy | Calculated $(R-I)_c$ colour |
|----------|-----------------------------------|
| NGC 3308 | 0.640 |
| NGC 4472 | 0.458 |
| NGC 5128 | 0.557 |

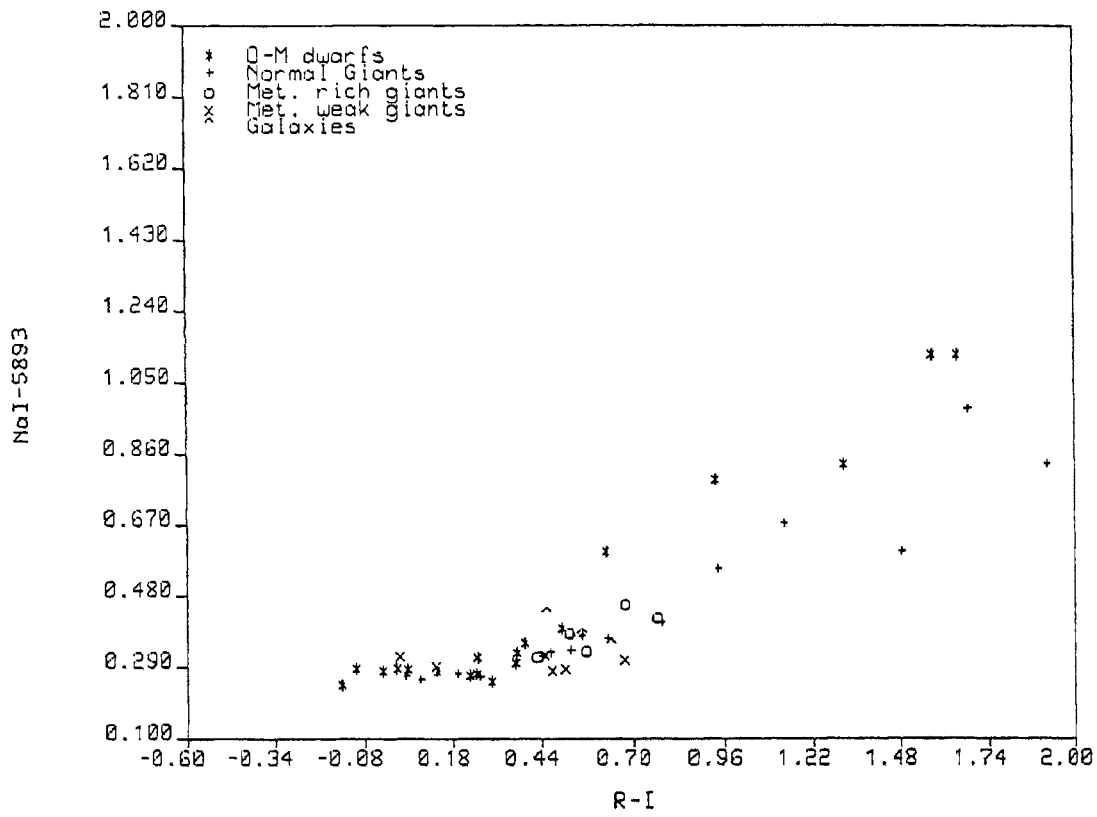


Figure 5.1(b)

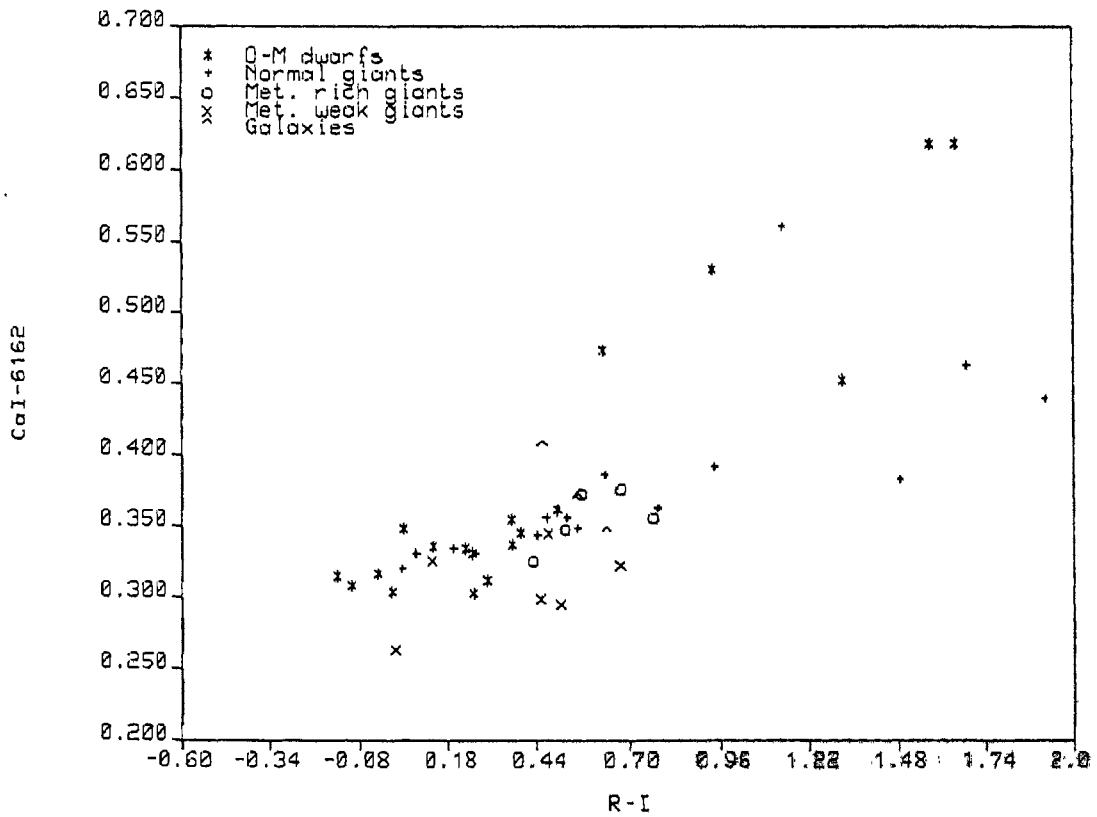


Figure 5.1(c)

stars later than spectral type K0. Although the absorption bands of TiO start contaminating this region from spectral class M2 onwards, the luminosity discrimination of this index is good down to the latest (M5-6) dwarfs present in the ASL. There is also a clear separation between metal rich and metal weak giant stars (see Figure 5.1b). Among the galaxies, NGC 4472 shows a clearly higher value for the given $(R-I)_c$ colour.

The NaI-ir index (Figure 5.1j), measures the lines at $\lambda 8183, 8195\text{\AA}$ in the near infra-red region of the spectrum. These lines provide very good luminosity separation between dwarf and giant stars and are used for spectroscopic luminosity classification of M stars (Sharpless 1956). The separation between dwarf and giant stars starts at about spectral type K0. The continuum sideband at 8050\AA used by O'Connell (1973) is not used here, since it is dominated by TiO and VO in very cool (M6 to M8) stars. A clear separation between metal weak and metal rich giant stars is also seen. Of the galaxies, NGC 3308 has the strongest value.

Ca I and Ca II

The line of Ca I at 6162\AA is enhanced in M dwarf stars (Turnshek et al 1985 and references therein). We find that the discrimination between dwarf and giant

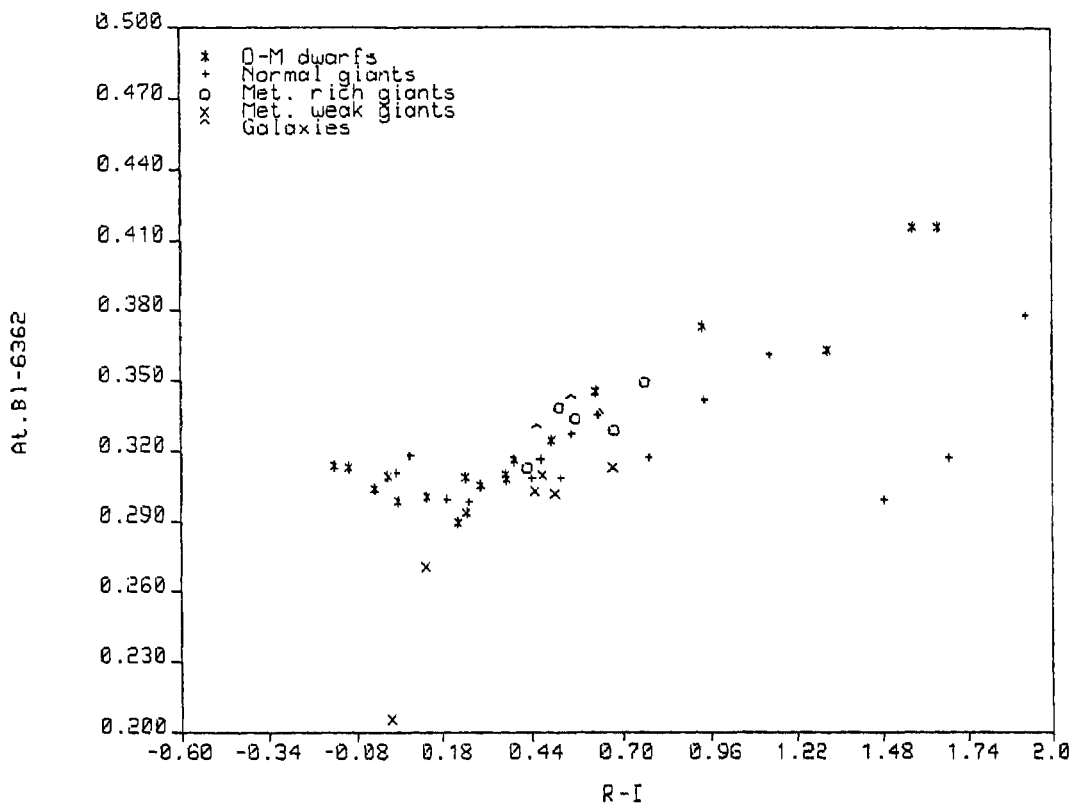


Figure 5.1(d)

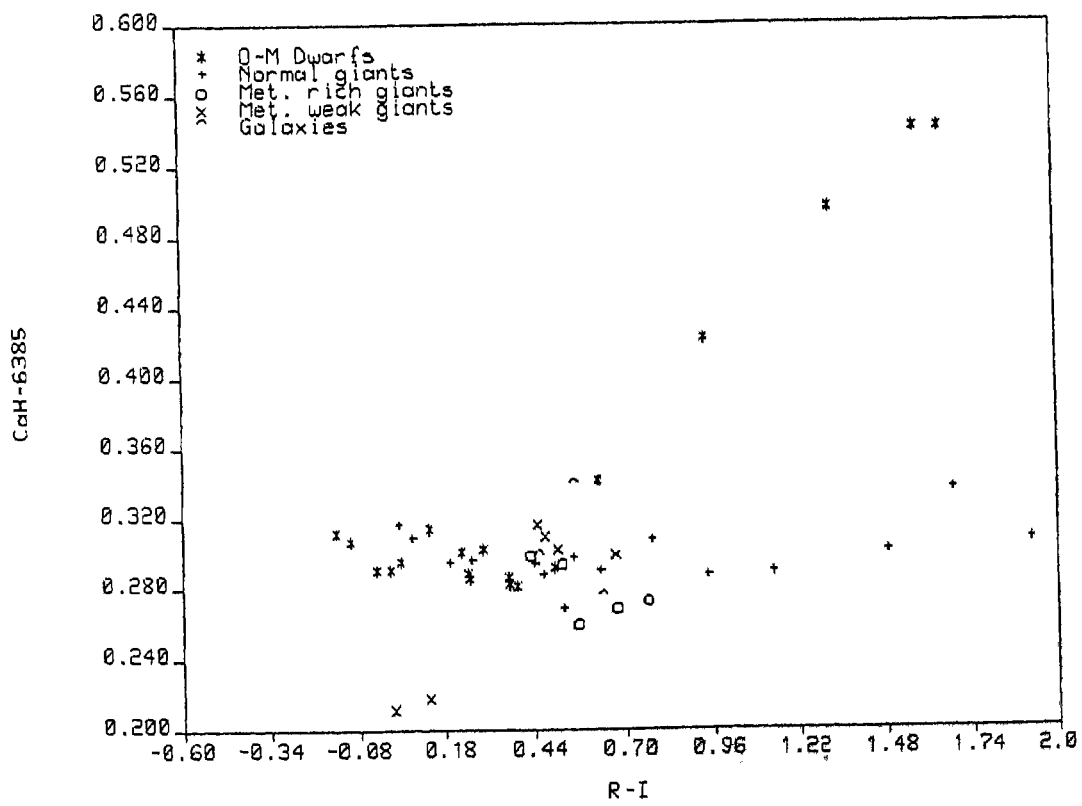


Figure 5.1(e)

stars by about spectral type K4. The Ca I-6162 index provides very clear separation after this spectral type. A fair level of separation between metal rich and metal weak giant stars is also seen. NGC 4472 has a fairly strong index value compared to the other galaxies.

The Ca II-8662 index measures the last line of the triplet at λ 8498, 8542 and 8662Å. These lines are known to be stronger in giants than in dwarf stars. O'Connell (1973) finds the line λ 8542Å to be a clear luminosity discriminant. Pickles (1985a) finds the summed local equivalent widths of the three lines to be a luminosity discriminant. The line λ 8662Å was studied here to see its individual behaviour. At the resolution of the spectra obtained here, we are unable to say that the index increases with spectral type of giants; blanketing due to molecular TiO bands (λ 8430) create a considerable scatter (see Figure 5.1k). However, contrary to the finding of Spinrad and Taylor (1969), this index shows a clear separation between metal weak and metal rich giant stars.

Mg I-5711

This index measures the only line of Magnesium detectable in the spectral range of the data; clear separation between metal rich and weak giants is seen

to be present (Figure 5.1a). Discrimination between giants and dwarfs is seen beyond spectral type K2-3 but the index decreases at later types for both luminosity classes. NGC 5128 clearly shows a lower value compared to the other two galaxies.

TiO

The strengths of the molecular absorption bands due to TiO are strongly temperature sensitive in stars cooler than around 4200 degrees; the strength increases with spectral type. These bands are used in temperature classification of stars of spectral type M (Sharpless 1956, Lockwood 1973, Solf 1978, Wing and Dean 1983). Figure 5.1f and g show the behaviour of the indices based on the bands at 7126\AA and 7198\AA , respectively. Both indices show an increase in strength with spectral type, beyond spectral type M0, and both indices are larger for giant than for dwarf stars. The indices do not discriminate between giant stars of different metallicities. It is apparent in the figure that all the galaxies show systematically higher values at the given $(R-I)_c$ colour.

The TiO-9918 index (Figure 5.1m) shows a different behaviour. Beyond spectral type around M3 to M4, the differences between giant and dwarf types is not seen. Though the quality of the data is poorer in this spectral region, it is evident that the latest dwarf groups show

TiO-7126

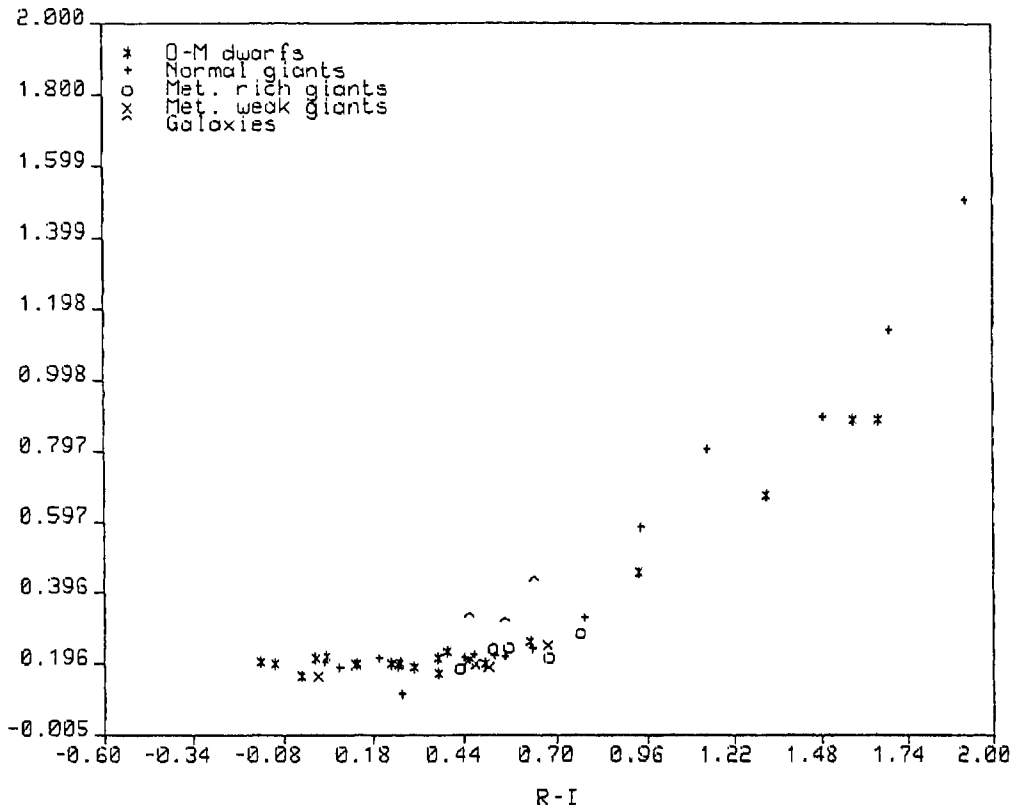


Figure 5.1(f)

TiO-7198

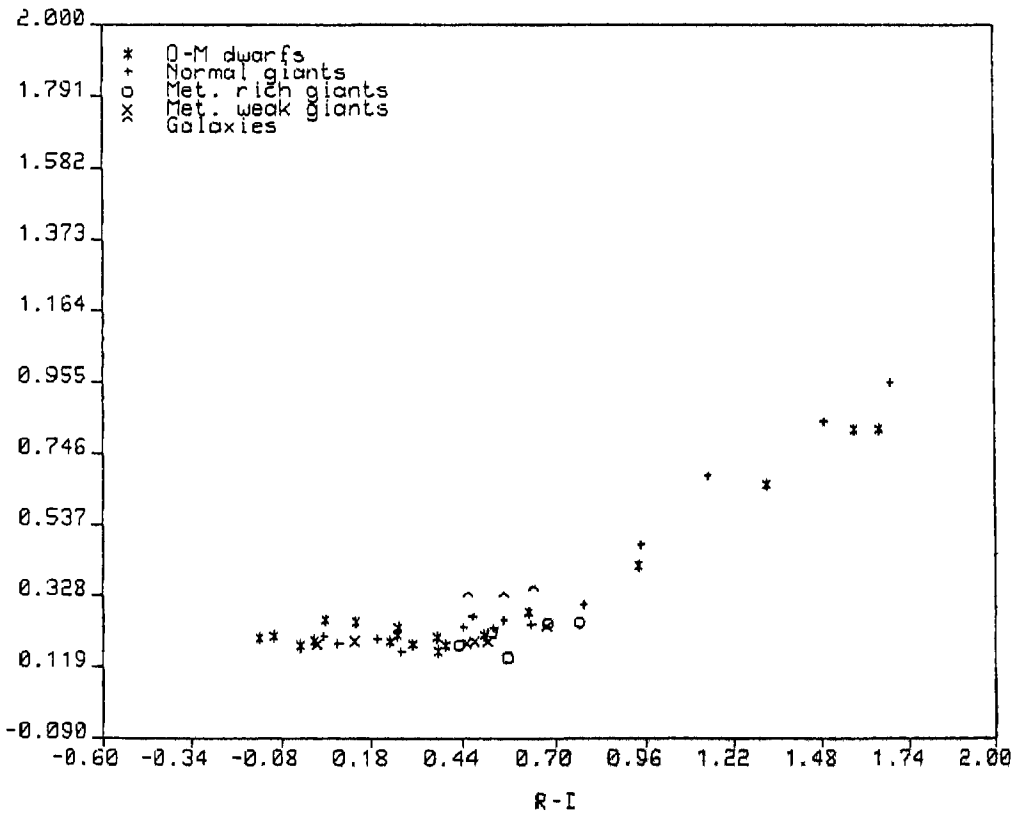


Figure 5.1(g)

enhanced values of this index. This is due to the presence of the Wing-Ford bands of FeH in stars of these types and later (see below).

Atomic line blend at $\lambda 6362\text{\AA}$

This blend of atomic lines of Fe I, Ti I, and Cr I is reportedly sensitive to luminosity, strengthening with increasing luminosity in K and M stars (Turnshek et al 1985). The index is plotted in Figure 5.1d, and though there is a scatter in the plot, the values for the dwarfs seem to be systematically higher than for the giants. The values discriminate between metal rich and metal weak giants. There is probably contamination by the bands of CaH at 6385\AA which have the opposite luminosity dependence.

CaH-6385

The absorption band system of CaH is strong in M-type dwarf stars (Turnshek et al 1985). The plot of the CaH-6385 index in Figure 5.1e shows this clearly. The giant stars of solar abundance show a very gradual increase in value with later spectral type. For the dwarf stars, on the other hand, the values increase sharply with type. The galaxy NGC 5128 has a significant value for the index, compared to the other two.

KI-7699

The line of neutral potassium, KI at λ 7699 \AA , can be used to distinguish M dwarfs from giants (Sharpless 1956). It is strong and wide in dwarfs by M3 and increases in strength to later spectral types (Turnshek et al 1985). The line (as also KI-7665 \AA) is in the region of the atmospheric 'A' band. Since all the spectra here were carefully corrected for atmospheric absorption, it was decided to study the behaviour of this feature. As seen in Figure 5.1h, the index grows significantly stronger with spectral type. It is, however, not clear if the values are systematically higher in dwarf stars. This uncertainty is probably due to contamination by TiO bands at λ 7672 \AA and λ 7705 \AA , which first appear at M2 and are very pronounced by M5 for all luminosity classes. The values for the galaxies is significant, being highest for NGC 4472 and decreasing with increasing $(R-I)_c$ colour.

VO-7929

This index includes the absorption bands due to Vanadium Oxide at λ 7919, 7929, 7939 \AA (Solf 1978). As seen in Fig. 5.1i, it does not show any clear cut trend with spectral type; this is so because the bands due to VO first appear at spectral type M7, which is not included in the ASL library. In the spectral range

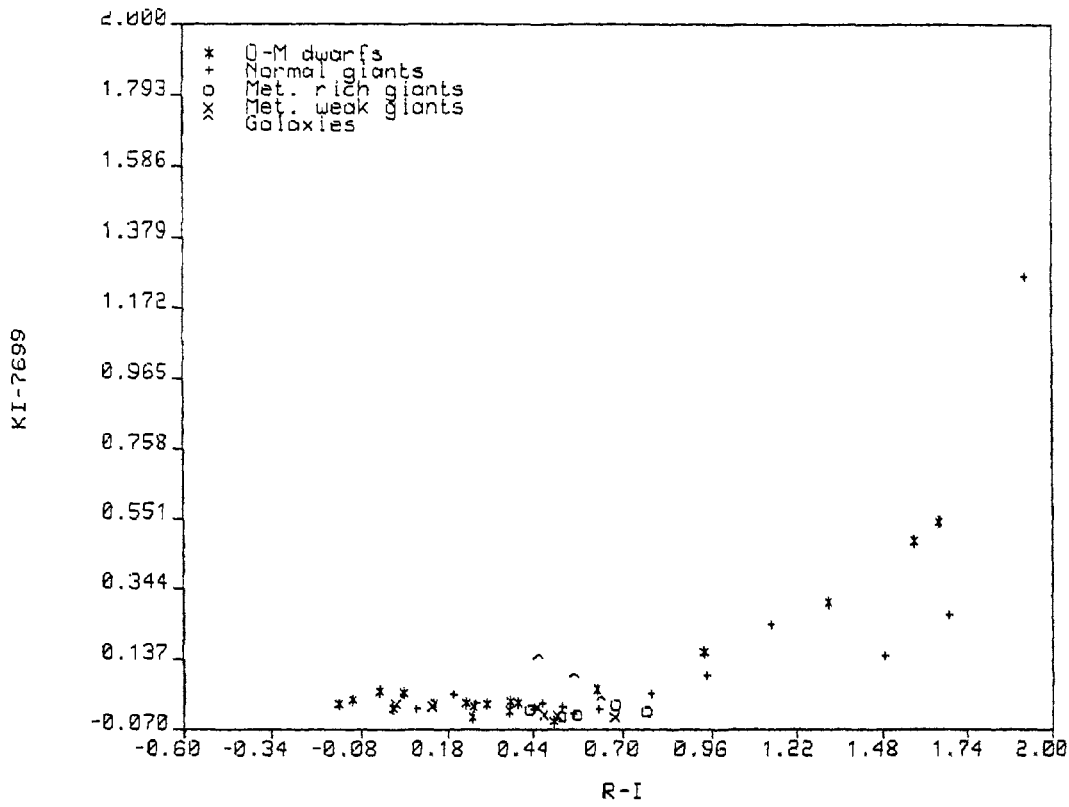


Figure 5.1(h)

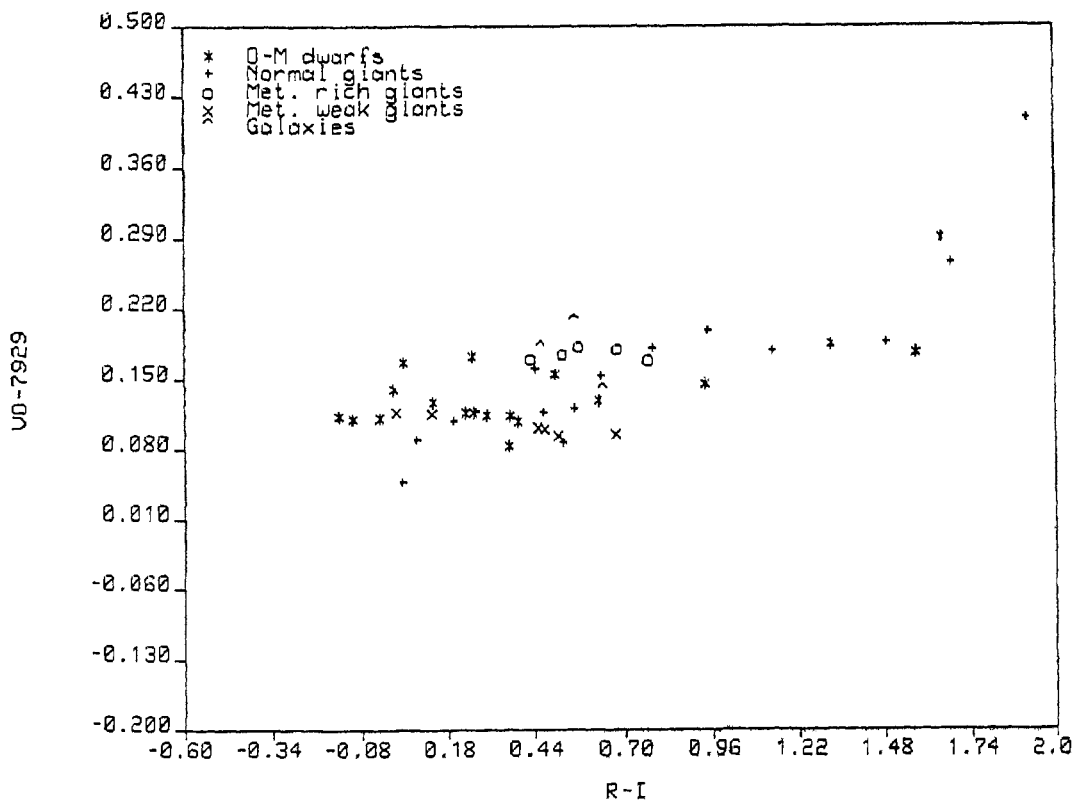


Figure 5.1(i)

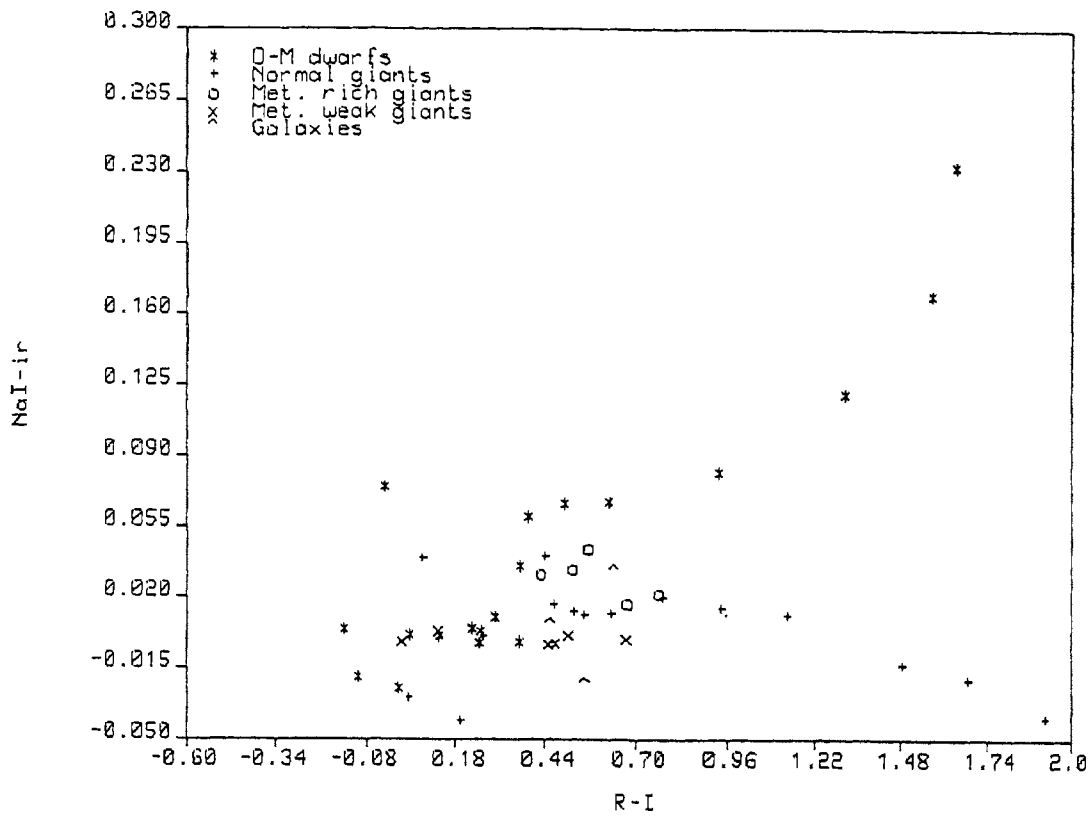


Figure 5.1(j)

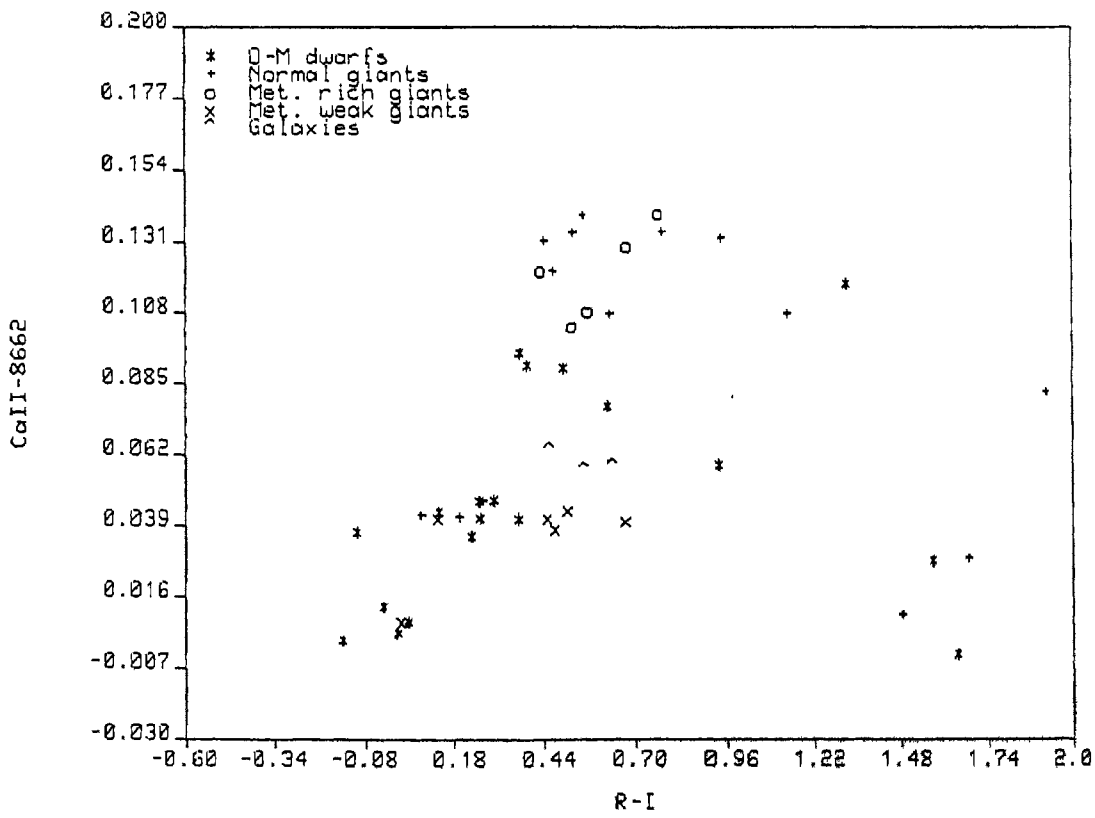


Figure 5.1(k)

covered here, the index is probably contributed to by TiO absorption bands at $\lambda 7907$ and 7949\AA which are marginally visible in M stars (Turnshek et al 1985). The index scans to discriminate systematically between metal rich and metal weak giant stars, which is not the case for TiO-7126 and TiO-7198.

WF-77

This index covers the Wing-Ford band due to FeH with band head at 9896\AA (Nordh et al 1977). The behaviour of this band was studied in detail by Whitford (1977 - hence the numerals in the index name), who found a sharp increase in the strength of the band for dwarf stars of spectral type later than M4. The index defined here is the same as that used by Whitford (1977).

Whitford found no evidence for the presence of this band in measures on galaxies. The resolution of his observations was 25\AA and he concluded that higher resolutions were required to detect it. The value he obtained for NGC 4472, the only galaxy in our sample observed by him, was 0.012, which was in the same range of values as for stars not showing the band. The value obtained for the galaxies here are:

| | |
|----------|--------|
| NGC 5128 | 0.091 |
| NGC 4472 | 0.106 |
| NGC 3308 | -0.025 |

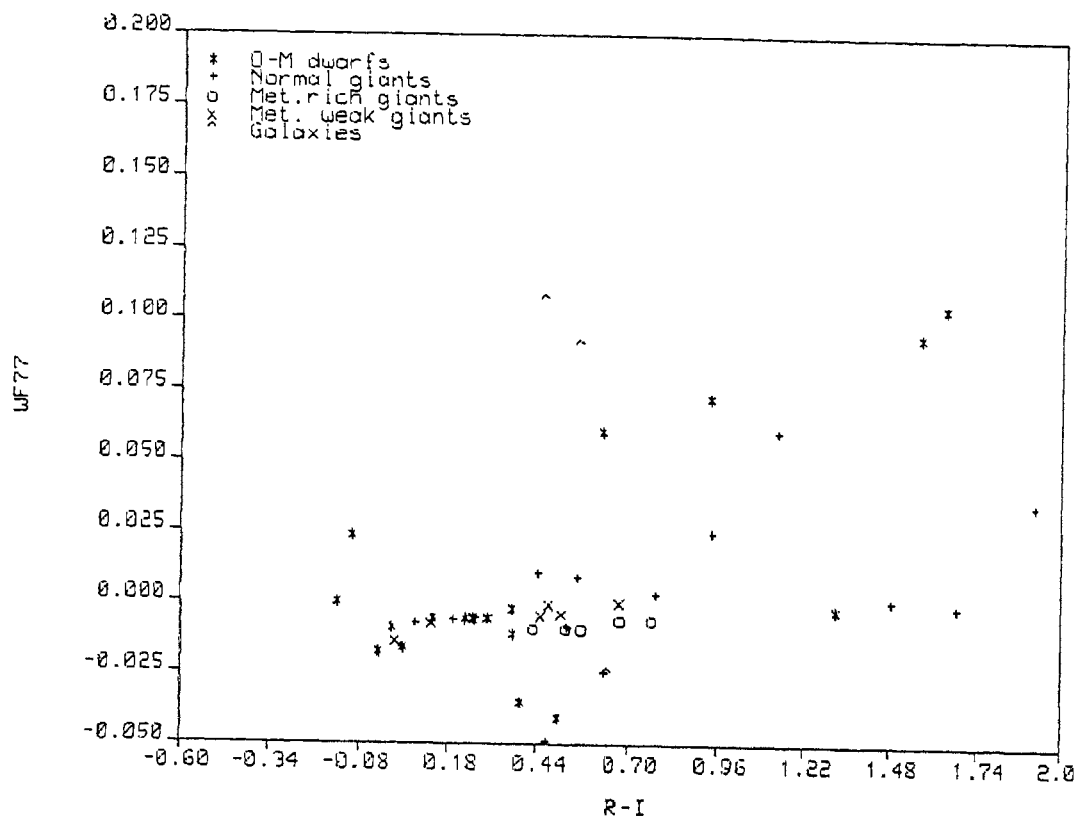


Figure 5.1(1)

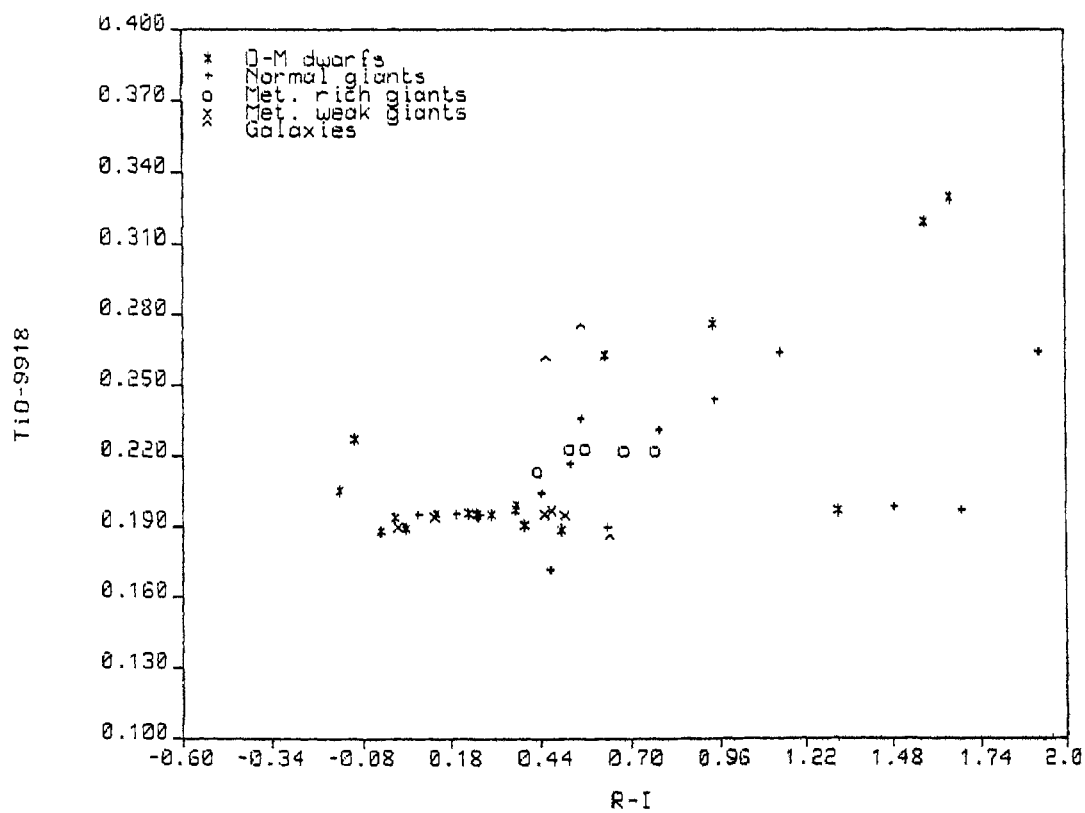


Figure 5.1(m)

In comparison, values obtained for some late type stellar groups are:

| | | | |
|-------------|--------|-------------|--------|
| M0-2 dwarfs | 0.073 | M0-2 giants | 0.025 |
| M3 dwarfs | -0.002 | M3 giants | 0.061 |
| M4 dwarfs | 0.095 | M4 giants | 0.001 |
| M5-6 dwarfs | 0.105 | M5 giants | -0.001 |
| | | M6 giants | 0.036 |

Cohen (1978) obtained spectra at resolutions of 3.3\AA using a solid state charge injection device (CID) array detector, of the region covering the WF bands, for several M dwarf and giant stars as well as the galaxies M31 and M32. The percentage depression below the continuum caused by the band was measured. A small detection ($\sim 7\%$) of the band was found in the galaxies.

The behaviour of the WF 77 index calculated for the stars in the ASL library and the galaxies is shown in Figure 5.1 l. The late dwarfs showing high values of the index, also show a high value of the TiO-9918 index (Figure 5.1m). The TiO-9918 band is peculiar to late giants and the WF band to late dwarfs; spectra of dwarfs as late as M8 do not show the TiO 9918 \AA band (Whitford 1977). Besides, the values of the TiO-9918 index for the M4 and M5-6 dwarf groups is much higher than for giants of similar spectral type. The late dwarfs in Figure 5.1m, would thus seem to be reflecting

the WF band (instead of the TiO band).

The galaxy NGC 4472 shows a strong value of the WF index, followed in strength by that for NGC 5128. The values of the index for these galaxies is the same or stronger than that for the M4 and M5-6 dwarf groups.

V.2. Method of Population Synthesis

As discussed in Chapter 1, the method of population synthesis involves matching the observed spectrum of the galaxy with a composite spectrum of different proportions of various stellar library groups, subject to astrophysical constraint. The technique used for synthesis in this study are those developed by Pickles (1985b), using an optimisation program developed at the Numerical Optimisation Centre, Hatfield (Bartholomew-Biggs, 1979). The routines for optimising synthesis were obtained from Pickles and used for this study.

The problem of optimisation can be stated as finding a vector \hat{x} with elements $x_1, x_2 \dots x_n$, for which a defined function $F(\hat{x})$ is optimum. However, since in most situations, the x_i may not be allowed to take any values whatsoever, these values can be constrained to lie in some range. Such constraints may in general be equality constraints of the type

$e(\hat{x}) = 0$ where e is a defined function or inequality constraints of the type

$$g(\hat{x}) \geq 0 .$$

The program named XOPRQP solves this optimisation problem.

The vector \hat{x} , in the application here can represent the fractional light contribution from different types of stars and the function $F(\hat{x})$ can define the goodness of the fit to the observed galaxy spectrum by the spectra of the stellar types summed in proportion to x_i . Thus if there are n stellar types and m wavelength points in the spectrum and x_j is the relative light contribution of the j^{th} stellar group at the normalising wavelength, then the computed spectrum at any wavelength is given by

$$S_i = \sum_{j=1}^n x_j F_{ji} \quad \dots (5.1)$$

where F_{ji} is the flux of the star of type j at wavelength i . The residual error in the fit at any wavelength is then

$$R_i = W_i \left(1 - \frac{S_i}{G_i} \right) \quad \dots (5.2)$$

where W_i are weights assigned to different wavelengths and G_i is the observed galaxy spectrum. The function to be minimised is thus

$$\text{FUNC} = \sum_{i=1}^m R_i^2 = \sum_{i=1}^m w_i^2 \left(1 - \frac{S_i}{G_i}\right)^2 \quad \dots (5.3)$$

and the merit of the fit is given by

$$\text{Merit} = \left(\frac{\text{FUNC}}{m}\right)^{\frac{1}{2}} \quad \dots (5.4)$$

The solution vector \hat{x} is to be found subject to constraints given by

$$\tilde{C} \cdot \hat{x} - \hat{K} = \hat{V} > 0 \quad \dots (5.5)$$

The residual in Equation (5.2) is in magnitudes; it may optionally be defined in flux units as $R_i = W_i (G_i - S_i)$.

The routine XOPRQP requires the values of the function, the constraint values V , and the gradients of these i.e. their partial derivatives with respect to all x_j .

In equation 5.5, the constraint matrix \tilde{C} has n rows by l columns, where n is the number of stellar groups in the ASL and l is the number of constraints imposed. The vector \hat{K} is a constant vector whose elements are usually zero.

For the synthesis problem undertaken here,

$n = 48$ (number of stellar groups in ASL)

$m = 743$ (number of pixels in the spectra)

x_j was the relative light contribution of group j at the normalising wavelength 5556\AA and $\sum x_j = 1$.

If the number of stars of type j is N_j and the luminosity of group j is L_j , then the total flux from the galaxy at wavelength i is

$$E_i = \sum_{j=1}^{48} N_j L_j F_{ji} / 100 \quad \dots (5.6)$$

where F_{ji} are normalised to a value of 100 at 5556\AA , and the total flux at 5556\AA is

$$E_{5556} = \sum_{j=1}^{48} N_j L_j \quad \dots (5.7)$$

Since the observed galaxy fluxes are also normalised to 100 at 5556\AA , the computed fluxes should also be normalised:

$$S_i = 100 \frac{E_i}{E_{5556}} \quad \dots (5.8)$$

Equations (5.6), (5.7) and (5.8) give

$$S_i = \sum_{j=1}^{48} \left(\frac{N_j L_j}{\sum_{k=1}^{48} N_k L_k} \right) F_{ji} = \sum_{j=1}^{48} x_j F_{ji} \quad \dots (5.9)$$

The factor $\sum_{k=1}^{48} N_k L_k$ can be normalised to 1, giving relative numbers of stars which can be scaled upto any total number of stars. In this case, the relative number of stars in group j is

$$n_j = \frac{x_j}{L_j} \quad \dots (5.10)$$

The mass to light ratio, M/L is given by the sum of the relative masses of each group:

$$M/L = \sum_{j=1}^{48} \frac{x_j M_j}{L_j} \quad \dots (5.11)$$

where M_j is the mass of stars in group j .

V.2.1. Stellar library parameters

The augmented stellar library (ASL) described in Section IV.2.4 was used to provide all the stellar fluxes for population synthesis.

The masses of the stellar groups were the same as used by Pickles (1985a) and tabulated in Table 4.3, except for the KO-1 and K2-3 dwarf groups. The masses for these groups, as taken for synthesis, were 0.85 and 0.76 solar masses instead of 0.8 and 0.6 solar masses respectively. The reason for this change is discussed below in relation to the assignment of absolute visual magnitudes M_v for the stellar groups.

Pickles (1985a) derived values of $\log T_e$ for the stellar groups as those appropriate to the measured group $(V-R)_c$ colour from the calibrations of Flower (1977) for early type dwarfs and giants, from Johnson (1966) for late type giants and from an average of these in cases of overlap. The bolometric corrections were obtained from Allen (1973), Flower (1977) and Tinsley

and Gunn (1976). For late M-giant stars, the bolometric corrections were taken from Bessel and Wood (1984) and are thought to be accurate to better than 0.1 magnitude. The masses for the groups were taken from Allen (1973) and Tinsley and Gunn (1976).

The absolute visual magnitudes for the different stellar groups were derived from bolometric magnitudes by applying the bolometric corrections. The bolometric magnitudes had been taken for the early type dwarfs and giants from Allen (1973) and for the M dwarfs from van den Berg (1983). The bolometric magnitudes for other groups were derived by interpolation between the Yale isochrone compilation. The age and abundance parameters of the isochrones used were selected by plotting the stellar groups on a diagram depicting isochrones of metal weak ($Z = 0.004$), solar abundance ($Z = 0.017$) and metal rich ($Z = 0.04$) compositions of ages 5, 10 and 15 giga years in the log-effective-temperature ($\log T_e$), bolometric magnitude (M_{bol}) plane. The values of M_{bol} for subgiant, G-K dwarfs and normal (solar abundance) G-K giants were taken for a solar composition, 10 gyr isochrone. Those for the metal-rich and metal weak G-K giants were similarly taken for 10 gyr metal rich ($Z = 0.04$) and metal weak ($Z = 0.004$) isochrones. All isochrones used were for a value of the helium abundance, $Y = 0.23$, and a ratio of the mixing length

to pressure scale height $\alpha = 1.6$. The metallicity estimates of the stellar groups have been taken from several sources for the individual stars compiled by Pickles (1985a) into the SLP library. Each group in the library includes a range of stellar abundances, particularly the dwarf stars. Stars with $[\text{Fe}/\text{H}]$ values in the range -0.7 to $+0.6$ dex are present in the dwarf sequence of spectral types G to M. The G-K giant sequence termed 'normal' in Table 4.3, similarly includes stars with $[\text{Fe}/\text{H}]$ values in the range -0.5 to 0.2 dex. Some of the group colours measured by Pickles (1985a), listed in the table, have poorly defined values and are enclosed in parentheses.

For the augmented stellar library, we used values of M_V from several sources. The calculation of stellar evolutionary sequences and isochrones has undergone revisions since the work of Pickles (1985a). The values of M_V for the dwarf stellar groups 1 to 4 in Table 4.3 were taken from Schmidt-Kaler (1982). The values for the groups A0-3 V to F5-6 V were taken at the zero age main sequence positions for stars of solar composition ($[\text{Fe}/\text{H}] = 0.0$ or $Z = 0.0169$) from Vanden Berg (1985), where the stellar models are based on a value of helium abundance $Y = 0.25$ and $\alpha = 1.6$ and incorporate extensive, new opacity data. Vanden Berg (1985) tabulates the calculated $(V-I)_c$,

$(V-R)_c$ colours on the Cousins system; the values of M_V were calculated using bolometric corrections derived from Vanden Berg and Bell (1985) and Buser and Kurucz (1978). The values for the main-sequence groups F7-8 to K2-3 were taken again from Vanden Berg (1985), appropriate to ages around 10 giga year. It must be clarified that the stellar models and isochrones used from various sources were not available to us on magnetic tape; some which have been ordered are yet to be received. We have, therefore, selected values by basically matching the $\log T_e$ and R-I values in the tabulated evolutionary models and isochrones. In the isochrones, this led to slightly different masses for the stellar groups as compared to the masses used by Pickles (1985a); the difference was usually a few hundredths of a solar mass. In some cases, the $\log T_e$ and R-I values could be matched better in the evolutionary tracks, but the ages were not as desired. Since the data was not available on tape, doing interpolations for all the required values between tabulated isochrones was a non-trivial task and was not done. In the light of the uncertainty in mass estimates for stellar groups, given the range of types in many groups, and the range in metallicities, the errors introduced by the above procedure are minimal and will not affect the results of population synthesis appreciably.

The ages for the groups F7-8V to K2-3V from the tracks/isochrones (Vanden Berg 1985) adopted are:

| | |
|-------|-----------------|
| F7-8V | 8 giga years |
| G0-4V | 10 giga years |
| G5-8V | 10.3 giga years |
| K0-1V | 10 giga years |
| K2-3V | 10 giga years |

For the last two groups (K0-1 and K2-3), the masses corresponding to the adopted values were significantly different from Pickles (1985a) and the new values of the masses (0.85 and 0.76 M_{\odot} respectively) were used.

The values of M_V for the dwarf groups K4-7 to M5-6 were derived from Vanden Berg et al (1983), using the tabulated values of M_{bol} and the bolometric corrections compiled by Pickles (1985a). The values of M_V for the subgiant groups were taken from an isochrone of 10 giga year of solar composition. The values for the early type solar abundance giants (groups 23 to 26) were taken from Schmidt-Kaler (1982).

For the normal (solar abundance) giant groups G5-9 III to M0-2 III, the M_V are from 'The Revised Yale isochrones and luminosity functions' (Green, Demarque and King 1987) which incorporate several improvements over the older Yale isochrones. The isochrones selected

were for $Y = 0.2$ and $Z = 0.01$ and age of 10 giga years. For the giant groups M3 and M4, the M_{bol} were taken from the isochrone mentioned above and the M_V values were derived using bolometric corrections from Bessel and Wood (1984). For the M3 and M4 giants we have retained the values used by Pickles (1985a).

For the metal rich giant groups mrG5-KO III to mrK5 III, two sources were considered. The recent calculations of Vanden Berg (1987) for $Z = 0.03, 0.06$ and 0.1 and $Y = 0.25$ and 0.35 which include effects of mass loss on the giant branch were examined. However, calculations were not available for all the groups and it was decided to use revised Yale isochrones (Green et al 1987, hereafter called Yale 87). The values of M_V were taken from Yale 87 with $Y = 0.2$, $Z = 0.04$ and an age of 10 giga years.

For the metal weak FOIII group we retain the value of Pickles (1985a). For the mwG5III and mwG8III groups, the M_V were taken from Yale 87 for an isochrone of age 10 giga year, $Y = 0.2$ and $Z = 0.0004$. For the mwK0-2 and K3-4III groups the values were also from Yale 87 for an isochrone of age 10 giga year, $Y = 0.2$, but $Z = 0.00001$. The values of Z were the closest values available in Yale 87, to the values of $[Fe/H]$ given in Table 4.3. The luminosity of the Horizontal branch

giant group (HBIII) was adopted from studies of the cluster NGC 288, members of which were included by Pickles (1985a) in the group. The value of M_V was taken from Penny (1984).

A comparison of the values M_V assigned in this work and those assigned by Pickles (1985a), shows significant differences; the values we have used are on an average brighter on the upper main sequence till about G5-8 and fainter below this. Our values are also slightly brighter for the subgiant groups, somewhat brighter for normal giants G5-9 to M0-2 and fainter for M3-M4 giants. The metal rich giant groups and metal weak giant groups later than the mwG5 group are significantly brighter in the assignment made here. The effects of these differences will be discussed later in this chapter.

V.2.2. Constraints on Synthesis Solutions

The solution obtained from a simple mathematical treatment of the population synthesis problem can often be untenable, astrophysically. The distribution of stars on the HR diagram, from the solutions are required to conform to the general ideas of stellar evolution theory and to the distributions of stars observed in the Galaxy.

The simplest and most important constraint requires that the contribution to the integrated light be non-negative. Such solutions often yield the best fit to the observed galaxy spectrum and give an indication of the dominant stellar groups supplying the light and especially, the main-sequence turnoff group. The non-negative solutions can, however, have unevenly varying numbers on the main-sequence and giant branches or even large gaps in the HR diagram, where a smoothly varying sequence is expected. Constraints are usually imposed on the solution to get results in reasonable agreement with stellar evolution theory.

It is important, however, to note that a group of stars formed at one time can be expected to yield close agreement with the theory; for galaxies, where stars may have formed over a period of several billions of years in a continuous fashion or in bursts, it would be unrealistic to force the idealised distributions. Most galaxies are truly composite systems and some disagreement is expected if idealised constraints are imposed (see Pickles 1986). The most important reason for disagreement are photometric errors in the data, in the presence of which solutions can be ambiguous (Peck, 1980).

In the study here we perform population synthesis with three types of constraint sets:

1. Simple constraints requiring non-negative numbers of stars of all groups. These constraints imply a single non-zero element in the corresponding row in the constraint matrix C in Section V.2. Synthesis runs with such constraints will be called 'non-negative synthesis' (NNS).
2. Constraints requiring non-negative numbers as well as increasing numbers along the main sequence and M-giant branches (in reverse order). Synthesis using such constraint will be called 'synthesis with sequences' (SS). In such cases the constraint specifies that the numbers in one stellar group exceed that in another by a minimum amount. This minimum amount can be controlled and usually kept very small to allow the algorithm greater flexibility in fitting.
3. Constraints requiring non-negative numbers, increasing numbers along the main sequence and giant branches as well as distinctly specified upper and lower limits to the ratios of stars of one spectral group to another. Synthesis using such constraints will be called 'synthesis with sequences and ratios' (SSR). This third type of constraint set permits virtually any kind of constraint to be imposed.

The above types of constraints are patterned after those of Pickles (1985a) and are broadly similar to those used by other authors (Faber, 1972, O'Connell, 1976, 1980).

The constraint sets with sequencing and sequencing plus ratios embody the following general inferences from stellar evolution theory.

The numbers of stars along the main sequence increase as one goes to later spectral types, since the mass decreases and lower mass stars live longer. There is no smoothing of the numbers since superimposition of successive generations of stars may not result in a smooth main sequence.

The number of stars decreases as one goes along the giant branch from spectral type M0 to M6 and beyond, because of faster evolution in the $M_{\text{bol}} - \log T_e$ plane as one goes up (to higher values of M_{bol}) the giant branch. The ratio of the total number of stars at the base of the giant branch (KO-2 giant stars which subsequently move up along the branch) to the number of M0-2 are expected to be compatible with the lifetimes in the corresponding stage of evolution.

The subgiant stars evolve to the base of the giant branch; the lifetimes at these evolutionary

stages would indicate roughly equal numbers of stars in these groups.

Along the G-K giant branches of solar, rich and weak metal abundances numbers would be expected to decrease as one goes from earlier to later types, again from considerations of the rate of evolution along these giant branches.

The range of values between which ratios of one stellar group to another are constrained to lie, have been kept large, to permit the algorithm more freedom in fitting. Tables 5.2a and b give a summary of the constraints and values for ratios for constraint sets of type SS and SSR.

V.2.3. Weights used for synthesis

In the discussion of the synthesis method in Section V.2, it was seen that the spectra could be weighted to give more weights to some spectral regions and less weight to others. Following the scheme used by Pickles (1985b), weight files have been generated by inverting the spectrum of the galaxy itself and then lowering the weights in the regions where subtraction of atmospheric absorption bands was done (see Section IV.2.1). Only the spectrum of NGC 4472 was used, since the turnup of fluxes in the near-infrared

Table 5.2a

Constraints for type SS synthesis

| Turnoff group selected | Standard non-negative groups | Extra non-negative groups | Excluded groups | Increasing sequence |
|------------------------|--|---------------------------|----------------------|---|
| 1. Earlier than F5-6 V | Early dwarfs till F4; Turnoff group; subgiants, B to late F III, K01 III, M6 III, mrK1-2 III, HB III, mw FO III, mwKO-2 III - for all cases. | None | None | From turnoff group to M5-6 V From M6 III to M0-2 III (for all cases). |
| 2. F7-8 V | | None | F5-6 V | |
| 3. G0-4 V | | F5-8 V | None | |
| 4. G5-8 V | | F5-8 V | G0-4 V | |
| 5. K0-1 V | | F5-8 V | G0-8 V early G IV | |
| 6. K2-3 V | | F5-8 V | G0-8 V early G IV | |

Table 5.2b

Additional constraints for type SSR synthesis

| Group A | Group B | Allowed range for ratio B/A |
|---|--|---|
| 1. KO-1 III + K2 III + mrK1-2 III | eG IV + mG IV + lG IV | 0.8 to 3.0 |
| 2. As in 1 + mwKO2 III | MO2 III | 0.003 to 0.1 |
| 3. mrK1-2 III | mrG5-KO III mrK3 III mrK4 III mrK5 III | 0.2 to 1.2 0.1 to 0.5 0.02 to 0.12 0.01 to 0.08 |
| 4. KO-1 III | G5-9 III K2 III K3 III K4 III K5 III | 0.3 to 1.5 0.3 to 1.1 0.1 to 0.8 0.03 to 0.2 0.01 to 0.05 |
| 5. mwKO-2 III | mwG5 III mwG8 III mwK3-4 III | 0.7 to 4.0 1.0 to 6.0 0.05 to 1.0 |

region of the spectrum for the other two galaxies are thought to be abnormal features not seen in 'normal' early-type galaxies.

The spectrum of NGC 4472 was smoothed to some extent and a continuum was fitted to it using a spline fitting technique. The continuum was then divided by the galaxy spectrum so that the result would be unity at the continuum at all wavelengths. The 'ratio' file (see Section IV.2.1) of several standard stars used for removal of atmospheric absorption bands were averaged, then corrected to the rest wavelength of NGC 4472. The two files were then multiplied together to give the weight file. The near infrared region was further derated to make the weights between 0.4 and 0.6. The resulting weight file gives high weight to the continuum points, since the overall shape of the spectrum is important, and stronger weight to the stronger spectral features. The weight file is shown plotted in Figure 5.2.

V.2.4. Population Synthesis of observed Galaxies

In this section we present details of population synthesis of the three galaxies observed. For each galaxy, synthesis was first done using non-negative constraints only (NNS), which allowed the approximate main sequence turnoff to be identified. Next, synthesis

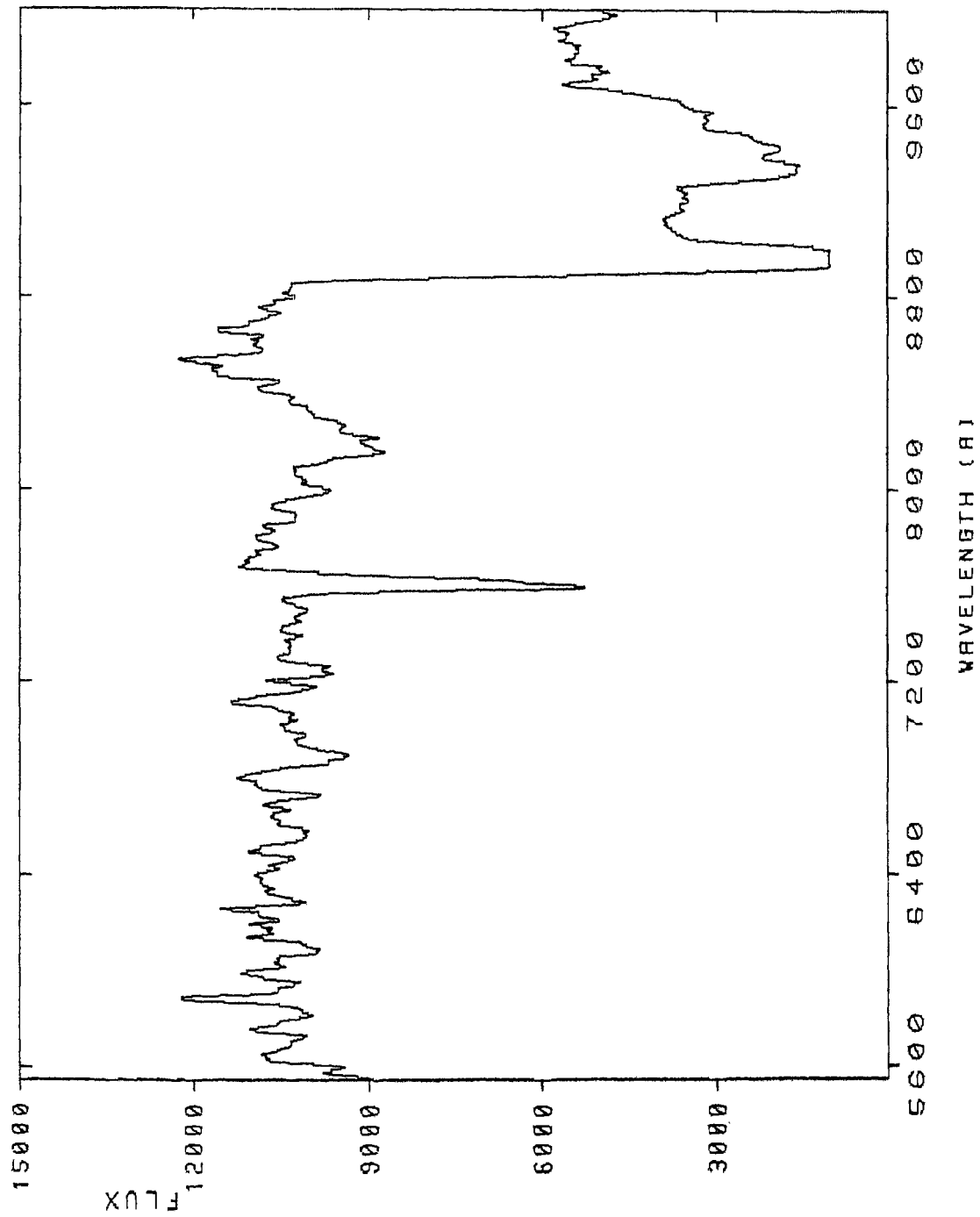


Figure 5.2. Weight file used for synthesis (scaled up by $\times 10^4$).

runs were done with constraints as in Table 5.2a (SS), where the main sequence turnoff was specified and numbers of stars were constrained to increase along it. Several SS runs were usually done, with different turnoff groups around the suspected one being specified. The merit of the fit indicated which specified turn-off group was most suitable. Usually, in an SS run, the solution did indicate the correct turnoff group, but the merit was poorer if the group specified (beyond which the numbers of stars along the main sequence were constrained to increase) was not the same as that indicated.

The next set of runs were those using non-negative constraints, sequences along the main sequence and M-giant branch as well as upper and lower limits to ratios between groups (SSR synthesis runs). SSR runs were tried out with the turnoff group indicated by the best SS run and also using turnoff groups on either side. The merit was usually best in the case of the correct turnoff group. The runs took from twenty minutes to one hour on the VAX 11/780 system at VBO.

Programs were written to display the observed and synthesized spectrum of the galaxy, the residuals and also the luminosity function as required. These were very useful in deciding the quality of the solutions.

V.2.4.1. Results for NGC 4472

The synthesis solution for non-negative constraints and the best solutions for the SS and SSR synthesis runs are presented in Table 5.3. Figure 5.3a shows the observed spectrum and the synthesized spectrum obtained by co-adding spectra of stellar groups in proportions present in the best SS solution. Figure 5.3b shows a plot of the logarithm of the numbers of stars of different stellar groups against their absolute visual magnitude; this plot is a form of the luminosity function for the galaxy. The main sequence, normal giants, metal rich giants and metal weak giants are marked with different symbols. Figure 5.4a and b show the same quantities for the best SSR solution.

The NNS solution shows maximum light contribution from the turnoff group, F7-8 V, at 5556\AA (50%), followed by the K4-7 V group (24.7%). The metal-rich G5-K0 III sequence provides only 10% of the visual light (5556\AA). Almost 9% of visual light comes from B6-9 dwarfs. These are stars of 4 solar mass and their presence would imply ongoing star formation in the nuclear region of the galaxy (where the aperture was centered for observations). NNS runs excluding the O, B and A dwarfs gave poorer values of the merit and the light contribution from the BIII group increased.

Table 5.3

Best Synthesis Solutions for NGC 4472

| Gurnoff specified Turnoff in solution Merit (mag.) M/L Ratio | NNS | | SS | | SSR | |
|---|--------------------------|------------------------------------|------------------------------------|------------------------------------|-----------------------------------|-----------------------------------|
| | F7-8 V 0.0306 3.91 | F7-8 V F7-8 V 0.0354 4.87 | F7-8 V F7-8 V 0.0354 4.87 | F7-8 V F7-8 V 0.0354 4.87 | F7-8 V F7-8 V 0.033 5.79 | F7-8 V F7-8 V 0.033 5.79 |
| <u>Groups</u> | <u>5556Å</u> | <u>10000Å</u> | <u>5556Å</u> | <u>10000Å</u> | <u>5556Å</u> | <u>10000Å</u> |
| B6-9 V | 8.73 | 2.45 | 8.14 | 2.78 | 2.75 | 0.78 |
| F7-8 V | 50.0 | 27.5 | 4.3 | 2.47 | 17.6 | 9.83 |
| G0-4 V | - | - | 4.1 | 2.78 | 16.8 | 11.1 |
| G5-8 V | - | - | 2.51 | 1.94 | 10.3 | 7.7 |
| K0-1 V | 2.53 | 2.14 | 22.3 | 19.7 | 15.2 | 12.6 |
| K2-3 V | - | - | 9.14 | 9.5 | 7.0 | 7.6 |
| K4-7 V | 24.7 | 35.4 | 8.64 | 12.9 | 12.3 | 16.0 |
| M0-2 V | - | - | 2.09 | 4.89 | 2.4 | 6.0 |
| M3-4 V | - | - | 0.49 | 3.25 | 0.39 | 2.55 |
| M5-6 V | - | - | - | 0.44 | - | 1.4 |
| mG1 V | 0.62 | 0.48 | 5.55 | 4.46 | - | 0.54 |
| BIII | - | - | 7.96 | 2.47 | - | - |
| M0-2 III | - | - | - | - | 0.24 | 0.76 |
| M3-4 III | - | - | - | 0.6 | - | - |
| M5-6 III | 0.62 | 19.8 | 0.3 | 8.3 | 0.1 | 14.1 |
| mG5-K0 III | 10.1 | 9.16 | 9.4 | 8.9 | - | - |
| mW5 III | - | - | - | - | 0.12 | 0.95 |
| mW8 III | 4.44 | 4.27 | 14.9 | 15.0 | 8.0 | 6.82 |
| mW0-2 III | - | - | - | - | 5.39 | 5.0 |
| mW3-4 III | - | - | - | - | 0.34 | 0.46 |

% Light contribution at

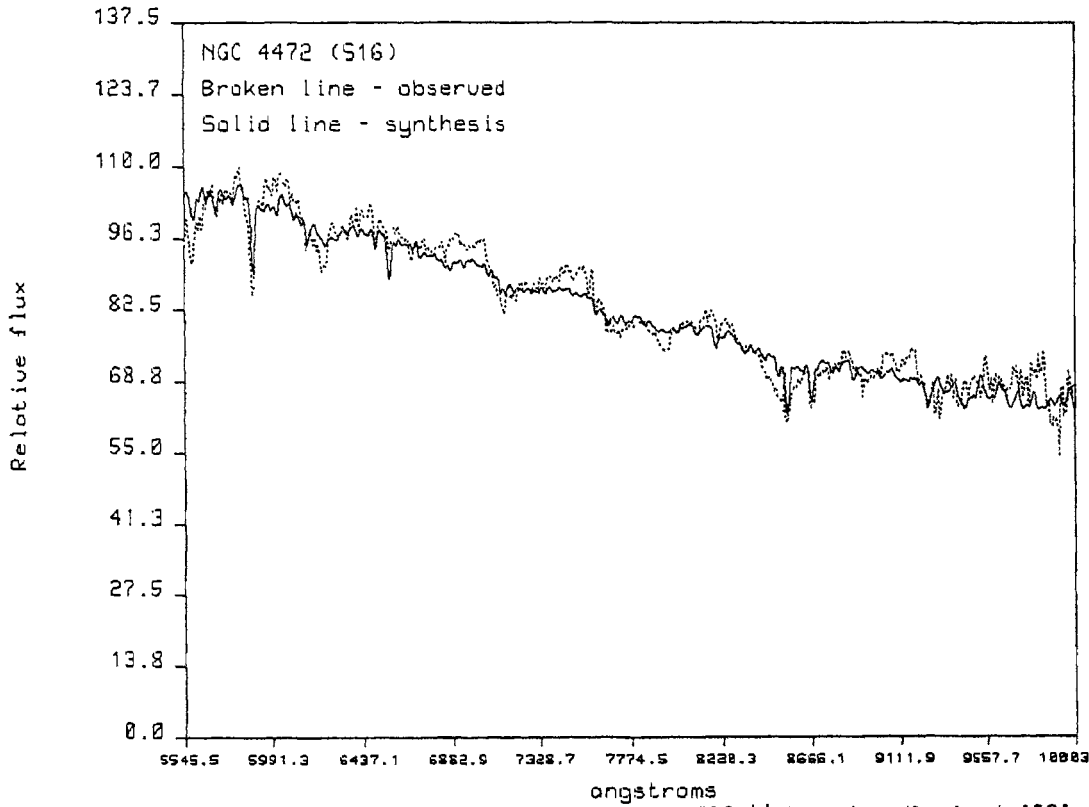


Figure 5.3a. Fit to the spectrum of NGC 4472 using the best 'SS' solution (the code in parentheses refers to the synthesis run number).

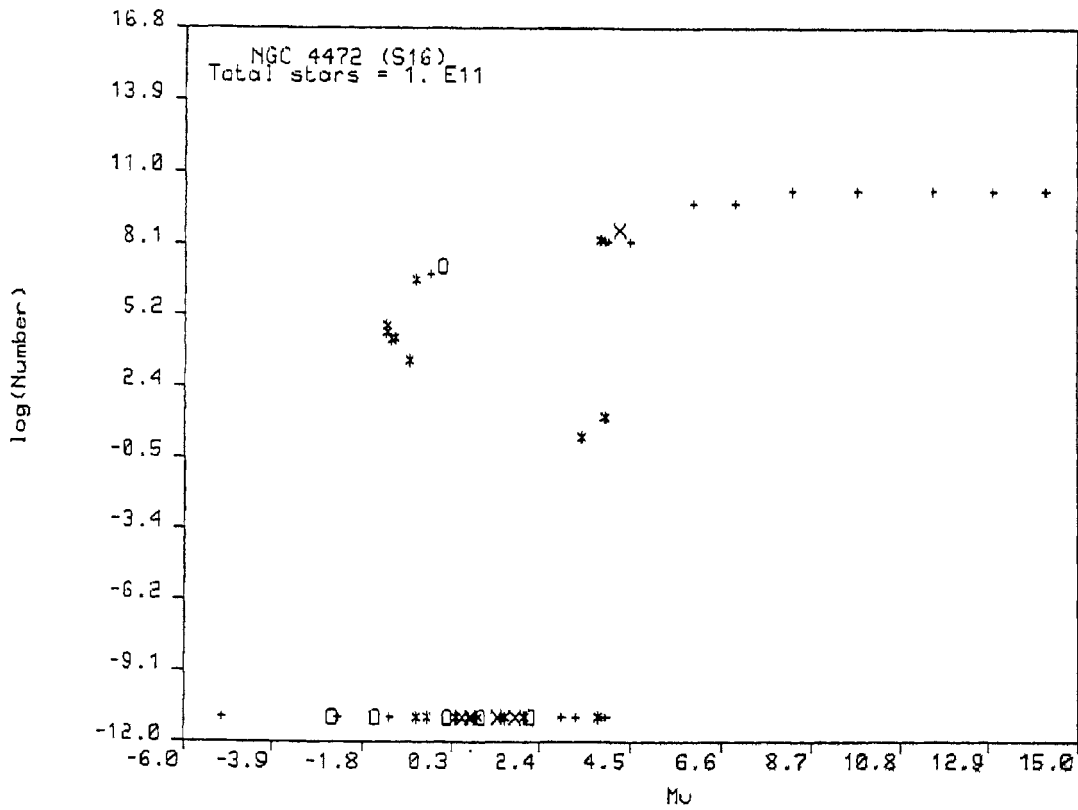


Figure 5.3b. Luminosity function for NGC 4472 (best 'SS' solution). Symbols are: + (main sequence); O (metal-weak giant + horizontal branch stars); x (metal-rich giants); * (normal giants).

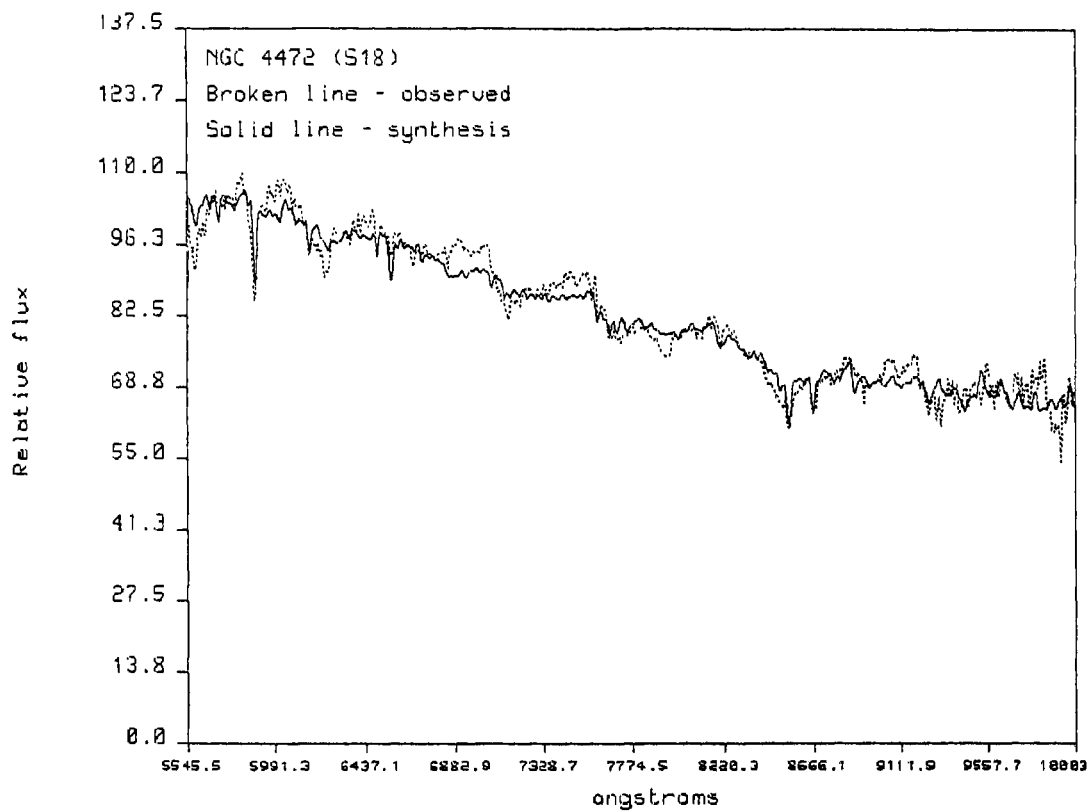


Figure 5.4a. Fit to the spectrum of NGC 4472 using the best 'SSR' solution (the code in parentheses refers to the synthesis run number).

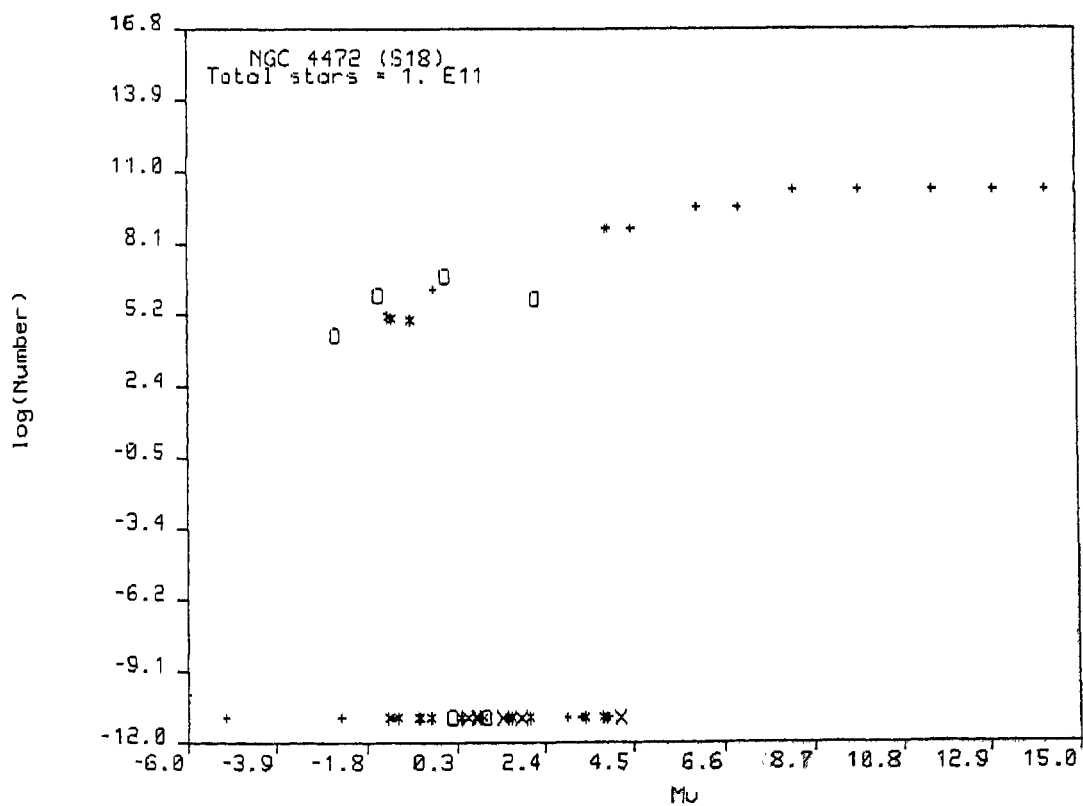


Figure 5.4b. Luminosity function for NGC 4472 (best 'SSR' solution)

The best solutions of the SS and SSR runs and indeed all other runs with different constraint sets showed from 2 to 8% of the light at 5556\AA to be from B6-9 dwarfs. In some of the SS and SSR runs, excluding the O, B and A groups increased the contribution from the groups at and below turnoff marginally, but there was no change in the contribution of the horizontal branch (HB) stars. The blue HB stars in the stellar library have the same photometric colours as the B6-9 dwarf group. These stars are, in fact indistinguishable in photometric properties from the latter types (O'Connell 1983, Pickles 1985b). If early type dwarf stars are in fact present, they would not change the spectrum appreciably in the region observed. In a study of nuclei of spiral galaxies and globular clusters with high precision ($\leq 5\%$) narrow band colours, O'Connell (1982) excluded the possibility that the nuclei are old metal poor systems and attributed the blue light to a young population less than 1 Gyr old.

Rose (1985) concluded from a study of several elliptical galaxy nuclei (including NGC 4472) that a maximum of only 2% of the light at wavelengths of the V band (close to 5556\AA) could be arising from young stars. The SSR best solution requires a V light contribution of 2.75% from the B6-9 V.

The turnoff group (B-V) colour corresponding to F7-8 V is near 0.55. An examination of the Vanden Berg (1985) isochrones of solar metallicity gives an age of 8 Gyr (turnoff (B-V) = 0.537) to 10 Gyr ((B-V) = 0.567). This is consistent with evidence that the light of nearby E/SO galaxies is dominated by a population that is 5 to 10 Gyr old (O'Connell, 1985). The last major star formation activity in NGC 4472, seen from the solutions here, occurred 8 to 10 Gyr ago.

It is a bit surprising that though metal rich stars of type mrg5-KO III were contributing about 10% V light in the NNS model, all metal rich stars are totally absent in the SSR model. The reason for this is not clear, especially since the fit to the observed spectrum is clearly better for the SSR model. One possible reason is that the SSR main sequence is better populated and since these groups have a range of metal abundances, the fit to the spectrum could be good even with the metal rich giants removed.

V.2.4.2. NGC 3308

The solution for synthesis with non-negative constraints and the best solutions for the SS and SSR synthesis runs for this galaxy are given in Table 5.4. The fit to the spectrum for the best SS solution is given in Fig. 5.5a and the luminosity function in

Table 5.4

Best Synthesis Solutions for NGC 3308

| Turnoff specified Turnoff in solution Merit (mag.) M/L Ratio | NNS | | SS | | SSR | |
|---|--------------------------|--|--------------------------|-----------------------------------|-----------------------------------|-----------------------------------|
| | K2-3 V 0.046 0.564 | - K2-3 V K2-3 V 0.045 1.59 | K2-3 V 0.046 0.564 | K2-3 V K2-3 V 0.045 1.59 | K2-3 V K0-1 V 0.047 1.05 | K2-3 V K0-1 V 0.047 1.05 |
| <u>Groups</u> | <u>5556Å</u> | <u>10000Å</u> | <u>5556Å</u> | <u>10000Å</u> | <u>5556Å</u> | <u>10000Å</u> |
| A0-3 V | 29.3 | 6.0 | 24.2 | 5.0 | 14.8 | 3.18 |
| K0-1 V | - | - | - | - | 20.2 | 12.5 |
| K2-3 V | 3.65 | 2.4 | 7.1 | 4.2 | 1.85 | 1.35 |
| K4-7 V | 2.86 | 2.4 | 2.4 | 2.42 | 0.55 | 0.58 |
| M0-2 V | - | - | 0.67 | 0.97 | 0.13 | 0.23 |
| M3-4 V | - | - | 0.45 | 0.65 | - | - |
| M5-6 V | - | - | - | 0.1 | - | 0.1 |
| eG IV | - | - | 1.78 | 0.7 | - | - |
| mG IV | - | - | - | - | 2.73 | 1.54 |
| BIII | 14.7 | 2.9 | 18.8 | 3.8 | 17.4 | 3.8 |
| eA III | - | - | 1.43 | 0.3 | - | - |
| K0-1 III | - | - | - | - | 3.98 | 2.46 |
| K2 III | - | - | - | - | 3.41 | 2.72 |
| K3 III | 1.85 | 1.38 | - | - | 14.7 | 13.4 |
| K4 III | - | - | - | - | 6.94 | 7.12 |
| K5 III | - | - | - | - | 2.19 | 2.97 |
| M0-2 III | 6.11 | 11.5 | 9.52 | 17.0 | 6.95 | 14.4 |
| M3 III | - | - | - | - | 0.42 | 1.09 |
| M4 III | - | - | - | - | 0.43 | 2.12 |
| M5 III | - | - | 0.95 | 9.6 | 0.66 | 5.79 |
| M6 III | 1.03 | 29.3 | 1.2 | 23.5 | 0.85 | 19.9 |
| mrK5 III | 23.8 | 29.1 | 22.4 | 27.3 | - | - |
| mwG8 III | - | - | - | - | 0.29 | 0.2 |
| mwK0 III | - | - | - | - | 1.23 | 0.93 |
| mwK3-4 III | 17.6 | 15.4 | 12.8 | 13.0 | 3.22 | 3.72 |

Table 5.4 .: contd.

| | <u>5556A</u> | <u>10000A</u> | <u>5556A</u> | <u>10000A</u> | <u>5556A</u> | <u>10000A</u> |
|------------|--------------|---------------|--------------|---------------|--------------|---------------|
| mWG8 III | - | - | - | - | 0.29 | 0.2 |
| mWKO III | - | - | - | - | 1.23 | 0.93 |
| mWX3-4 III | 17.6 | 15.4 | 12.8 | 13.0 | 3.22 | 3.72 |

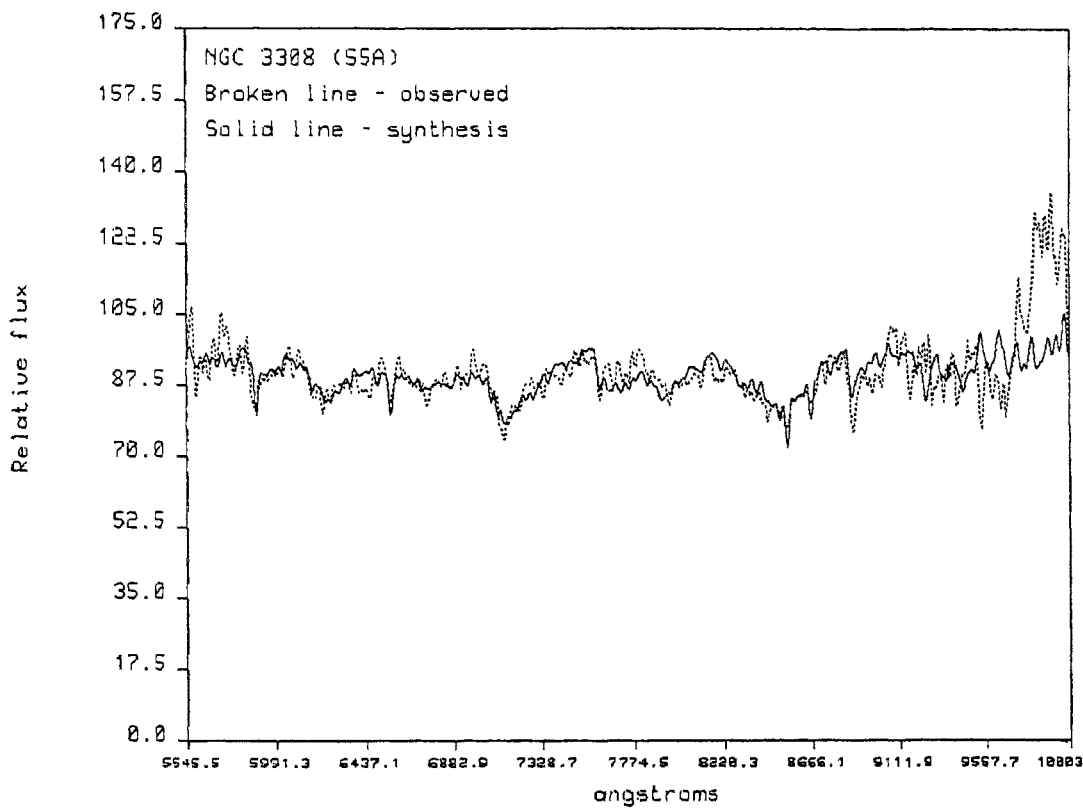


Figure 5.5a. Fit to the spectrum of NGC 3308 using the best 'SS' solution (the code in parentheses refers to the synthesis run number).

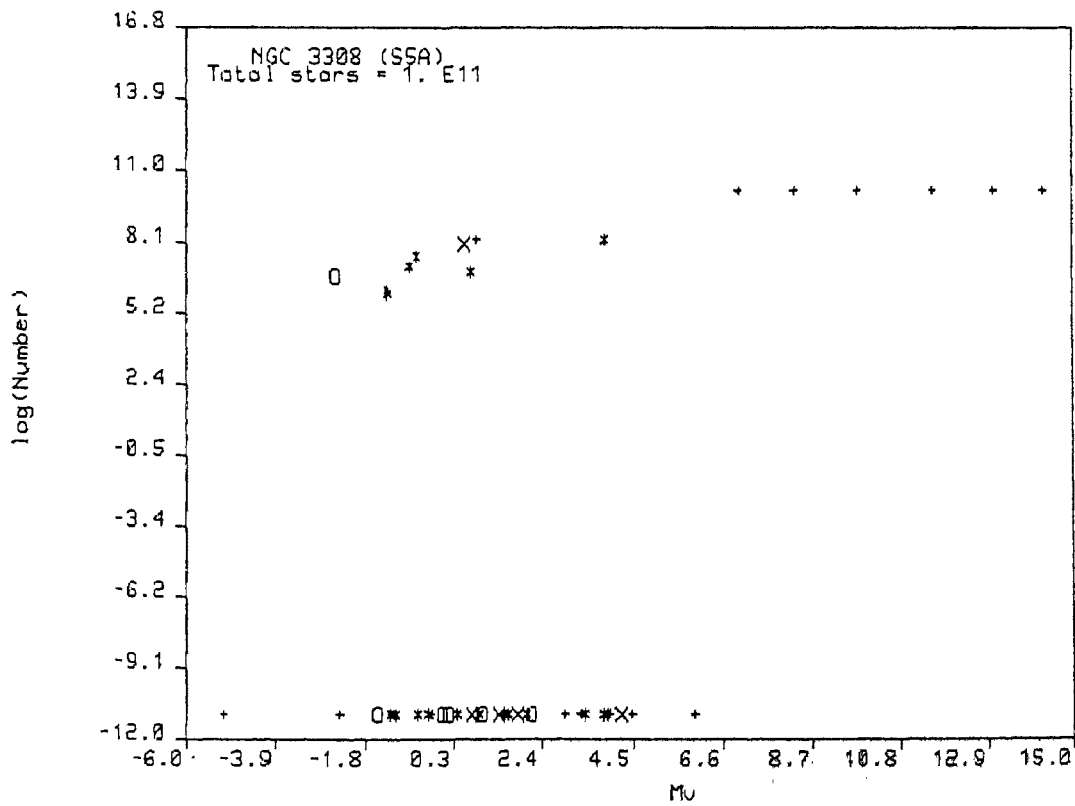


Figure 5.5b. Luminosity function for NGC 3308 (best 'SS' solution).

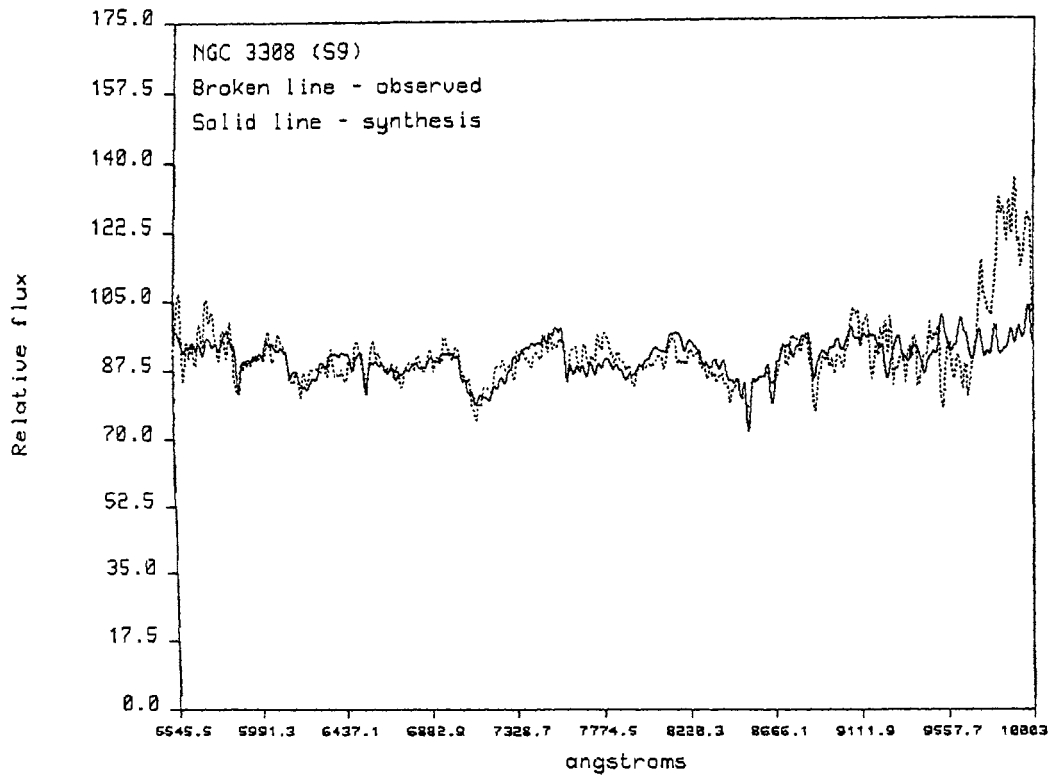


Figure 5.6a. Fit to the spectrum of NGC 3308 using the best 'SSR' solution (the code in parentheses refers to the synthesis run number).

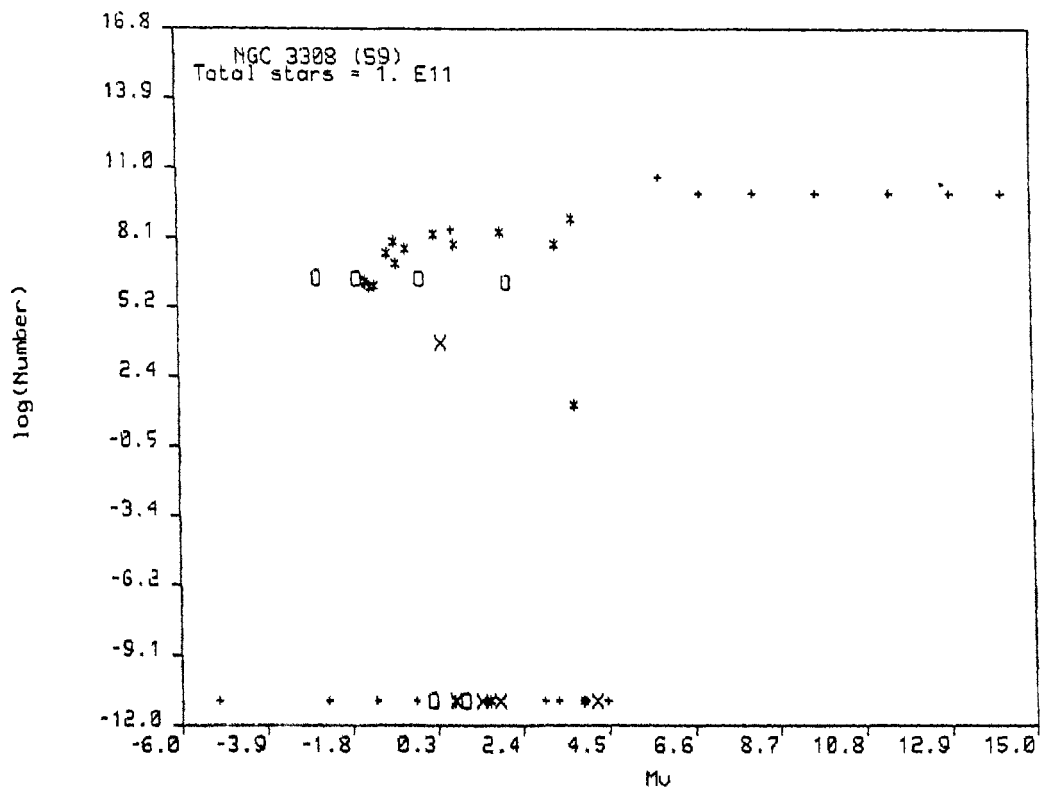


Figure 5.6b. Luminosity function for NGC 3308 (best 'SSR' solution).

Figure 5.5b. The fit for the best SSR solution is given in Figure 5.6a and the corresponding luminosity function in Figure 5.6b.

The most striking aspect about the solutions is the large light contribution from the A0-3 dwarf group and B III groups to the V-light. In the NNS solution 29% of the V-light is from A0-3 V stars and 14.7% from B III stars. Metal rich K5 III giants contribute 23.8% and are the next largest contributors to the light after the A0-3 V. The metal weak K3-4 III group also contributes a large fraction of the V-light. The light at 10000\AA is fully dominated by the M6 III and mrK5 III. The SS solution is similar except that M0-4 dwarfs and early M giants are also seen. In the SSR solution the contribution from the A0-3 V goes down, but is still high at V (14%); normal abundance K giants contribute significantly to the light, the metal rich giants are excluded from the solution and the metal weak giants though contributing less, are still significant. An interesting aspect is that the contribution of the BIII group is about the same in all three syntheses.

The main sequence turnoff group indicated by all the synthesis runs is either K0-1 V or K2-3 V, which for a solar abundance yields ages of greater than

20 Gyr. If a turnoff at K2-3 V has to be possible at lower ages, this would call for higher metallicities. None of the line indices for this galaxy, which discriminate between metal rich and metal poor giant stars are strong; the only exception to this is the Ca II-8662 index, which, however, suffers from TiO contamination. The TiO indices at 7126\AA and 7198\AA are quite strong in this galaxy, implying large numbers of giants, though not necessarily metal rich giants. On the strength of the TiO bands alone, one would expect more light from M stars and the SS solution would seem more appropriate. The SS solution also indicates a high incidence of the mrK5 III group.

In Section IV.1.9, we found that the magnitudes obtained from our spectra for the flux standard stars were systematically fainter in the visual and brighter in the red region; if the galaxy spectrum is corrected for this, then an even larger number of stars from the blue stellar groups would be required. From the considerations in O'Connell (1983), if the blue light fitted by the A0-3 V and BIII groups were actually from horizontal branch stars then this would imply too many horizontal branch stars. If the galaxy had to be corrected for reddening using the larger value of $E(B-V)$ in Table 3.3, that would also increase the light in the visual region further.

As mentioned in Chapter III, this galaxy has not been studied well earlier and further observational studies, of NGC 3308 and of other members of the cluster Abell 1060 (of which it is a member), are required before a proper interpretation of the results obtained here can be made.

V.2.4.3. NGC 5128

The best results of population synthesis runs for the galaxy NGC 5128 are presented in Table 5.5. Around forty different runs were done on this galaxy using both the original stellar library of Pickles (1985), with luminosities and masses for stellar groups as assigned by him, and the augmented stellar library (ASL) with luminosity and mass values assigned in this study. Since NGC 5128 is known to be a peculiar object, a whole range of turnoff groups were tried out with different kinds of constraint sets. As for the other two galaxies, the merit of the fit was always better using the ASL. It was found that no SS run could produce reasonable fits of merit close to the best NNS and SSR runs. Therefore, in Table 5.5 we present only the best results of NNS and SSR synthesis. The fit to the spectrum using the NNS solution is in Figure 5.7a and the luminosity function in Figure 5.7b. The fit for the best SSR solution is shown in Figure 5.8a and the luminosity function in Figure 5.8b.

Table 5.5

Best synthesis solutions for NGC 5128

| | <u>NNS</u> | | <u>SSR</u> | |
|---------------------|-----------------------------|---------------|--------------|---------------|
| Turnoff specified | - | | KO-1 V | |
| Turnoff in solution | K2-3 V. | | G0-4/KO-1 V | |
| Merit (mag) | 0.062 | | 0.060 | |
| M/L Ratio | 4.79 | | 8.87 | |
| | <u>% Light contribution</u> | | | |
| <u>Groups</u> | <u>5556Å</u> | <u>10000Å</u> | <u>5556Å</u> | <u>10000Å</u> |
| O-B3 V | 43.7 | 6.05 | 24.6 | 4.06 |
| G0-4 V | - | - | 1.38 | 0.83 |
| G5-8 V | - | - | 1.38 | 0.94 |
| K0-1 V | - | - | 15.4 | 12.0 |
| K2-3 V | 43.4 | 33.5 | 6.15 | 5.67 |
| K4-7 V | - | - | 3.07 | 4.08 |
| M0-3 V | - | - | 0.68 | 1.75 |
| M4 V | 0.75 | 6.14 | 0.57 | 0.56 |
| M5-6 V | - | - | 0.22 | 2.67 |
| BIII | - | - | 20.0 | 5.52 |
| G5-9 III | - | - | 0.30 | 0.26 |
| K0-1 III | - | - | 1.58 | 1.24 |
| K2-3 III | - | - | 8.46 | 9.54 |
| K4-5 III | - | - | 4.42 | 5.96 |
| M0-5 III | - | - | - | 0.92 |
| M6 III | 1.61 | 39.6 | 0.43 | 26.6 |
| mrG5-KO III | - | - | 0.39 | 0.33 |
| mrK1-3 III | - | - | 5.10 | 5.22 |
| mrK4 III | 1.96 | 2.50 | 4.54 | 6.92 |
| mrK5 III | 8.81 | 13.2 | 3.82 | 6.82 |

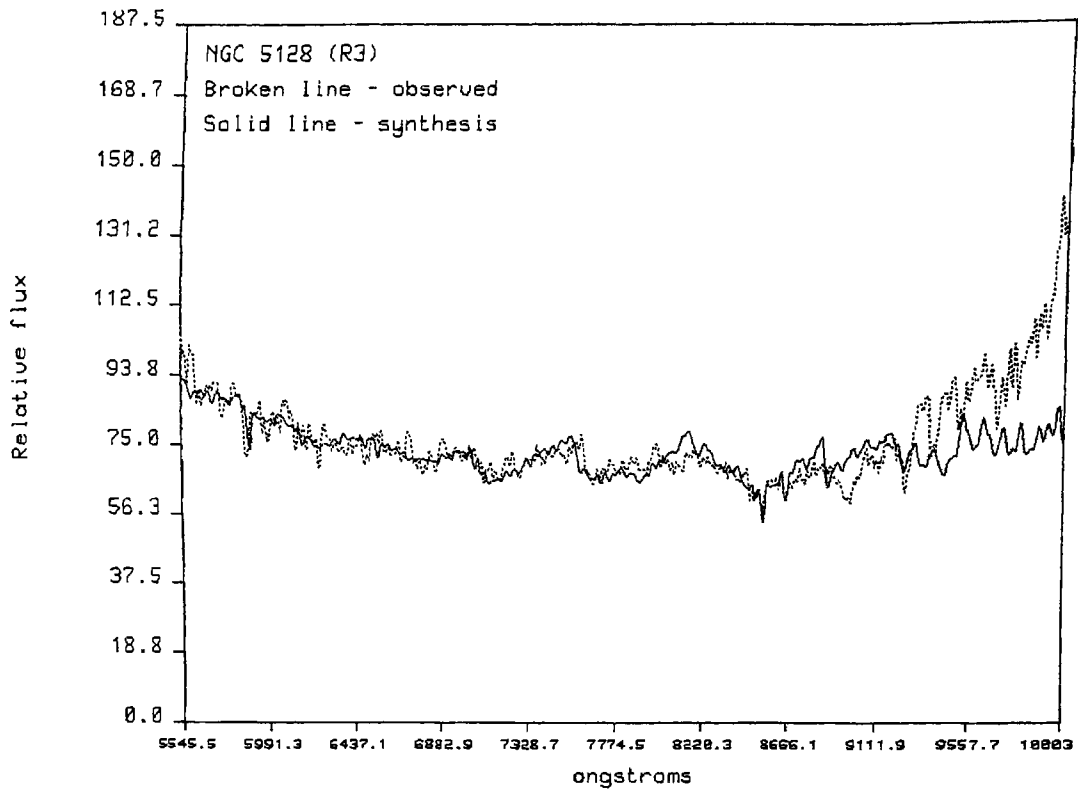


Figure 5.7a. Fit to the spectrum of NGC 5128 using the NNS solution (the code in parentheses refers to the synthesis run number).

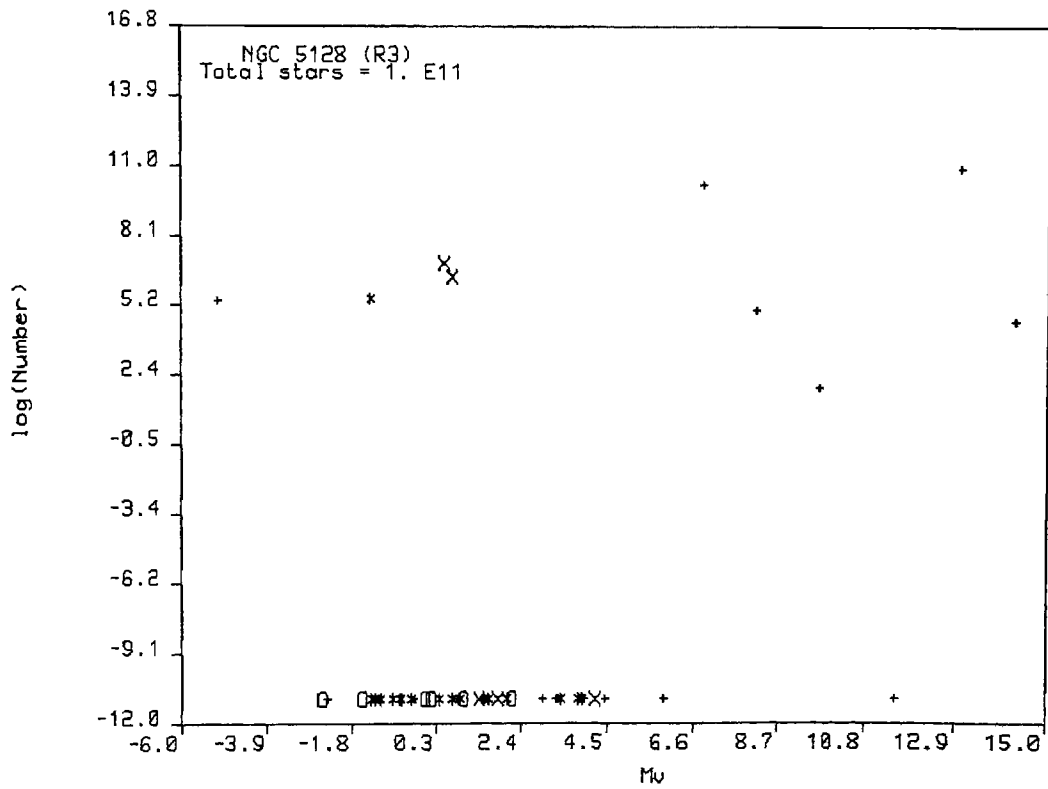


Figure 5.7b. Luminosity function for NGC 5128 ('NNS' solution).

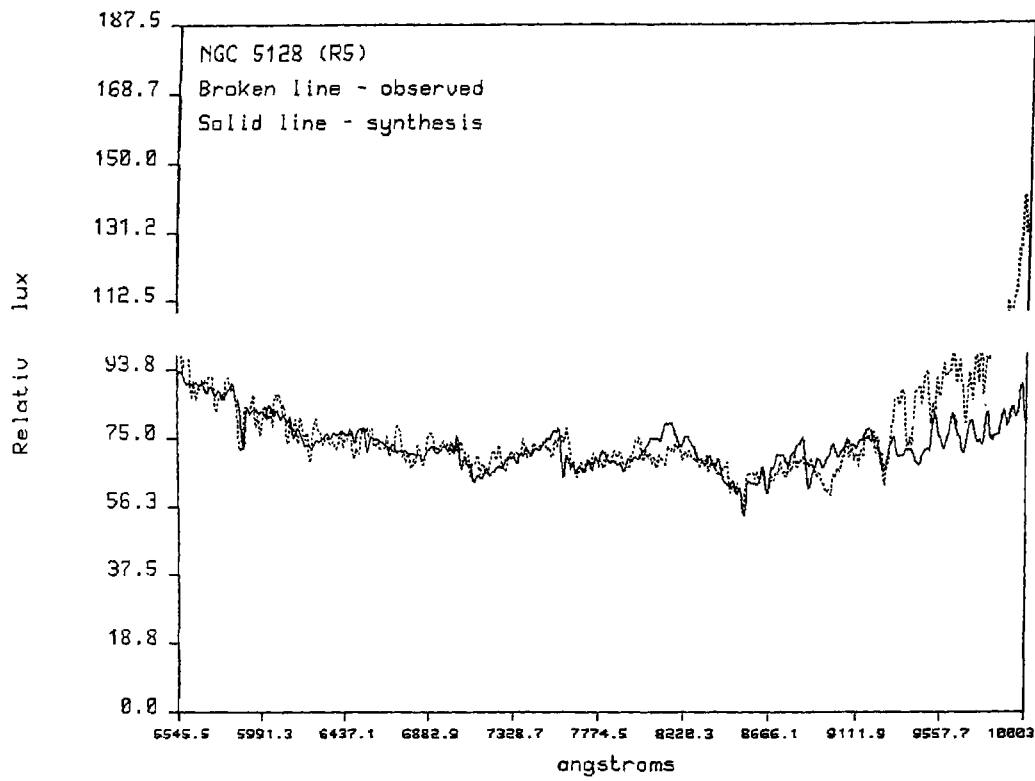


Figure 5.8a. Fit to the spectrum of NGC 5128 using the best 'SSR' solution (the code in parentheses refers to the synthesis run number).

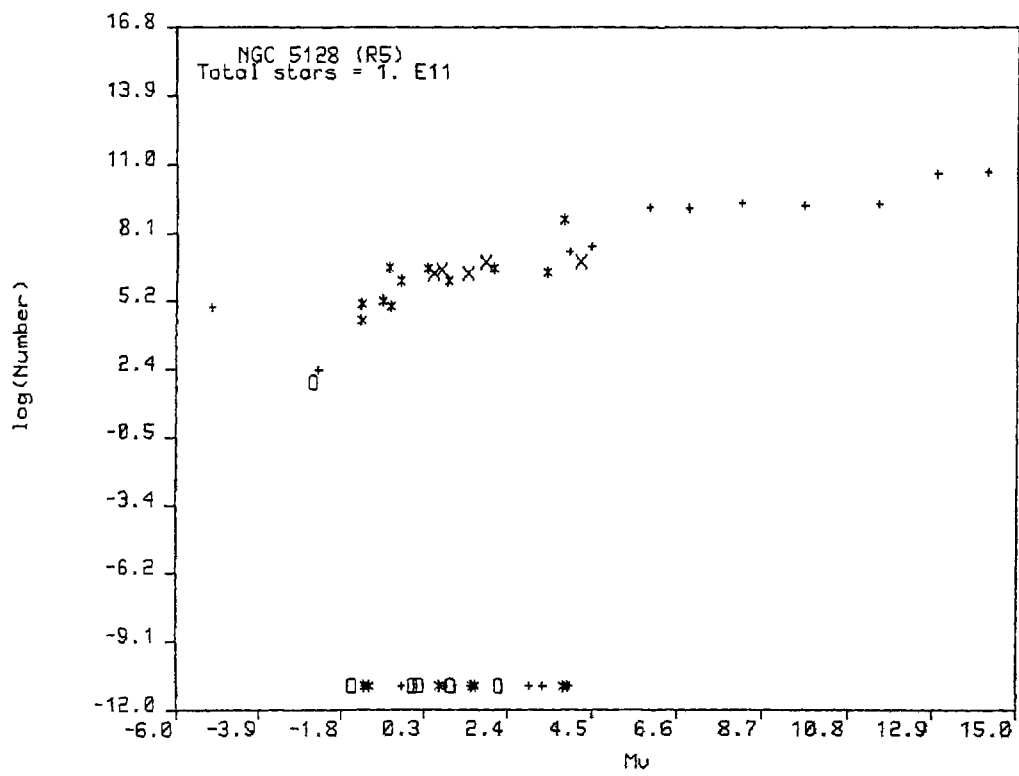


Figure 5.8b. Luminosity function for NGC 5128 (best 'SSR' solution).

The NNS solution shows few dominant stellar groups, the most remarkable of which are the earliest O-B3 dwarf groups contributing 43.7% of the light at visual wavelengths (5556\AA). The next biggest contributor at 5556\AA is the K2-3 dwarf group followed by the mK5 III giant group. At 10000\AA , the light is dominated almost equally by the latest M giants in the library and the K2-3 dwarfs. The luminosity function shown in Figure 5.7b immediately shows the lack of a well defined main sequence, suggesting perhaps the effect of multiple generations of stars.

The best SSR solution, shown in Table 5.5 shows maximum light on the lower main sequence of 15% at the K0-1 group, suggesting that the bulk of the stars in the region observed are old (discussed later). However, above this apparent turnoff point there are enough numbers of stars of type G0-8 to produce a significant contribution to the light. This implies a later generation of stars. There is appreciable contribution to the V light from O-B3 V (24.6%) and BIII groups (20%). SSR runs excluding the early main sequence, increases the BIII contribution; runs excluding, in addition, the BIII group, transferred the V light contribution to the wFO III. In this latter case, however, the merit deteriorated to unacceptable values. It would, therefore, seem that there is a significant amount of blue light from hot young stars.

The SSR solution also shows the dominance of the near-infrared radiation by the latest M giant group available in the stellar library, the M6 III group. Also worth noting in both Figures 5.7a and b is the inadequacy of the synthesis solution in fitting the sharp upturn in the spectrum towards longer wavelengths, despite the dominance by M6 giants. The shape of the spectrum seems to need hot stars to fit the rising continuum towards the blue region, which is achieved using the earliest dwarf groups, and cooler and redder stars to fit the infra-red, which is not possible. Synthesis runs were tried, in which increasing numbers of stars with later spectral type on the M giant branch were forced on the solution; this only resulted in the fit worsening towards lower wavelengths without improving appreciably in the 1 micron region.

A brief description of the properties of NGC 5128 was given in Section III.1.3.3. The galaxy has a disk of gas, dust and young stars rotating rapidly with respect to the main ellipsoidal body (Phillips 1981 and references therein). According to Dufour et al (1979), the photometric colours of various regions are consistent with a scenario that the optically dominant stellar population formed in a burst of star formation starting about 5×10^7 years ago and continuing till the present. The maximum star formation occurs at the outer perimeter

of the disk; Van den Bergh (1976) infers that the dust is rich in heavy elements, implying that it comes from gas ejected from evolved stars.

Our synthesis solution using the SSR constraint sets (and in its broad features also that using the NNS constraints) seem to be generally consistent with this picture. The blue light comes mainly from hot, young stars. Whether these stars are massive ($\sim 30 M_{\odot}$), O-type stars or less massive (~ 5 to $10 M_{\odot}$) B-type stars is a matter bearing further discussion. Stellar evolutionary models of massive stars incorporating mass loss and convective overshooting of the core shows that the core helium burning stage of evolution occurs partly in the red and partly in the blue region of the HR diagram (Chiosi 1986). A typical $20 M_{\odot}$ star spends about 30% of its Helium burning lifetime as a red super-giant; stars of 10 to $20 M_{\odot}$ are likely to spend their entire core-helium burning phase as red super-giants. The formation of massive O5 stars is apparently required to account for the far infrared emission from galaxies with dust lanes, such as NGC 5128.

The excess red light seen in our spectra at 1 micron by a few M super-giant stars, whose predecessors would be the massive O stars providing the upturn towards the blue. Cool M giants of late spectral type (M7 to M9 III)

can also account for this excess light. Unfortunately, the stellar library contains neither of these types. It would be interesting to see if the cool M giants found in the Galactic centre in large numbers (Frogel 1985) match the near infra-red spectrum observed here.

The G0-4 main sequence stars above the turnoff would imply that formation of stars of lower masses (as compared to the massive O stars) has taken place in the course of the last few billion years. The turnoff point of G0 for this intermediate generation, for a metal rich composition $Z = 0.03$ from Vanden Berg (1987) implies an age of about 6 Gyr. It would, therefore, seem that star formation has not only occurred in NGC 5128 in the recent past but also over a period of a few giga years.

Chapter VI

SUMMARY AND FUTURE DIRECTIONS

In the foregoing chapters we have detailed a study of the populations of stars in early type galaxies. The method used for the study is that of population synthesis, in which the observed spectrum of a galaxy is matched by the co-added spectra of stars of known types within the Galaxy.

We have obtained spectroscopic data of galaxies and stars belonging to standard stellar types and carried out reduction of the data to finally obtain the energy distribution as a function of wavelength. The library of stellar spectra for use in population synthesis has to cover the entire range of stars seen and studied within the galaxy. The compilation of such a library, with each stellar group observed a sufficient number of times to get good representative averages, can take a lot of observing time. Since such compilations have been made earlier, it is prudent to use them, if possible. We have used an existing library after augmenting it with our own stellar observations.

Three early type galaxies were studied in this work; of these, NGC 4472 in the Virgo cluster has been the subject of many earlier investigations, including

the derivation of its stellar content using population synthesis. The second galaxy is a typical early type galaxy, in the sense that it was not known to show any signs of activity characterised by emission lines in the spectrum, abnormal colours or morphology or radio emission. There has hardly been any earlier work on this galaxy, except for measurements of radial velocities and photometry. The third galaxy, NGC 5128, also known as Centaurus A, is in that class of elliptical galaxies classified as peculiar. It is one of the most powerful sources of radiowave radiation in the sky and had other features such as the gigantic band of dust and gas obscuring part of the light, which have attracted much attention; strangely no population synthesis using optical spectra have been made before.

For the galaxy NGC 4472, we find evidence for star formation activity in the region observed (which was the optically bright centre of the galaxy) to the extent thought possible by others, from studies of strengths of spectral lines (Rose 1985). We also find that the last major star formation activity in the galaxy occurred 8 to 10 giga years ago as indicated by the main sequence turnoff point derived. One puzzling result that we get in the best constrained synthesis model is that contrary to what is believed of giant elliptical galaxies, NGC 4472 does not have a significant proportion of

metal rich giant stars. We feel that the stellar libraries used in population synthesis should discriminate between different metallicities among dwarf stars, particularly of late spectral type, to resolve this problem. Very cool metal rich giant stars such as now known to exist at the centre of our Galaxy, should also be used in the stellar library.

The galaxy NGC 3308 has been studied in such detail for the first time. It is a member of the A 1060 cluster of galaxies and is also the most distant of the three. The best synthesis solutions show a main sequence turnoff group at K2-3 V, implying that the stars belong to an old population. The solutions also show about 14% light contribution from dwarf stars of spectral type A0-3 and about 17% contribution from B-type giant stars. It is not possible to say for certain if this component of light is really from young hot stars or from horizontal branch stars.

We find interesting solutions for the stellar content of NGC 5128, which is consistent with the findings from photometry, that star formation on widespread scales is currently going on in this galaxy. There seems to be appreciable contribution to light at visual wavelengths from massive main sequence stars and the light at wavelengths near 1 micron are dominated by

the latest M-giant group available in the library (M6 III). NGC 5128 shows an enhanced metal rich giant sequence which contributes about 19% of the light at 1 micron. The spectrum of NGC 5128 turns up towards bluer wavelengths and also toward the infra-red. This seems to suggest massive young stars being formed and evolving to provide late M giants or even supergiants. The existing stellar library components are not, in our finding, adequate to match the increasing flux towards the infrared.

It would be very useful to obtain observations at several positions on the patchy surface of the galaxy and obtained the distribution of the stellar populations spatially, over both the old ellipsoidal component and the young star forming disk.

One of the main conclusions from the analysis of line indices is that they can be exploited in choosing between solutions. During the analysis of line indices in both the stellar library and the galaxies we find several useful indicators of metallicity and luminosity, which, though used for stars have not been used commonly for galaxies e.g. CaH at 6385, CaI 6162.

Our immediate aim in the continuance of this study is to use the recently acquired CCD (charge coupled device) detector system at the Vainu Bappu Observatory

to compile flux calibrated libraries for stellar groups covering metal rich and metal poor dwarf stars, super metal rich M giant stars found at the Galactic centre, M supergiant groups and extreme populations in general.

We would like to extend population synthesis studies to cover as many objects of a given type as possible, so that conclusions may be taken as statistically significant. This calls for sustained effort over the years using a standardised observing pattern. The effort would be well worth it since it would enable us to extend the understanding of the stars around us to the distant galaxies.

REFERENCES

- Aaronson, M.,
Cohen, J.G.,
Mould, J.,
Malkan, M. 1978 *Astrophys. J.* 223, 824
- Allen, C.W. 1973 *Astrophysical Quantities*,
University of London.
- Arimoto, N.,
Yoshii, Y. 1986 *Astr. Astrophys.* 164,
260.
- Babcock, H.,
Moore, C. 1947 *The Solar Spectrum λ 6600
to λ 13495*, Carnegie Inst.
Washington, No.579.
- Baldwin, J.E.,
Danziger, I.J.,
Frogel, J.A.,
Persson, S.E. 1973 *Astrophys. Lett.* 14, 1.
- Barbaro, G.,
Olivi, F.M. 1986 in *Spectral Evolution of
Galaxies*, Eds. C. Chiosi
& A. Renzini, *Astrophysics
and Space Science Library
122*, D. Reidel, Dordrecht,
p. 283.
- Bartholomew-Biggs,
M.C. 1979 *Numerical Optimisation
Centre, Hatfield Polytech-
nic, Tech. Rep. No.105.*
- Bessell, M.S. 1979 *Publ. astr. Soc. Pacific*,
21, 593.
- Bessell, M.S. 1983 *Publ. astr. Soc. Pacific*,
25, 480.
- Bessell, M.S.,
Wood, P.R. 1984 *Publ. astr. Soc. Pacific*,
26, 247.
- Blanco, V.M.,
Demers, S.,
Douglas, G.G.,
Fitzgerald, M.P. 1968 *Publ. US Naval Obs. Vol.21.*
- Breger, M. 1976 *Astrophys. J. Suppl. Ser.*
32, 1.

- Brosch, N. 1987 Mon. Not. R. astr. Soc. 225, 257.
- Bruzual, A.G. 1983 Astrophys. J., 273, 105.
- Buscombe, W. 1984 MK Spectral Classifications, Sixth General Catalog, Northwestern University, Evanston.
- Buser, R. 1978 Astr. Astrophys., 62, 411.
- Buser, R.,
Kurucz, R.L. 1978 Astr. Astrophys. 70, 555.
- Chiosi, C. 1986 in Spectral Evolution of Galaxies, Eds. C. Chiosi and A. Renzini, Astrophysics and Space Science Library, 122, D. Reidel, Dordrecht, p. 237.
- Code, A.D. 1959 Publ. astr. Soc. Pacific, 71, 118.
- Cohen, J.G. 1978 Astrophys. J. 221, 788.
- Cousins, A.W.J. 1975 Mon. Not. R. astr. Soc. Sth. Africa, 34, 68.
- Cousins, A.W.J. 1980 S. African Astr. Obs. Circ. Vol.1, No.5, p. 234.
- Cousins, A.W.J. 1981 S. African Astr. Obs. Circ. Vol.1, No.6, p.4.
- de Vaucouleurs, G. 1975 in Galaxies and Universe, Eds. A. Sandage, M. Sandage & J. Kristian, Univ. Chicago Press, p. 557.
- de Vaucouleurs, G.,
de Vaucouleurs, A. 1958 Lowell Obs. Bull., No.92, 58.
- de Vaucouleurs, G.,
de Vaucouleurs, A. 1959 Publ. astr. Soc. Pacific, 71, 83.
- de Vaucouleurs, G.,
de Vaucouleurs, A. 1973 Astr. Astrophys., 28, 109.

- de Vaucouleurs, G., 1976 Second Reference Catalog
de Vaucouleurs, A., of Bright Galaxies,
Corwin, H.G. Univ. Texas Press, Austin
(RC2).
- Dufour, R.J. et al. 1979 Astr. J., 84, 284.
- Ebnetter, K., 1983 Publ. astr. Soc. Pacific,
Balick, B. 95, 675.
- Ekers, R.D., 1978 Astr. Astrophys. 67, 47.
Kotanyi, C.G.
- Faber, S.M. 1972 Astr. Astrophys., 20, 361.
- Faber, S. 1977 in The Evolution of Galaxies
and Stellar Populations,
Eds. B.M. Tinsley & R.B.
Larson, Yale Univ. Obs.
p. 157.
- Flower, P.J. 1977 Astr. Astrophys. 54, 31.
- Frogel, J.A. 1986 in Spectral Evolution of
Galaxies, Eds. C. Chiosi
& A. Renzini, Astrophysics
and Space Science Library
122, D. Reidel, Dordrecht,
p. 143.
- Frogel, J.A., 1975 Astrophys. J. Lett. 195, L15.
Persson, S.E.,
Aaronson, M.,
Becklin, E.E.,
Mathews, K.,
Neugebauer, G.
- Gliese, W. 1969 Catalog of Nearby Stars :
Ver. Astr. Rechen Inst.
Heidelberg No .22.
- Gunn, J.E., 1981 Astrophys. J., 249, 48.
Stryker, L.,
Tinsley, B.
- Hayes, D.S., 1975 Astrophys. J. 197, 593.
Latham, D.W.
- Hoffleit, D. 1982 The Bright Star Catalog,
4th Rev. Edn., Yale Univ.
Obs., New Haven.

- Johnson, H.M. 1966 A.Rev. Astr. Astrophys. 4, 193.
- Kron, G.E., 1953 Astrophys. J. 118, 502.
White, H.S.,
Gascoigne, S.C.B.
- Kron, G.E., 1957 Astr. J., 62, 205.
Gascoigne, S.C.B.,
White, H.S.
- Lockwood, G.W. 1973 Astrophys. J. 180, 845.
- Malin, D.F., 1983 Astrophys. J. 272, L5.
Quinn, P.J.,
Graham, J.A.
- McClure, R.D., 1968 Astr. J., 73, 313.
Bergh, S. van den.
- Moore, C.E., 1966 National Bureau of Stan-
Minnaert, M.G.J.,
Houtgast, J. dards Monograph, 61.
- Morgan, W.W. 1956 Publ. astr. Soc. Pacific,
68, 509.
- Morgan, W.W. 1958 Publ. astr.. Soc. Pacific,
70, 364.
- Morgan, W.W., 1957 Publ. astr. Soc. Pacific,
Mayall, N.V. 69, 291.
- Nordh, H.L., 1977 Astr. Astrophys. 56, 1.
Lindgren, B.,
Wing, R.F.
- O'Connell, R.W. 1973 Astr. J., 78, 1074.
- O'Connell, R.W. 1974 Astrophys. J. Lett., 193,
L49.
- O'Connell, R.W. 1976 Astrophys. J., 206, 370.
- O'Connell, R.W. 1980 Astrophys. J., 236, 430.
- O'Connell, R.W. 1982 Astrophys. J., 257, 89.
- O'Connell, R.W. 1983 Astrophys. J., 267, 80.

- O'Connell, R.W. 1985 in Spectral Evolution of Galaxies, Eds. C. Chiosi and A. Renzini, Astrophysics and Space Science Library 122, D. Reidel, Dordrecht, p. 321.
- Palumbo, G.G.C., 1983 Catalog of Radial Velocities of Galaxies, Gordon & Breach, New York.
Tanzella-Nitti, G.,
Vettolani, G.
- Peck, M.L. 1980 Astrophys. J., 238, 79.
- Penny, A.J. 1984 in IAU Symp. 105 : Observational Tests of the Stellar Evolution Theory, Eds. A. Maeder & A. Renzini, D. Reidel, Dordrecht, p.157.
- Phillips, M.M. 1981 Mon. Not. R. astr. Soc. 197, 659.
- Pickles, A.J. 1985a Astrophys. J. Suppl. Ser., 59, 33.
- Pickles, A.J. 1985b Astrophys. J. 296, 340.
- Pickles, A.J. 1986 in IAU Symp. 127 (in press)
- Pritchett, C. 1977 Astrophys. J. Suppl. Ser. 35, 397.
- Rose, J.A. 1985 Astr. J. 90, 1927.
- Renzini, A., 1986 in Spectral Evolution of Galaxies, Eds. C. Chiosi & Buzzoni, A. A. Renzini, Astrophysics and Space Science Library 122, D. Reidel, Dordrecht, p.195.
- Richter, U.-G 1987 Astr. Astrophys. Suppl. Ser., 67, 237.
- Sadler, E. 1984 Astr. J., 89, 34.
- Sandage, A. 1973 Astrophys. J., 183, 711.
- Schmidt-Kaler. 1982 Numerical Data and Functional Relationships in Science and Technology, New Series, Vol.2.

- Seaton, M.J. 1979 Mon. Not. R. astr. Soc.,
187, 73P.
- Sharpless, S. 1956 Astrophys. J. 124, 342.
- Solf, J. 1978 Astr. Astrophys. Suppl.
Ser. 34, 409.
- Spinrad, H.,
Taylor, B.J. 1969 Astrophys. J., 157, 1278.
- Spinrad, H.,
Taylor, B.J. 1971 Astrophys. J. Suppl. Ser.
22, 445.
- Stebbins, J.,
Whitford, A.E. 1948 Astrophys. J., 108, 413.
- Straizys, V.,
Sviderskiene, Z. 1972 Vilnius Obs. Bull.No.35,
p.23.
- Taylor, B.J. 1984 Astrophys. J. Suppl. Ser.
54, 259.
- Thomas, P.A. 1986 Mon. Not. R. astr. Soc.,
220, 949.
- Thonnard, N. 1983 in IAU Symp. 100 : Internal
Kinematics and Dynamics of
Galaxies, Ed. E. Athanassoula,
D. Reidel, Dordrecht, p.305.
- Tinsley, B.M. 1980 Fund. Cosmic Phys. 5, 287.
- Tinsley, B.M.,
Gunn, J.E. 1976 Astrophys. J., 266, 747.
- Turnshek, D.E.,
Turnshek, D.A.,
Craine, E.R.,
Boeshaar, P.C. 1985 An Atlas of Digital Spectra
of Cool Stars, Western
Research Company Tucson,
Arizona.
- van den Bergh, S. 1976 Astrophys. J. 208, 673.
- van den Bergh, S.,
Henry 1962 Publ. David Dunlap Obs.,
2, 281.
- VandenBerg, D.A.,
Hartwick, F.D.A.,
Dawson, P.,
Alexander, D.R. 1983 Astrophys. J., 266, 747.

- VandenBerg, D.A. 1985 *Astrophys. J. Suppl. Ser.*
58, 711.
- VandenBerg, D.A.,
Bell, R.A. 1985 *Astrophys. J. Suppl. Ser.*
58, 561.
- VandenBerg, D.A.,
Laskarides, P.G. 1987 *Astrophys. J. Suppl. Ser.*
64, 103.
- Whipple, F. 1935 *Harvard Obs. Circ.*, No.404.
- Whitford, A.E. 1958 *Astr. J.*, 63, 201.
- Whitford, A.E. 1977 *Astrophys. J.*, 211, 527.
- Williams, T.B. 1976 *Astrophys. J.*, 209, 716.
- Wing, R.F.,
Dean, C.A. 1983 in IAU Coll. 76 : The
Nearby Stars and the
Stellar Luminosity Function,
Eds. A.G.D. Philip & A.R.
Upgren, L. Davis Press,
New York, p. 385.
- Wood, D.B. 1966 *Astrophys. J.*, 145, 36.
- Wood, D.B. 1969 *Astr. J.*, 74, 177.
- Wyse, R.F.G. 1985 *Astrophys. J.*, 299, 593.